LIAM COATMAN

BLACK HOLE MASSES AND OUTFLOWS IN HIGH REDSHIFT QUASARS

BLACK HOLE MASSES AND OUTFLOWS IN HIGH REDSHIFT QUASARS

LIAM COATMAN
UNIVERSITY OF CAMBRIDGE
INSTITUTE OF ASTRONOMY
ROBINSON COLLEGE
SUBMITTED TO THE BOARD OF GRADUATE STUDIES APRIL 2017
UNDER THE SUPERVISION OF
PROF. PAUL C. HEWETT
DR. MANDA BANERJI

Ohana means family.
Family means nobody gets left behind, or forgotten.

— Lilo & Stitch

Dedicated to the loving memory of Rudolf Miede.

$1939 - 2005$

ABSTRACT

Short summary of the contents in English. . . a great guide by Kent Beck how to write good abstracts can be found here:

https://plg.uwaterloo.ca/~migod/research/beckOOPSLA.html

ZUSAMMENFASSUNG

Kurze Zusammenfassung des Inhaltes in deutscher Sprache. . .

ACKNOWLEDGMENTS

Put your acknowledgments here.

CONTENTS

LIST OF TABLES

LISTINGS

ACRONYMS

INTRODUCTION

1

A NEAR-INFRARED SPECTROSCOPIC DATABASE OF HIGH-REDSHIFT QUASARS

Super-massive black holes (BHs) are found at the centres of most nearby massive galaxies and the BH mass and mass of the host galaxy spheroid are strongly correlated (Ferrarese and Merritt, 2000; Gebhardt et al., 2000; Kormendy and Ho, 2013). Although any underlying causal mechanism(s) responsible for the correlation is yet to be conclusively identified, there is considerable observational and theoretical support for models that involve BH-fuelling, outflows and a 'feedback' relationship (e.g. King and Pounds, 2015). The number density of quasars, which evolves strongly with redshift, peaks at redshifts $2 \lesssim z \lesssim 3$ (e.g. Brandt and Hasinger, 2005; Richards et al., 2006b) and the most massive ($M_{BH} \gtrsim 10^9 M_\odot$) present-day BHs experienced much of their growth during this epoch. The star formation rate, which closely follows the cosmological evolution of the quasar luminosity function, also peaks during this epoch (e.g. Boyle and Terlevich, 1998). Quantifying the growth-rate of massive BHs at $2 \lesssim z \lesssim 3$ would therefore help significantly in understanding the role quasars play in galaxy evolution.

Reliable estimates of BH masses are a prerequisite for investigating the relationship between BHs and their host galaxies. If the line-emitting clouds in the broad line region (BLR) are assumed to be virialized and moving in a potential dominated by the central BH, then the BH mass is simply a product of the BLR size and the square of the virial velocity. The reverberation-mapping technique uses the time lag between variations in the continuum emission and correlated variations in the broad line emission to measure the typical size of the BLR (Peterson, 1993; Peterson, 2014). The full width at half maximum (FWHM) or dispersion (σ; derived from the second moment) velocity of the prominent broad emission line of Hβ (4862.7Å)[1] is used as an indicator of the virial velocity, with extensions to other low-ionization emission lines such as Hα (6564.6Å) and Mg II - - 2796.4,2803.5 (e.g. Vestergaard, 2002; McLure and Jarvis, 2002; Wu et al., 2004; Kollmeier et al., 2006; Onken and Kollmeier, 2008; Wang et al., 2009; Rafiee and Hall, 2011). Extensive reverberation mapping campaigns have provided accurate BH masses for ~50 active galactic nuclei (AGN) at relatively low redshifts and of modest luminosity (e.g. Kaspi et al., 2000; Kaspi et al., 2007; Peterson et al., 2004; Bentz et al., 2009; Denney et al., 2010).

---

1 Vacuum wavelengths are employed throughout the thesis.

Reverberation mapping campaigns have also revealed a tight relationship between the radius of the BLR and the quasar optical (or ultraviolet) luminosity (the $R - L$ relation; e.g. Kaspi et al., 2000; Kaspi et al., 2007). This relation provides a much less expensive method of measuring the BLR radius, and large-scale studies of AGN and quasar demographics have thus become possible through the calibration of single-epoch virial-mass estimators using the reverberation-derived BH masses (e.g. Greene and Ho, 2005; Vestergaard and Peterson, 2006; Vestergaard and Osmer, 2009; Shen et al., 2011; Shen and Liu, 2012; Trakhtenbrot and Netzer, 2012). The uncertainties in reverberation mapped BH masses are estimated to be ~ 0.4 dex (e.g. Peterson, 2010), and the uncertainties in virial masses are similar (e.g. Vestergaard and Peterson, 2006). Since the structure and geometry of the BLR is unknown, a virial coefficient f is introduced to transform the observed line-of-sight velocity inferred from the line width in to a virial velocity. This simplification accounts for a significant part of the uncertainty in virial BH masses (in addition to, for example, describing the BLR with a single radius R and scatter in the $R - L$ relation; Shen, 2013). Furthermore, if the BLR is anisotropic (for example, in a flattened disk; e.g. Jarvis and McLure, 2006) then the line width will be orientation-dependent (e.g. Runnoe et al., 2013b; Shen and Ho, 2014; Brotherton et al., 2015).

At redshifts of $z \gtrsim 2.0$ the low-ionization hydrogen and Mg II emission lines are no longer present in the optical spectra of quasars and it is necessary to employ an emission line in the rest-frame ultraviolet. The strong C IV - - 1548.2,1550.8 emission doublet is visible in the optical spectra of quasars to redshifts of $z \sim 5$ and C IV-derived BH masses have become the standard (e.g. Vestergaard and Peterson, 2006; Park et al., 2013) for both individual quasars and in studies of quasar population demographics.

The luminosities of quasars at redshifts $z \gtrsim 2$ are much greater than the majority of AGN at lower redshifts for which reverberation mapping results are available. Therefore, the reliability of the existing calibration involving C IV FWHM velocity measurements and ultraviolet luminosity is not established definitively when extrapolating to high-redshifts and luminosities. While some authors have found good agreement between BH mass-estimates based on C IV and Hβ (e.g. Vestergaard and Peterson, 2006; Assef et al., 2011; Tilton and Shull, 2013), others have questioned the consistency (e.g. Baskin and Laor, 2005a; Trakhtenbrot and Netzer, 2012; Shen and Liu, 2012).

Denney, (2012) presented evidence that the interpretation of the FWHM velocity of the C IV-emission being due primarily to virial motions within the quasar BLR requires care. Specifically, both a low-velocity core component and a blue excess to the C IV-emission, both of which do not reverberate, can be present and Denney, (2012) pro-

poses that a contribution from an accretion disc wind or from a more distant narrow emission line region is important.

Certainly, in contrast to the hydrogen Balmer lines and Mg II, the C IV emission line in quasar spectra exhibits a broad range of line shapes, including significant asymmetry, with shifts of the line-centroid to the blue ('blueshifts') of up to several thousand $km\,s^{-1}$ (Richards et al., 2002; Baskin and Laor, 2005a; Sulentic et al., 2006). Shen and Liu, (2012) found, using a sample of 60 luminous quasars, that the scatter between the FWHM of C IV and Hβ was correlated with the blueshift of C IV relative to Hβ. Shen et al., (2008) found a similar result by comparing C IV with Mg II for quasars from SDSS DR5. The blueshifting of C IV is usually interpreted as evidence for strong outflows (e.g. Sulentic et al., 2007; Richards et al., 2011) which, most likely, result from the presence of a radiation line-driven accretion-disc wind (e.g. Konigl and Kartje, 1994; Murray et al., 1995; Proga, Stone, and Kallman, 2000; Everett, 2005; Gallagher et al., 2015). In this picture, the non-virial wind component makes a significant contribution to the observed C IV-emission FWHM in quasars with large C IV blueshifts ('wind-dominated quasars') and hence increases the inferred BH masses. A primary goal of this chapter is to present the full range of C IV-emission line blueshifts present among high-luminosity quasars at redshifts $z \sim 2.5$ and investigate potential systematic trends in the derived C IV-based BH masses as a function of blueshift.

Changes in the C IV blueshift and equivalent width are correlated with changes in the velocity widths and strengths of other optical and ultra-violet emission lines. In the spectra of lower-redshift AGN, the FWHM of the broad Hβ emission line and the relative strengths of optical Fe II and Hβ have been identified as the features responsible for the largest variance in the population. These parameters form part of 'Eigenvector 1' (EV1), the first eigenvector in a principal component analysis which originated from the work of Boroson and Green, (1992). The underlying driver behind EV1 is thought to be the Eddington ratio (e.g. Sulentic et al., 2000; Shen and Ho, 2014). Sulentic et al., (2000) proposed a two-population model to classify AGN by their EV1 properties. In this scheme AGN with FWHM(Hβ) < 4000 $km\,s^{-1}$ and FWHM(Hβ) > 4000 $km\,s^{-1}$ are classified as population A and B objects respectively, although there is a continuous distribution of parameter values across this divide. Sulentic et al., (2007) added a measure of the C IV asymmetry to EV1, and found a strong association between blue-asymmetry and their population A quasars.

Denney, (2012) found the level of contamination in single-epoch spectra from non-reverberating gas to be correlated with the shape (FWHM/σ) of the C IV profile. Runnoe et al., (2013a) found the scatter between the C IV and Hβ line widths to be correlated with the continuum-subtracted peak flux ratio of the ultraviolet emission-line blend of Si IV+O IV (at 1400 Å) to that of C IV. Both authors used these

correlations to propose empirical corrections to the C IV line width which can improve the consistency between C IV and Hβ-based virial BH mass estimates. In fact, the shape, peak flux relative to the 1400 Å blend, and blueshift of C IV all correlate with one another and with other parameters in EV1. Therefore, EV1 provides a useful context for understanding systematic trends in C IV velocity widths, and hence virial BH masses.

Currently, the number of reverberation mapped quasars is both small (~50 quasars; Park et al., 2013) and, as highlighted by Richards et al., (2011), includes a restricted range of the C IV emission line shapes seen in the quasar population. In particular, the reverberation mapped objects generally possess high C IV equivalent widths and low C IV-blueshifts. Nevertheless, the derived scaling relations based on the reverberation-mapped sample are regularly applied to the quasar population with low C IV EWs and/or large C IV-blueshifts, where any non-virial outflow-related contribution to the dynamics is significant. Much more complete coverage of the C IV-emission properties within the population of luminous quasars will come from the new SDSS-IV reverberation mapping project (Shen et al., 2015) but, for now, additional direct comparison of C IV-emission and low-ionization emission-line properties in the same quasars offers a way forward.

Near-infrared spectra, including the Hα emission line, for a sample of 19 quasars, at redshifts $2.0 < z < 2.7$, have been obtained to complement existing SDSS optical spectra covering the C IV emission line. The 19 quasars were chosen to include a broad range of C IV line blueshifts. Our aim is to directly test the reliability of C IV-based BH mass estimates at high redshift for objects with a diverse range of C IV-line shapes. In particular, we will investigate potential systematic effects on the C IV-emission based BH masses for quasars with large, $\gtrsim 1200 \mathrm{km\,s^{-1}}$, C IV blueshifts, using the properties of the Hα emission line to provide BH-mass estimates for the objects unbiased by non-virial contributions to the emission-line profile. Examining higher redshifts, our work complements other studies which attempt to improve the reliability of BH mass estimates which use the C IV line (e.g. Runnoe et al., 2013a; Denney, 2012). However, the range of C IV blueshifts in our sample is significantly more extended, which will allow us to study systematic biases in C IV-based virial BH masses more directly, i.e. as a function of the C IV blueshift. Established relations to derive BH masses from emission-line properties are employed but an advantage of our approach is that C IV and Hα can be directly compared as a function of C IV-emission line shape.

Throughout this thesis we adopt a ΛCDM cosmology with $h_0 = 0.71$, $\Omega_M = 0.27$, and $\Omega_\Lambda = 0.73$. All wavelengths and equivalent width measurements are given in the quasar rest-frame, and all emission line wavelengths are given as measured in vacuum.

SAMPLE SELECTION FOR LIRIS/NTT PROGRAM

The parent sample for our investigation is the spectroscopic quasar catalogue of the Sloan Digital Sky Survey (SDSS; York et al., 2000) Seventh Data Release (DR7; Schneider et al., 2010). The SDSS DR7 catalogue contains moderate resolution $\sim 3800 - 9180$Å spectra for 105,783 quasars. Shen et al., (2011) have compiled a catalogue of properties for the SDSS DR7 quasars including, at $z > 1.5$, measurements of the broad C IV--1548.2,1550.8 emission line. Our aim is to explore the relationship between the Hα and C IV emission-line properties over the full dynamic range in C IV-emission shapes, with particular emphasis on quasars possessing large C IV-blueshifts (see Section 2.2). The sample was restricted to objects with redshifts $2.14 < z < 2.51$ (7,258 quasars), to ensure that the Hβ and Hα emission lines fall within the H- and K-bands respectively, allowing us to observe both simultaneously with the appropriate grism configuration. Given the limited number of quasars for which near-infrared spectra could be obtained, the quasar sample was further restricted to objects that are radio-quiet (5,980 quasars), show no evidence of broad absorption lines (BALs) in their spectra (5,299 quasars), and are free from significant dust extinction. We removed radio-loud objects from our sample using the same radio-loud classification as Shen et al., (2011), and BAL quasars using the classifications of both Shen et al., (2011) and Allen et al., (2011). The removal of quasars with significant dust extinction was achieved by identifying quasars with $i - K$ colours redder than a parametric spectral energy distributions (SED) model + SMC-like extinction curve with $E(B - V)$=0.05 (see Maddox et al., 2012). The K-magnitude was taken from the UKIRT Infrared Deep Sky Survey (UKIDSS; Lawrence et al., 2007) Large Area Survey (ULAS). The requirement to be in the ULAS footprint and have reliable K band photometry reduced our sample of possible targets to 1,683, and the $E(B - V)$ cut left 1,204 in our sample. Finally, a flux-limit of K < 18.5 (AB) was applied to ensure that spectra of sufficient signal-to-noise ratio (S/N) could be obtained (412 quasars).

We were able to obtain new infra-red spectra for 19 quasars from this sample of 412 possible targets (Section 2.3). The quasars included in this sub-sample were selected to have C IV-emission shapes which span the full range observed in the population. Reliably quantifying the distribution of C IV-emission shapes has been made possible thanks to redshift-determination algorithms (Hewett and Wild, 2010, Allen & Hewett 2016, in preparation) which are independent of the C IV-emission shape. Calculation of the C IV emission line parameters is described in detail in the next section.

C IV BLUESHIFTS IN THE QUASAR POPULATION

Recognition that the C IV emission line in quasars can exhibit significant asymmetric structure, with an excess of flux to the blue of the predicted rest-frame transition wavelength, extends back to Gaskell, (1982). Significant progress in understanding the relationship between changes in C IV-emission shape and quasar properties has come about through studies in which near-infrared spectra of the hydrogen Balmer lines have been obtained. Such studies typically involve samples of modest size and the location of the Balmer lines provides a reliable estimate of the quasar systemic redshifts; recent examples include Shen and Liu, (2012) and Marziani et al., (2016). In Section 2.4 we adopt the same approach to estimate systemic redshifts for the quasar sample presented here with near-infrared spectra. However, improvements in the estimation of systemic redshifts from ultraviolet quasar spectra means that it is now possible to quantify the distribution of C IV-blueshifts in the observed quasar population as a whole.

Quasar systemic redshifts

Historically, the parametrisation of the C IV emission-line properties for quasars in large surveys has not proved straightforward because the C IV emission line has itself been used in the determination of the quasar redshifts. The SDSS provided the first catalogue of tens of thousands of redshift $z >1.6$ quasars with spectra of adequate velocity resolution and S/N that effective statistical studies of the rest-frame ultraviolet emission-line properties, including line-shape, have proved possible.

The comprehensive compilation of quasar properties for the SDSS DR7 quasars by Shen et al., (2011) provides a natural starting point for population studies. In Fig. 21a we plot the C IV-blueshift versus C IV-emission equivalent width (EW) using the SDSS pipeline redshifts and the blueshifts calculated by Shen et al., (2011). The grey points show all SDSS DR7 quasars for which measurements exist and the orange circles show the 19 quasars with near-infrared spectra presented in this paper. A strong trend in the blueshift values as a function of line EW is not evident in Fig. 21; structure in the parameter space is being masked because the C IV emission line is itself being used in the determination of the quasar redshifts.

The redshift-determination scheme of Hewett and Wild, (2010) provided much improved redshifts, not least because the redshift estimates for the majority of quasars were derived using emission-lines other than the C IV-line itself. Figure 21b shows SDSS DR7 quasars in the same C IV parameter space as Figure 21a, but now using Hewett and Wild, (2010) redshifts. The improved redshift estimates are predominantly responsible for the differences seen in Fig. 21a and b; the
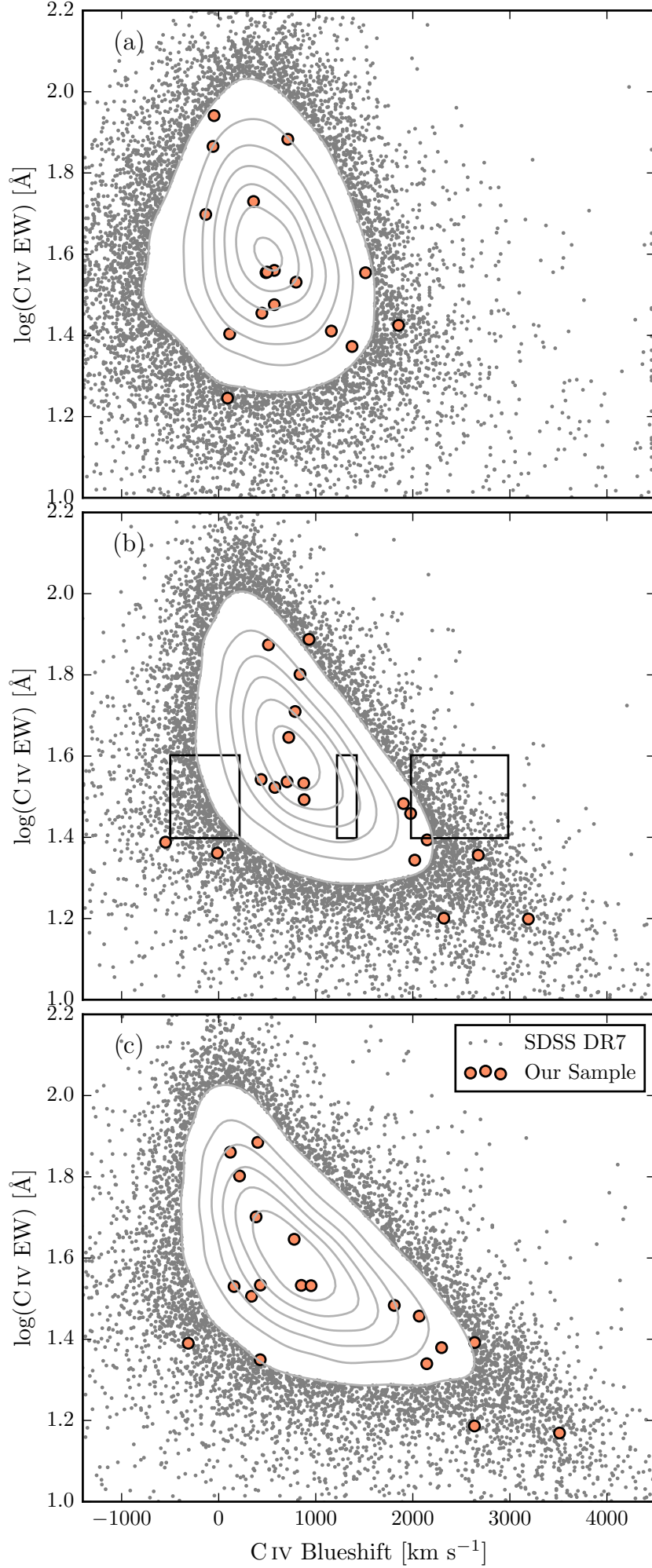
appearance in Fig. 21b of the extension to high blueshift for quasars with low C IV EW is particularly evident.

The large systematic variation in the C IV emission-line profile within the population is evident from figures 11 and 12 of Richards et al., (2011). The plots and analysis in Richards et al., (2011) employ the quasar redshifts from Hewett and Wild, (2010) but, as is evident from the figures, the systematic variation in the C IV shape is correlated with changes in the quasar SEDs, including the strengths of the Si IIIλ1892 and C IIIλ1908 emission lines in the rest-frame ultraviolet. As a consequence, the redshifts from Hewett and Wild, (2010) still suffer from systematic errors that are correlated with the shape, and particularly the blueshift, of the C IV emission line. The nature of the systematic variations in the quasar ultraviolet SEDs are such that for quasars with close-to symmetric C IV profiles and line centroids close to the systemic redshift, the Hewett and Wild, (2010) redshifts result in C IV blueshifts that are overestimated by a few hundred $\mathrm{km\,s^{-1}}$, whereas, for quasars with strong blue-asymmetric C IV profiles and line centroids displaced significantly to the blue of the systemic redshift, the C IV blueshifts are underestimated by, in the most extreme cases, up to 1200$\mathrm{km\,s^{-1}}$.

Figure 21c shows the C IV emission line parameters calculated using a new redshift-estimation algorithm (Allen & Hewett 2016, in preparation) that takes account of the quasar SED variations, producing redshifts independent of the large systematic shape changes seen in the C IV emission line. The low-ionization emission lines visible in the rest-frame ultraviolet (over wavelengths from Mg II$\lambda\lambda$2796,2803 down to the O Iλ1304+Si IIλ1307 blend) using the new redshift-algorithm are located at rest-frame wavelengths in excellent agreement with the systemic redshift defined using the rest-frame narrow-line optical O III$\lambda\lambda$4960,5008 and broad-line Hβ and Hα.

The systematic trends seen in Fig. 21b, in particular the extension to high blueshift at low C IV EW, become more apparent in Fig. 21c, as expected from consideration of the known SED-related errors in the redshifts from Hewett and Wild, (2010). A population of quasars with only modest blueshifts and low EW is also apparently still present.

C IV emission line blueshift measurements

The differences in the distribution of C IV emission line properties seen in the three panels of Fig. 21 are due primarily to the change in the systemic redshift estimates. It is also necessary, however, to obtain a measure of the C IV emission line 'location' in order to calculate the blueshifts. When working with moderately-sized samples, parametric fits to the emission-line profile may be undertaken using careful mask-definition to minimise the effect of absorption features on the profiles used for the parametrization, and this is the approach

we follow below in Section 2.4. Effective analysis of the tens of thousands of spectra from SDSS DR7, and now DR12, however, requires a more robust scheme to determine a C IV-blueshift estimate that is not very sensitive to the range of S/N among the spectra or the presence of narrow absorption systems within the C IV-emission profile. Shen et al., (2011) provide a discussion (their section 3) of the factors that effect the measurement of broad emission lines in quasar spectra of modest S/N. Their careful analysis of the C IV emission properties employed the results of parametric fits of three Gaussians to the spectra. Our own experiments in quantifying the C IV emission properties of SDSS spectra showed that a simple non-parametric measure of the C IV emission location reduced the number of outliers significantly. Visual inspection of spectra demonstrated that the improvement is due primarily to the identification of, and interpolation over, associated and outflow absorption systems, which forms part of the non-parametric measurement scheme.

We therefore chose to use a non-parametric scheme to measure the blueshift of the C IV line, which we will now describe. A continuum is first defined as a power-law of wavelength, $f(\lambda) \propto \lambda^{-\alpha}$, with the slope, α, determined using the median[2] values of the flux in two continuum windows at 1445–1465 and 1700–1705Å (the same wavelengths as adopted by Shen et al., (2011)). The C IV emission line is taken to lie within the wavelength interval 1500-1600Å, a recipe that is commonly adopted (e.g. Shen et al., 2011; Denney et al., 2013). To reduce the impact of narrow absorption systems on the emission-line profile a 'pseudo continuum' is defined by applying a 41-pixel median filter to the quasar spectrum. Pixels within the C IV profile that lie more than 2σ below the pseudo-continuum are deemed to be affected by absorption and added to an 'absorber'-mask. Two pixels on either side of each such pixel are also included in the mask. For each masked pixel, the flux values in the spectrum are replaced by values from the pseudo-continuum.

The wavelength that bisects the cumulative total line flux, λ_{half}, is recorded and the blueshift (in $km\,s^{-1}$) defined as $c\times(1549.48-\lambda_{half})/1549.48$ where c is the velocity of light and 1549.48Å is the rest-frame wavelength for the C IV doublet[3]. Positive blueshift values indicate an excess of emitting material moving towards the observer and hence outflowing from the quasar. Hewett and Wild, (2010) redshifts are used to define the quasar rest-frame.

---

2 The median is used to improve the robustness of the continuum estimate from the relatively small wavelength intervals.

3 The adopted C IV rest-frame wavelength assumes an optically thick BLR, in which case the contribution from each component is equal. Adopting a 2:1 ratio (appropriate for an optically thin BLR) changes the blueshifts by $\sim 80km\,s^{-1}$.

Sample selection - C IV properties

The primary aim of the paper is to investigate the potential systematic effects on the C IV-emission based BH masses for quasars with large, $\gtrsim$1200km s^{-1}, C IV blueshifts, using the properties of the Hα emission line to provide BH-mass estimates for the objects unbiased by non-virial contributions to the emission-line profile. The orange symbols in Fig. 21 show the C IV parameters of our quasar targets for which near-infrared spectra of adequate S/N were obtained. These quasars were selected using our non-parametric blueshift measures (based on the Hewett and Wild, (2010) redshifts). The sample of 19 quasars spans the full dynamic range in C IV-parameters based on the Hewett and Wild, (2010) systemic redshifts and the coverage is in fact even more complete when using the forthcoming SED-independent redshifts from Allen & Hewett (2016, in preparation). As is evident from the sparsity of quasars with large C IV blueshifts when the SDSS pipeline systemic redshifts are used (Fig. 21a), improvements in the estimation of systemic redshifts from ultraviolet spectra have been a crucial factor in allowing us to reliably select a sample of quasars with a range of C IV blueshifts. In subsequent sections we re-derive the systemic redshifts and C IV blueshifts for this sample using parametric fits to the Hα and C IV emission (the former from our-near infrared observations). Thus, while the systematic trends in BH masses inferred from measurements of the C IV emission line depend on the distribution of C IV emission line properties within the quasar population, the results of our analysis of the Hα and C IV emission line properties are independent of the redshifts used to produce the panels in Fig. 21.

Relation to virial BH mass estimates

In general, researchers studying quasar demographics at high-redshift adopt estimates of BH masses based on the width of C IV-emission, without reference to the blueshift of the C IV-emission (e.g. Vestergaard, 2004; Kollmeier et al., 2006; Gavignaud et al., 2008; Vestergaard et al., 2008; Vestergaard and Osmer, 2009; Kelly et al., 2010; Kelly and Shen, 2013). The systemic redshift is often assumed to be given by the peak of the C IV emission, regardless of whether there is evidence that the line is shifted or not. Figure 2 shows the shape of the C IV-emission in composite spectra constructed from SDSS DR7 quasars with EW(C IV)=25-40Å, as a function of C IV blueshift. Quasars classified as BALs, or possessing strong associated absorbers have been excluded, and the composite-spectra shown are derived using an arithmetic mean of a minimum of 200 spectra at each blueshift. The blueshifts and EWs of the quasars contributing to each of the composites are indicated by the boxes in Fig. 21b. The profiles show how, at
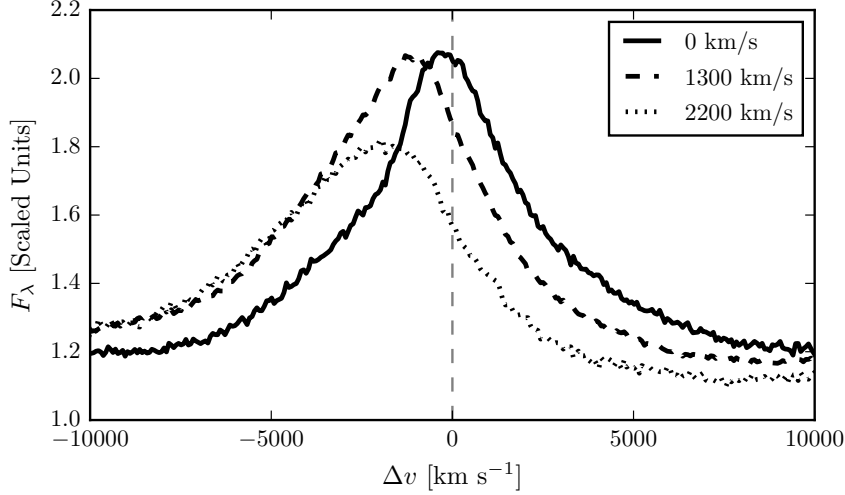
Figure 2: Composite spectra of the C IV-emission line as a function of C IV blueshift for SDSS DR7 quasars. The quasars contributing to each composite are indicated in Fig. 21b. Virtually the entire C IV-profile appears to shift blueward and the change in line shape is not simply an enhancement of flux in the blue wing of a still identifiable symmetric component. In order of increasing C IV blueshift, the composite spectra have FWHM 4870, 5610, and 6770 $km\,s^{-1}$ and EW 33.1, 31.6, and 28.8 Å.

large values of blueshift ($\gtrsim$2000$km\,s^{-1}$) the C IV-profile is displaced to the blue by amounts comparable to the FWHM of the profile.

A possible origin of the blueshifts is the presence of a disc-wind (see Gallagher et al., 2015; Higginbottom and Proga, 2015, for recent papers) but, irrespective of the physical origin of the high-blueshift C IV-profiles, measures of the emission-line 'width' do not relate simply to virialized motions of the emitting gas under the gravitational influence of the BH. On the other hand, Denney et al., (2013) point out that any radiatively driven wind will have a velocity comparable to the escape velocity, i.e. approximately twice the virial velocity. Even if dominated by an outflow component, the C IV line width might therefore still be expected to relate to the BH mass.

OBSERVATIONS

Near-infrared spectra were obtained with the Long-slit Intermediate Resolution Infrared Spectrograph (LIRIS) mounted on the 4.2m William Herschel Telescope (WHT) at the Observatorio del Roque de los Muchachos (La Palma, Spain). Observations took place over four non-contiguous nights from 2015 March 31 to April 4. Approximately one night was lost due to poor weather and a further half-night was affected by poor transparency due to cloud. A one arc-

Table 1: Summary of near-infrared spectroscopic observations with LIRIS.

SDSS Name	SDSS DR	z^a	i_{SDSS}	UTC Date	T_{exp} (s)	S/N(C IV)^b	S/
073813.19+271038.1	DR12	2.4508	18.80	2015-04-01	720	29.13	
074352.61+245743.6	DR12	2.1659	19.09	2015-04-04	2160	8.64	
080651.54+245526.3	DR12	2.1594	18.91	2015-04-01	1200	10.37	
085437.59+031734.8	DR7	2.2504	18.41	2015-03-31	2520	26.58	
085856.00+015219.4	DR12	2.1675	17.62	2015-04-04	1800	66.16	
110454.73+095714.8	DR12	2.4238	19.12	2015-04-03	1440	19.41	
123611.21+112921.6	DR12	2.1527	18.53	2015-04-04	1680	35.24	
124602.04+042658.4	DR12	2.4473	18.49	2015-04-01	960	35.34	
130618.60+151017.9	DR12	2.4020	19.00	2015-04-05	840	29.83	
131749.78+080616.2	DR12	2.3791	19.04	2015-04-05	2880	19.25	
132948.73+324124.4	DR12	2.1684	18.40	2015-04-01	2520	32.58	
133646.87+144334.2	DR7	2.1422	18.84	2015-04-01	1200	15.2	
133916.88+151507.6	DR12	2.3157	18.52	2015-04-03	2880	20.52	
140047.45+120504.6	DR12	2.1722	18.29	2015-04-02	840	36.64	
152529.17+292813.2	DR12	2.3605	17.52	2015-04-04	1440	80.55	
153027.37+062330.8	DR12	2.2198	18.62	2015-04-04	1800	29.9	
153848.64+023341.1	DR12	2.2419	17.56	2015-04-01	2520	64.82	
161842.44+234131.7	DR7	2.2824	18.49	2015-04-04	1320	23.37	
163456.15+301437.8	DR12	2.4901	18.29	2015-04-01	1920	36.06	

a From Hewett and Wild, (2010).
b Measured in the continuum and quoted per resolution element.

second slit-width was employed and the LIRIS H + K low-resolution grism was selected, which covers the spectral ranges 1.53–1.79 μm and 2.07–2.44 μm with a dispersion of 9.7Å/pixel. The spatial scale of the instrument is 0.25 arcsec/pixel. Observations were divided into 60 s sub-exposures and performed in an ABBA nodding pattern, with the object placed at two positions along the slit 12 arcsec apart. Bright A0-5V stars were observed at similar air-masses to the targets in order to provide both telluric absorption corrections and a flux calibration of the quasar spectra.

The raw LIRIS data frames incorporate a known 'pixel shift' which was first removed from all frames using the LIRIS data reduction package LIRISDR. Subsequent data reduction was undertaken with standard IRAF[4] procedures. The flat-field images, which were taken at the beginning of each night via illumination of the dome, were averaged and normalised to remove any wavelength-dependent signature. Each individual two-dimensional spectrum was then flat-field corrected. Consecutive AB and BA pairs of two-dimensional spectra were subtracted to remove the sky background. All the subtracted AB/BA-pairs for a target were then averaged to give the final two-dimensional spectrum.

The size of the one-dimensional spectrum extraction windows, in the slit direction, varied from 6-10 pixels. To increase the S/N, optimal variance-weighted extraction with sigma clipping was employed. For the fainter objects in our sample we were unable to trace the spectrum across the dispersion axis reliably and the trace from a telluric standard-star observation, observed at a similar air mass and time, was used instead. The wavelength calibration, using argon and xenon lamp exposures, resulted in root mean square errors in the range 1.01–1.71 Å, with a mean of 1.47Å. The telluric standard star observations were reduced using the same steps described above. The stellar continuum was divided out of the standard star spectrum, which was then divided into the quasar spectrum to remove telluric absorption features. The spectral type and magnitude of the standard star were used to flux calibrate the quasar spectrum both in a relative and absolute sense. Variable atmospheric conditions combined with the narrow slit width resulted in a significant level of uncertainty in the absolute flux calibration for the quasar observations. The use of the UKIDSS broadband magnitudes (H and K) to normalise the spectra results in a significantly improved calibration.

Spectra with sufficient S/N for analysis of the Hα emission line properties were obtained for a total of 19 quasars. Sixteen of the 19 quasars have been re-observed in the Sloan Digital Sky Survey-III: Baryon Oscillation Spectroscopic Survey (SDSS-III/BOSS; Dawson et

---

4 IRAF is distributed by the National Optical Astronomy Observatory, which is operated by the Association of Universities for Research in Astronomy (AURA) under a cooperative agreement with the National Science Foundation.
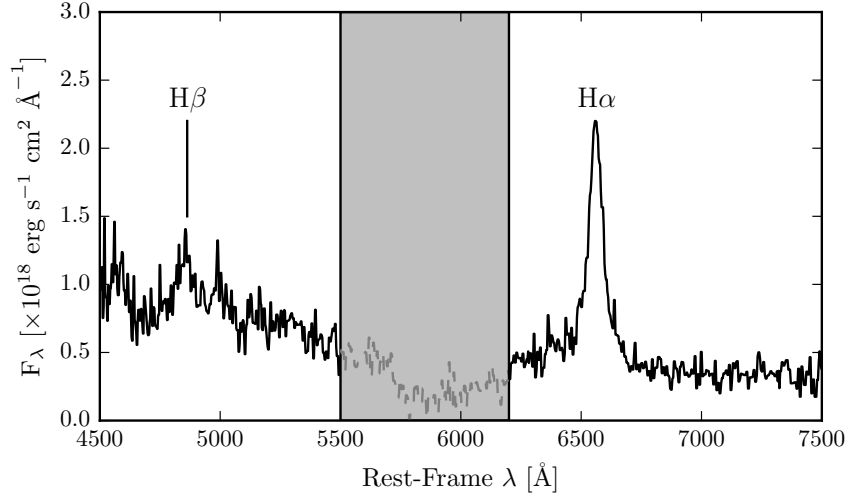
Figure 3: LIRIS spectrum of SDSSJ1246+0426. The gap between the H and K bands (~5500-6300 Å) has been greyed-out.

al., 2013) and the spectra are available in the SDSS DR12 quasar catalogue (Pâris et al., 2017). As the BOSS-spectra have higher S/N compared to those in DR7, we have used the BOSS spectra when available. A typical reduced LIRIS spectrum is shown in Fig. 3. A log of the observations, the quasar positions, magnitudes and redshifts, along with the S/N achieved for the Hβ, Hα and C IV emission line regions (the last from the optical SDSS/BOSS spectra) are listed in Table 1. The S/N, which is given per resolution element, was measured in the continuum in the region around the emission lines. The full SDSS name is given in Table 1; in the subsequent tables and text we will refer to objects using an abbreviated name of the form SDSSJHHMM+DDMM.

Although the S/N is similar in the continuum regions adjacent to the Hα and Hβ emission lines, in practice the much lower EW of Hβ compared to Hα meant that both parametric and non-parametric characterisation of the emission-line parameters did not produce results that could be used in this investigation. The individual Hβ profiles were thus not employed, although a composite spectrum of the Hβ region is used below.

EMISSION LINE MEASUREMENTS

Virial BH mass estimators are calibrated using either the FWHM or dispersion (σ; derived from the second-moment velocity) of a broad emission line (e.g. Vestergaard and Peterson, 2006; Park et al., 2013). Complications which are encountered when measuring line widths include how to model the 'continuum' flux, where to define the limits of the line emission, and how to deal with absorption. All of these

issues are exacerbated when working with low S/N data (see Denney et al., 2013, for a discussion). In Section 2.2.2 we measured the blueshift of C IV for tens of thousands of SDSS DR7 quasar spectra. This allowed us to quantify the distribution of C IV blueshift values and hence select a subset for near-infrared observations which have C IV blueshifts spanning the full range of this distribution (Fig. 21). A non-parametric scheme was employed because, in comparison to recipes involving the fitting of multiple Gaussian (or other parametric) profiles, it was found to be more robust and less sensitive to the range of S/N among the spectra and to the presence of narrow absorption systems within the C IV-emission profile. In this section we will use a different approach, and measure the line properties by fitting a parametric model to the data. When working with a small number of spectra, it is possible to use careful mask-definition to minimise the effect of absorption features on the profiles used for the parametrization. The purpose of the model fits is purely to best represent the intrinsic line profile, and no physical meaning is attached to the individual model components. We will now describe the parametric model and fitting procedure used for each emission line. The models were fit using a standard variance-weighted least squares minimisation procedure employing the Levenberg-Marquardt algorithm. Prior to the fit, the spectra were visually inspected and regions significantly affected by absorption were masked and excluded.

C IV

We first measure and subtract the local continuum emission, by fitting a power-law to two windows on either side of the line emission, as described in Section 2.2.2. For a small number of objects, absorption features, or artefacts, in the spectrum necessitated modest adjustments to the window extents, which are specified in Table 2. The continuum-subtracted spectra are then transformed from wavelength units into units of velocity relative to the rest-frame line-transition wavelength for the C IV doublet (1549.48Å, assuming equal contributions from both components). The parametric model is ordinarily fit within the same 1500–1600 Å window used in Section 2.2.2, which corresponds to approximately $\pm 10\,000$ km s^{-1} from the rest-frame transition wavelength. The line-window was extended if significant flux in the profile was present blueward of the short wavelength limit. The adopted line-fitting windows, in units of velocity from the rest-frame transition wavelength, are given in Table 2.

To fit the C IV profile we employed Gauss-Hermite (GH) polynomials, using the normalisation of van der Marel and Franx, (1993) and the functional forms of Cappellari et al., (2002). We allowed up to six components in the GH polynomial model, but in many cases a lower order was sufficient; the polynomial order used for each line

Table 2: Summary of the fitting regions and the parameters of the models used to fit the C IV and Hα emission lines.

| | Fitting Region [km s^{-1}] | | Continuum Region[Å] | |
Name	C IV	Hα	C IV	Hα
0738+2710	-9570,9770	-7530,10740	1445-1465, 1700-1705	6000-6250, 6800-7000
0743+2457	-9570,9770	-7530,10740	1445-1465, 1700-1705	6004-6210, 6800-7000
0806+2455	-9570,9770	-9219,10759	1445-1465, 1700-1705	6000-6250, 6800-7000
0854+0317	-9570,9770	-7530,10740	1445-1465, 1700-1705	5989-6135, 6800-7000
0858+0152	-20000,7400	-7530,10740	1423-1428, 1700-1705	6000-6200, 6800-7000
1104+0957	-9570,9770	-7530,10740	1445-1465, 1700-1705	6000-6250, 6801-6845
1236+1129	-15363,7650	-8904,10590	1445-1465, 1700-1705	6063-6210, 6800-7000
1246+0426	-9570,9770	-7530,10740	1445-1465, 1700-1705	6000-6250, 6799-6906
1306+1510	-13000,7800	-7530,10740	1445-1465, 1700-1705	6000-6250, 6800-7000
1317+0806	-9198,9755	-7530,10740	1445-1465, 1700-1705	6000-6250, 6800-7000
1329+3241	-12000,9000	-7605,7406	1445-1461, 1700-1705	6000-6250, 6800-7000
1336+1443	-14000,10000	-10131,10674	1445-1465, 1700-1705	6000-6250, 6800-7000
1339+1515	-12000,11000	-7530,10740	1445-1465, 1700-1705	6046-6250, 6800-7000
1400+1205	-15000,10000	-2000,10815	1445-1465, 1700-1705	6000-6250, 6800-7000
1525+2928	-9570,9770	-7586,8080	1459-1466, 1700-1705	6055-6251, 6800-7000
1530+0623	-12000,10000	-7530,10740	1445-1465, 1700-1705	6127-6186, 6800-7000
1538+0233	-13500,9000	-7530,10740	1450-1465, 1700-1705	6000-6250, 6855-7002
1618+2341	-9190,9770	-7530,10740	1445-1465, 1689-1697	6000-6250, 6800-7000
1634+3014	-9570,9770	-8400,8500	1445-1465, 1700-1705	6000-6250, 6736-6779
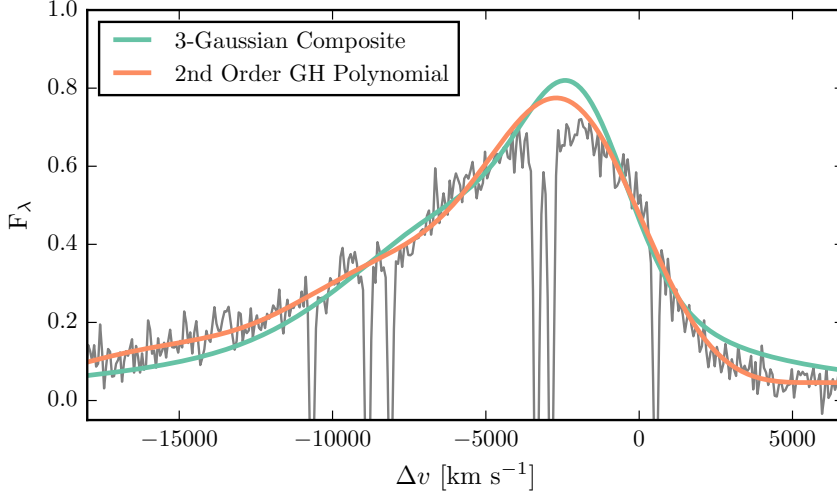
Figure 4: 2nd-order Gauss-Hermite (GH) polynomial and 3-component Gaussian fit to the C IV-emission line of SDSSJ0858+0152, which is the most blueshifted in our sample. We derive line parameters from the GH polynomial fit; using the Gaussian model changes the FWHM, line dispersion, and blueshift by -250, -150, and 500 $km\,s^{-1}$ respectively. For the C IV lines of all other quasars in our sample the GH polynomial and Gaussian models provide equally good fits.

is given in Table 2. It is also a common practice to fit the C IV emission profile with two or three Gaussian components (e.g. Shen et al., 2011). We opted to use a GH-polynomial model primarily because it provided a significantly better fit to the most blueshifted and asymmetric C IV line (in SDSSJ0858+0152). Figure 4 shows how a model with three Gaussian components underestimates the flux in the blue wing and overestimates the flux in the red wing of the line profile. Using the Gaussian model rather than the GH polynomial changes the FWHM, line dispersion, and blueshift by -3, -3, and 10 per cent respectively. We have highlighted SDSSJ0858+0152 because, of all the objects in our sample, the choice of model leads to the largest change in C IV line parameters. Even in this case, however, the differences are modest.

For every other C IV line in our sample we found only marginal differences in our best-fit line parameters when, rather than using a GH polynomial model, the C IV emission was fit using a composite model of up to three Gaussians. Our best-fit parameters are also in good agreement with Shen et al., (2011), who employ a multi-Gaussian parametrization[5]. The scatter between the Shen et al., (2011) results and our own is 0.1 dex about the one-to-one relation and, as expected, is larger for lines with smaller EWs.

---

5 The Shen et al., (2011) parameters are derived from the SDSS DR7 spectra, whereas 16 out of 19 of our fits are to higher S/N BOSS DR12 spectra.

Hα

We employ the same continuum subtraction and fitting method as for C IV, with the continuum and fitting windows as given in Table 2. We adopt a rest-frame transition wavelength of 6564.89 Å to transform wavelengths into equivalent Doppler velocities. We used a simple model with up to three broad Gaussian components to fit the Hα emission line. We opted against parametrizing the Hα line using a GH polynomial because the extra degrees of freedom in this model did not improve the quality of the fits[6]. Upon inspection of the residuals from the fit, we also found no evidence that additional model components for narrow Hα, N II - -6548,6584 and S II - -6717,6731 were required. Furthermore, narrow O III - -4960,5008 emission is relatively weak in these spectra.

The sole exception is the Hα line in the spectrum of SDSSJ0738+2710. In addition to having the narrowest Hα line, this spectra also has the strongest narrow O III component (EW = 63 Å), which suggests that a contribution from the narrow-line region might be important. Introducing a single Gaussian for the narrow emission, while retaining a double Gaussian for the broad emission, the FWHM of the broad component increases to 3400 km s^{-1}(compared to 1580 km s^{-1}without the narrow component). For consistency, the parameters quoted in Table 3 are from the model with no narrow component. However, because the properties derived from the emission line width (the BH mass and the mass-normalised accretion rate) are strongly biased by the probable contribution from the narrow-line region, SDSSJ0738+2710 is excluded from the analysis in Section 2.5.

Comparison of Hα and Hβ profiles

Virial BH mass estimators are typically based on the width of Hβ. However, the Hα and Hβ emission is believed to originate from the same gas and the transformation between the emission-line velocity widths is expected to be well defined. Greene and Ho, (2005), using a sample of 162 quasars with high S/N SDSS spectra, established the following relation between the Hα and Hβ FWHM:

$$\mathrm{FWHM(H_\beta)} = (1.07 \pm 0.07) \times 10^3 \left(\frac{\mathrm{FWHM(H_\alpha)}}{10^3 \ \mathrm{km \ s^{-1}}} \right)^{(1.03 \pm 0.03)} \tag{1}$$

Greene and Ho, (2005) found the root-mean-square scatter about this relation to be ∼ 0.1 dex. We do not have a sufficient number of robust Hβ line measurements to test this relation directly. However, we are in the process of acquiring a much larger sample of quasars

---

6 The emission line parameters and subsequent analysis do not depend on whether line parameters from multiple-Gaussian or GH-polynomial model fits are used.
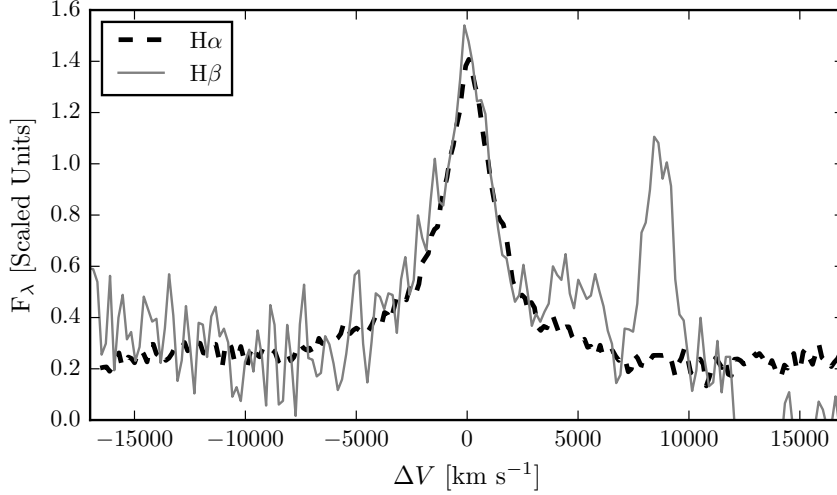
Figure 5: The Hα and Hβ emission line regions in the median composite spectrum, shown as function of the velocity shift from the respective predicted line peak wavelengths. The line fluxes have been scaled in order for the profile shapes to be readily compared. The Hα and Hβ line profiles are very similar, which suggests a tight correlation between the Hα and Hβ line widths. Quasar narrow-line emission from O III-5008.2 is visible but, overall, the O III--4960,5008 emission is relatively weak in these spectra.

with near-infrared spectra covering Hα and Hβ at similar redshifts and luminosities to the sample presented here. The Hα and Hβ line widths of this sample are in excellent agreement with the Greene and Ho, (2005) relation. To indirectly test the Hα/Hβ line width relation for the sample presented here, we first constructed mean composite spectra in the Hα and Hβ emission line regions to increase the S/N. The individual rest-frame spectra (defined using the wavelength of the Hα centroid) were interpolated on to a common wavelength grid. The spectra were then normalised using the continuum flux under the line centre, which was found by linearly interpolating between two emission-line free windows on either side of the line. Figure. 5 shows the composite Hα and Hβ line regions overlaid and, as expected, the line profiles are closely matched.

Emission line parameters

In Fig. 6 we show our best-fitting models overlaid on the observed flux in the spectral regions around C IV and Hα. The spectra are presented in order of increasing C IV blueshift. The Doppler velocities have been shifted so that the Hα emission line centroid is at 0 km s^{-1}. The y-axes of the data-minus-model residual plots have deliberately been scaled by the spectrum flux errors. The model fits are generally

Table 3: Summary of emission line properties derived from parametric model fits to Hα and C IV.

Name	z (Hα)	Blueshift [km s^{-1}] C IV	FWHM [km s^{-1}] C IV	FWHM [km s^{-1}] Hα	σ [km s^{-1}] C IV	σ [km s^{-1}] Hα
0738+2710	2.4396	50 ± 21	2255 ± 42	1503 ± 95	2916 ± 42	1789 ± 95
0743+2457	2.1662	692 ± 210	5924 ± 536	6036 ± 511	3801 ± 536	3904 ± 51
0806+2455	2.1542	389 ± 115	3435 ± 267	4059 ± 403	3387 ± 267	1724 ± 40
0854+0317	2.2475	-403 ± 134	3940 ± 354	4436 ± 522	3448 ± 354	3146 ± 52
0858+0152	2.1692	4354 ± 82	8412 ± 384	3155 ± 80	5298 ± 384	3758 ± 80
1104+0957	2.4217	-299 ± 55	3590 ± 112	3307 ± 334	3259 ± 112	2723 ± 33
1236+1129	2.1559	2828 ± 99	7540 ± 271	3152 ± 131	4168 ± 271	3277 ± 13
1246+0426	2.4393	325 ± 145	4126 ± 88	4268 ± 472	3901 ± 88	2543 ± 47
1306+1510	2.3989	2043 ± 84	6660 ± 158	2626 ± 330	3905 ± 158	2145 ± 33
1317+0806	2.3748	437 ± 289	5256 ± 182	7188 ± 946	3675 ± 182	3033 ± 94
1329+3241	2.1637	652 ± 113	4528 ± 491	4908 ± 410	3819 ± 491	3350 ± 41
1336+1443	2.1466	3668 ± 345	8780 ± 1003	2954 ± 67	3772 ± 1003	3227 ± 67
1339+1515	2.3207	133 ± 184	3865 ± 935	8816 ± 1072	4501 ± 935	3627 ± 107
1400+1205	2.1672	2492 ± 107	7590 ± 290	3231 ± 227	4363 ± 290	3103 ± 22
1525+2928	2.3572	612 ± 536	5697 ± 128	6360 ± 1915	4303 ± 128	2696 ± 191
1530+0623	2.2169	1471 ± 108	5397 ± 302	3073 ± 145	4092 ± 302	2664 ± 14
1538+0233	2.2420	2018 ± 80	5567 ± 100	2892 ± 253	3596 ± 100	2415 ± 25
1618+2341	2.2755	42 ± 53	2516 ± 161	2669 ± 175	3312 ± 161	2359 ± 17
1634+3014	2.5018	1509 ± 223	6835 ± 745	6210 ± 900	4566 ± 745	3236 ± 90
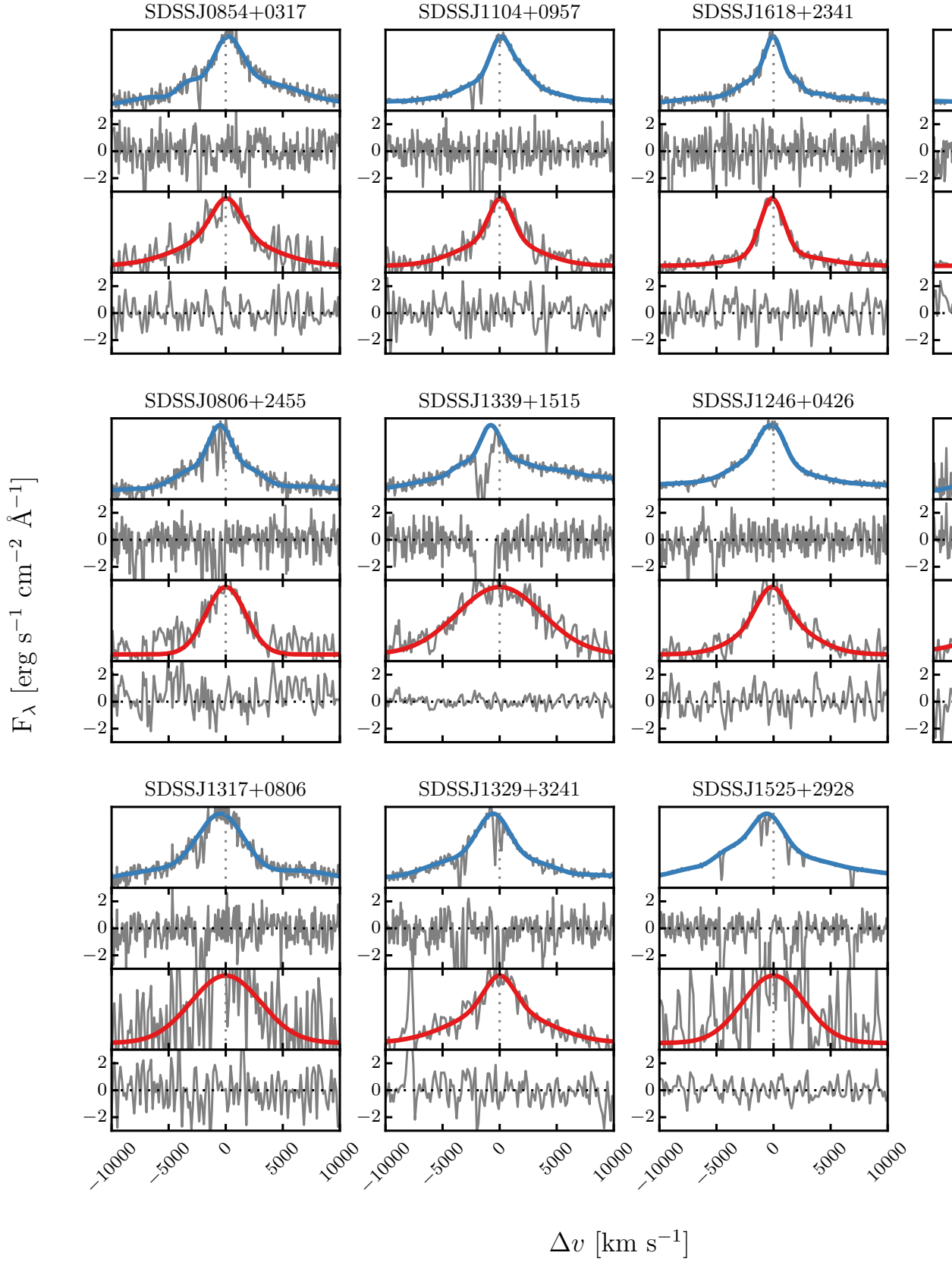
Figure 6: C IV (SDSS/BOSS) and Hα (LIRIS) emission lines and best-fitting model. Δ*v* is the velocity shift from the line rest-frame transition wavelength, with the systemic redshift defined using the centroid of the fit to Hα. Objects are presented in order of increasing C IV blueshift relative to the Hα centroid. Below each fit we plot the
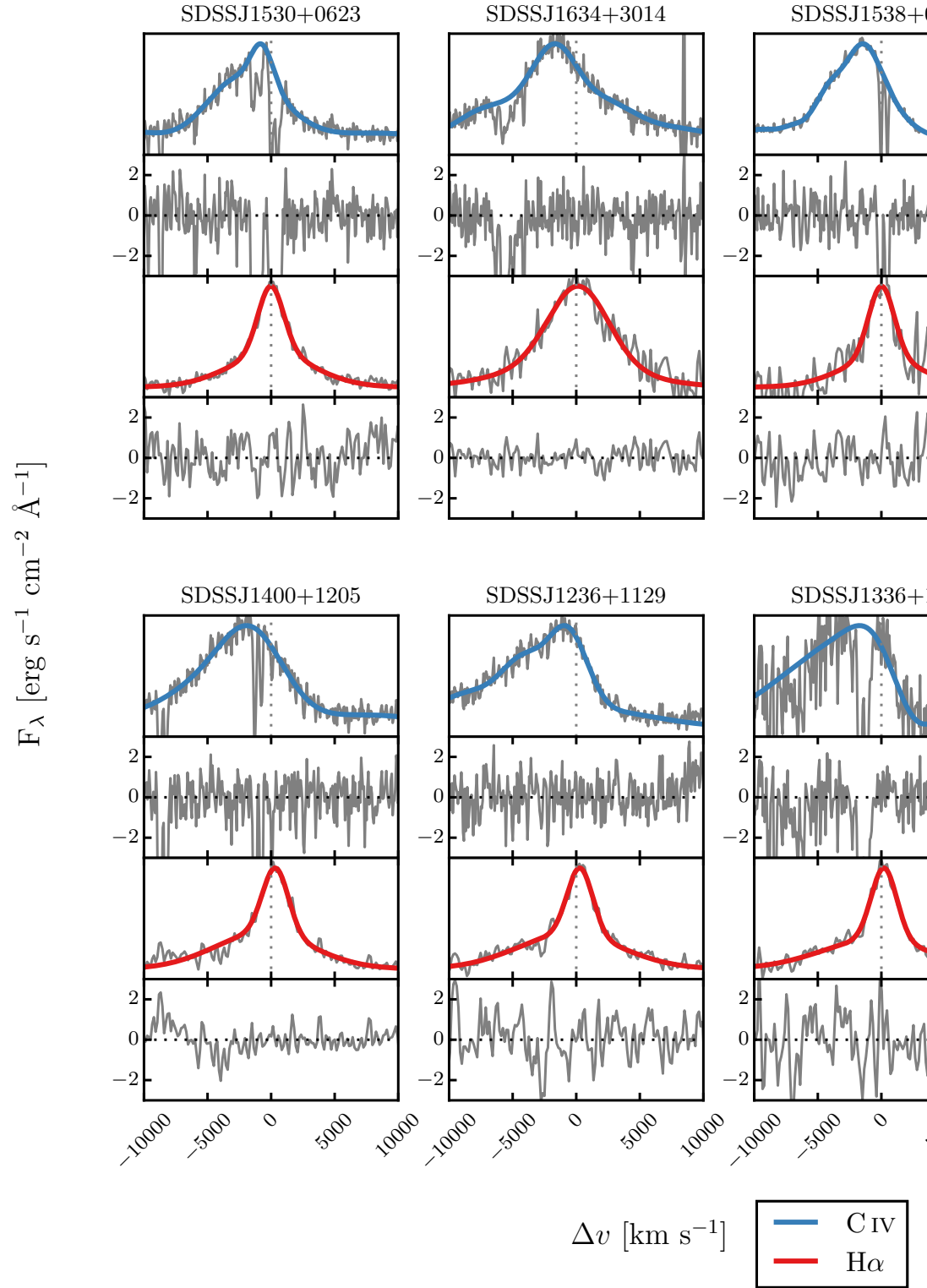
Figure 6: *Continued*

very good with only minimal systematic residuals. The only significant features seen in the residual C IV spectra correspond to the location of narrow absorption lines which were excluded in the fitting procedure. The continuum windows for a number of the Hα lines extend close to the edges of the K-band and uncertainties in the flux calibration, and hence continuum level, are almost certainly responsible for the low-amplitude, large-scale, systematic residuals seen in a number of objects (e.g. SDSSJ 0806+3455, 0858+0152, 1400+1205, 1538+0233). The amplitudes are, however, small and redefining the continuum levels to eliminate the residuals has only a very small effect on the line-profile parameters used in the analysis.

The systemic redshift (defined using the Hα peak), the C IV blueshift, the line FWHM, dispersion, and EW of Hα and C IV are all given in Table 3. Both the FHWM and the dispersion (σ) have been corrected for instrumental broadening by subtracting the FWHM resolution (152 and $477\,\mathrm{km\,s^{-1}}$ for SDSS/BOSS and LIRIS respectively) in quadrature[7].

Our definition of the C IV blueshift differs slightly in two ways from the values plotted for the quasar population in Fig. 21. Firstly, we use the peak of our parametric model fit to the Hα line to define the quasar systemic-redshift[8]. Secondly, the centre of the C IV line is now defined as the wavelength that bisects the cumulative total flux of our best-fit GH-polynomial model rather than of the data.

The monochromatic luminosity of the continuum at 1350 and 5100 Å, which are used to calculate virial BH mass estimates, are given in Table 4. The luminosity at 1350 Å was taken from the spectral fits of Shen et al., (2011). The quasar rest-frame continuum at 5100Å often lies at the edge, or beyond, the wavelength coverage of the LIRIS spectra. Monochromatic 5100Å luminosities were therefore calculated from the fit of our parametric quasar model (described in Maddox et al., (2012)) to the UKIDSS H- broadband magnitude for each quasar. The model fits to the quasars are excellent, with residuals in SDSS and UKIDSS passbands under 10 per cent.

Emission line parameter uncertainties

The 1σ error bars calculated from the covariance matrix in least-squares minimisation will underestimate the true uncertainties on the line parameters, since they do not account for systematic errors such as the significant uncertainty introduced in the continuum subtraction procedure. To calculate more realistic uncertainties on our fitted variables we employed a Monte Carlo approach. Artificial spectra were

---

7 For the dispersion we first divide the FHWM resolution by 2.35, which assumes that the line profile is Gaussian.
8 The Hα-derived redshifts are very closely in agreement with those from the forthcoming Allen & Hewett redshifts, which are plotted in Fig. 21c.

Table 4: Monochromatic continuum luminosities used to derive bolometric luminosities and BH masses.

	Log L_λ [erg s^{-1}]	
Name	1350Å	5100Å
0738+2710	46.43 ± 0.02	46.14 ± 0.01
0743+2457	46.07 ± 0.02	45.93 ± 0.02
0806+2455	46.09 ± 0.01	45.95 ± 0.02
0854+0317	46.28 ± 0.01	46.27 ± 0.01
0858+0152	46.82 ± 0.00	46.37 ± 0.01
1104+0957	46.11 ± 0.03	45.92 ± 0.02
1236+1129	46.45 ± 0.01	46.01 ± 0.01
1246+0426	46.46 ± 0.01	46.13 ± 0.01
1306+1510	46.35 ± 0.01	46.00 ± 0.02
1317+0806	46.31 ± 0.01	46.02 ± 0.01
1329+3241	46.35 ± 0.01	46.08 ± 0.02
1336+1443	45.84 ± 0.02	45.95 ± 0.01
1339+1515	46.42 ± 0.01	45.97 ± 0.01
1400+1205	46.45 ± 0.01	46.05 ± 0.01
1525+2928	46.84 ± 0.01	46.50 ± 0.01
1530+0623	46.26 ± 0.01	45.97 ± 0.01
1538+0233	46.94 ± 0.00	46.51 ± 0.01
1618+2341	46.59 ± 0.01	46.10 ± 0.01
1634+3014	46.66 ± 0.01	46.16 ± 0.01

synthesised, with the flux at each wavelength drawn from a Normal distribution (mean equal to the measured flux and standard deviation equal to the known error). Our emission-line fitting recipe was then implemented on five thousand artificial spectra. Our parameter uncertainties are defined as the standard deviation of the best-fitting parameter values from these five thousand realisations. The uncertainty on the monochromatic continuum luminosity at 5100 Å was estimated via a very similar method – using the error on the UKIDSS H-band magnitude to run a number of realisations of our SED-fitting routine. The uncertainties on all derived quantities, such as the BH mass, are propagated through by assuming that the uncertainties are uncorrelated and independent.

Because of its sensitivity to the flux in the wings of the line profile, care must be taken to define an appropriate range over which to measure the line dispersion. This is particularly true of Lorentzian-like profiles with extended wings. In spectra of only moderate S/N the line limits are difficult to determine unambiguously, which introduces an extra degree of uncertainty in line dispersion measurements. In common with previous work (e.g. Vestergaard and Peterson, 2006), by default, the dispersion was calculated within $\pm 10\,000 \, \text{km s}^{-1}$ of the line centre, but this was extended when appropriate to avoid excluding a significant amount of line flux.

RESULTS

A fundamental assumption on which single-epoch virial BH-mass estimates are based is that the widths of the broad emission lines are directly related to the virial motions of the emitting clouds moving in the gravitational potential of the central BH. However, the C IV line profiles of the quasars in our sample with the largest C IV blueshifts indicate that non-virial motions, very likely due to outflows, are having a significant effect on the observed C IV emission velocity profile (e.g. Gaskell, 1982; Baskin and Laor, 2005a; Sulentic et al., 2007; Richards et al., 2011; Wang et al., 2013). As shown in Fig. 2, at fixed emission-line EW, virtually the entire C IV-profile appears to shift blueward and the change in line shape is not simply an enhancement of flux in the blue wing of a still identifiable symmetric component. While gravity almost certainly plays a key role, determining the escape velocity for out-flowing material for example, it is clear that the virial assumption, on which single-epoch BH-mass measurements are predicated, is not straightforwardly applicable for the C IV-emission line in quasars exhibiting large blueshifts.

The main aim of this paper is to investigate potential systematic trends in C IV-based single-epoch virial BH masses as a function of the C IV blueshift. Calibrations using Hβ (and therefore also Hα) are generally accepted to be the most reliable, since most reverberation

mapping employs the Hβ line and the R − L relation has been established using Hβ. Therefore, we will test the reliability of the C IV-based estimates by comparing C IV line profiles to Hα profiles in the same quasars.

Characterising the emission-line profiles

There has been a considerable degree of attention paid to the effectiveness of different velocity-width measures of the C IV-emission; specifically, the line FWHM and the dispersion, σ, derived from the second-moment velocity (e.g. Assef et al., 2011; Denney et al., 2013). The FWHM and line dispersion trace different parts of the broad line velocity field, with the FWHM relatively more sensitive to any low-velocity core present and the line dispersion relatively more sensitive to the high velocity wings. The shape of the line can be characterised by the ratio FWHM/σ. FWHM/σ $\simeq$ 2.35 for a Gaussian profile, while FWHM/σ $\simeq$ 1 for a peakier Lorentzian profile[9]. In practice, the line dispersion is almost certainly a more robust velocity indicator when the assumptions underlying the virial-origin of the emission-line velocity width are true and the spectral S/N and resolution are adequate. This was demonstrated by Denney et al., (2013) for a sample of quasars possessing a significantly smaller range in C IV-blueshift than investigated here.

In reality, however, as highlighted by Denney, (2012), contributions to the C IV-emission line profile from gas where virial motions do not dominate can be significant. Looking to the future, the results of the new reverberation-mapping projects (Shen et al., 2015; King et al., 2015) will show what fraction of the C IV-emission line, as a function of velocity, does reverberate for quasars with an extended range of C IV-emission shapes. The derivation of quantitative corrections to transform velocity-width measures from single-epoch to reverberation-only line profiles should then be possible.

As such information is not yet available, there is a strong rationale for investigating whether the systematic changes in the C IV-emission line profile can be used to improve the single-epoch BH-mass estimates derived using the C IV line. In the left panels of Fig. 7 we show how the C IV FWHM, line dispersion, σ, and line shape, FWHM/σ, vary as a function of the blueshift. The C IV FWHM is correlated with the blueshift, with the median FWHM of quasars with the largest blueshifts a factor of 2-3 higher than quasars with only moderate blueshifts. The dispersion, however, does not show a similarly strong systematic variation.

---

9 Strictly FWHM/σ $\rightarrow$ 0 for a Lorentzian profile, but values close to unity are typical when the dispersion is calculated over a velocity range, $\simeq \pm 10\,000\,\mathrm{km\,s^{-1}}$, used to parametrize broad emission lines in quasar spectra.
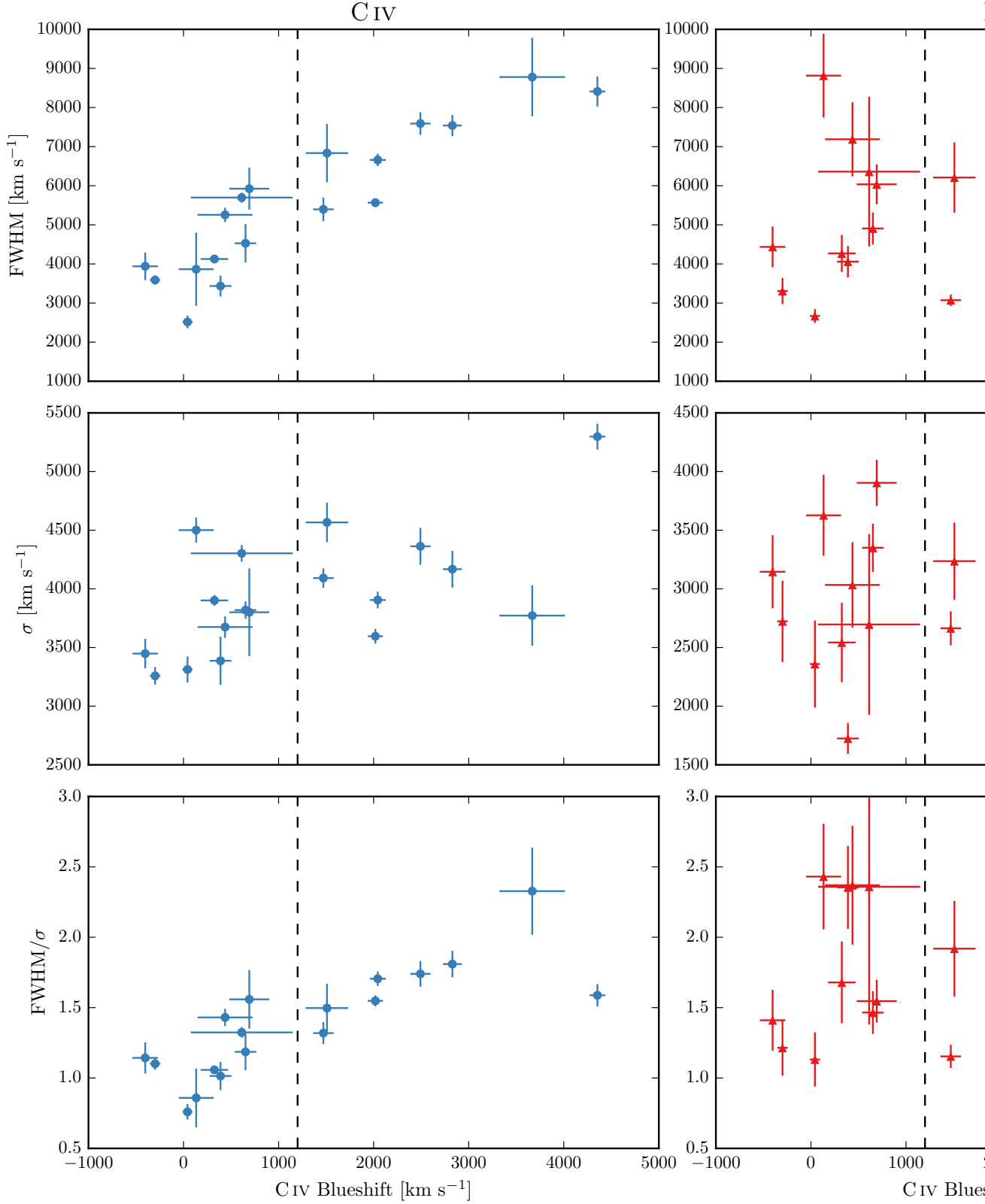
Figure 7: The FWHM, dispersion (σ) and shape (FWHM/σ) of C IV and Hα as a function of the C IV blueshift. The vertical line demarcates the 'high' and 'low' C IV blueshift regimes discussed in the text. At high blueshift it is clear that BH masses estimated from the C IV FWHM (as is typically done at the redshifts considered) will be significantly larger than those estimated from the Hα FWHM.

Without knowledge of the C IV-blueshifts, the dynamic range present in the FWHM and line dispersion measurements accords with the expectations from the study of Denney et al., (2013); the factor of $\simeq 4$ spread in the FWHM measurements indicating greater sensitivity to the emission-line profile shape than is the case for the dispersion, which varies by a factor of only $\simeq 2$. Adopting a value of $1200\,\mathrm{km\,s^{-1}}$ to define 'low' and 'high' blueshift, the median C IV-emission dispersion for the low and high-blueshift samples differ by only 10 per cent. It follows, therefore, that while the dispersion provides a relatively line-profile independent measure of the velocity width for quasars where the underlying assumption regarding the virial-origin of the velocity width applies, quasars where the assumption is not true can be assigned apparently normal velocity-widths and hence potentially incorrect BH-masses.

To emphasise this point, in Fig. 8 we overlay the C IV line profiles of SDSSJ1236+1129 and SDSSJ1525+2928, whose dispersions (Table 3) are indistinguishable (4168 ± 271 and $4303\pm128\,\mathrm{km\,s^{-1}}$ respectively). Notwithstanding the very similar dispersion values, the emission-line velocity fields differ dramatically and, therefore, the dispersion values cannot be measuring accurately the virial-induced velocity spread of the C IV emission in both quasars.

The analysis here, building on earlier work (including Shen and Liu, 2012; Sulentic et al., 2007), confirms a link between C IV emission-line shape and blueshift, raising the prospect of developing a blueshift-dependent correction to single-epoch BH-mass estimates based on the C IV line. Expressed in another way, we are interested in testing if the significant systematic change in line shape as a function of C IV blueshift can be used to provide improved single-epoch BH-masses from the C IV emission line. The tightness of the correlation we observe between the C IV FWHM and blueshift implies that such an approach may be more effective than using the C IV emission-line velocity dispersion without reference to blueshifts. A further practical advantage is that, given the typical S/N of current survey-quality spectra, virial BH mass estimates for high-redshift quasars are usually based on the FWHM rather than the dispersion (e.g. Shen et al., 2011), which, being strongly affected by the continuum placement, is often found to be difficult to measure robustly (e.g. Mejía-Restrepo et al., 2016). As a first step towards the goal, below (Sec. 2.5.5) we investigate the apparent systematic trends in the Hα FWHM and line shape as a function of C IV blueshift (shown in the right of Fig. 7).
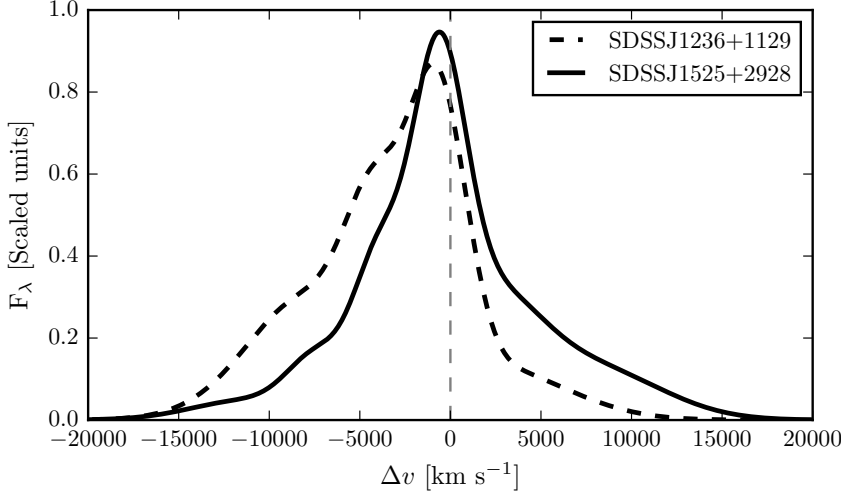
Figure 8: Comparison of the C IV line profiles of SDSSJ1236+1129 and SDSSJ1525+0426. Notwithstanding the essentially identical dispersion values, the emission-line velocity fields differ dramatically and, therefore, the dispersion values cannot be measuring accurately the virial-induced velocity spread of the C IV emission in both quasars.

Computing BH mass estimates

Single-epoch virial BH mass estimates normally take the form

$$M_{BH} = 10^a \left(\frac{\Delta V}{1000 \text{ km s}^{-1}} \right)^b \left[\frac{L_\lambda}{10^{44} \text{ erg s}^{-1}} \right]^c \tag{2}$$

where ΔV is a measure of the line width (from either the FWHM or dispersion), L_λ is the monochromatic continuum luminosity at wavelength λ, and a, b, and c are coefficients, determined via calibration against a sample of AGN with reverberation-mapping BH mass estimates. Several calibrations have been derived using different lines (e.g. Hβ, Mg II, C IV) and different measures of the line width (FWHM or dispersion) (e.g. Vestergaard, 2002; McLure and Jarvis, 2002; Vestergaard and Peterson, 2006; McGill et al., 2008; Wang et al., 2009; Rafiee and Hall, 2011; Park et al., 2013).

Reverberation mapping measurements of nearby AGN have revealed the BLR to be stratified, with high-ionisation lines, including C IV, emitted closer to the BH than low-ionisation lines, including Hα and Hβ (e.g. Onken and Peterson, 2002). Vestergaard and Peterson, (2006) found that the C IV-emitting region is at approximately half the radius of the Hβ/Hα emitting region. Given the $\Delta V \propto R_{BLR}^{-0.5}$ virial relation, this leads to the prediction that the C IV line widths should be $\simeq 1.4$ times broader than Hα for a given BH mass. More recently, Denney, (2012) found that there is a significant contribution from gas at larger

radii to the C IV emission line, enhancing the profile at lower-velocity and leading to smaller FWHM or dispersion values. The ratio of the line widths is therefore predicted to be lower than the factor of $\simeq 1.4$.

An alternate virial BH-mass calibration is proposed by Park et al., (2013), using an improved sample of AGN with reverberation mapped masses. A major difference from the calibration of Vestergaard and Peterson, (2006) is that Park et al., (2013), recognising the poor correlation sometimes observed between the C IV and Hβ FHWM, allow the exponent on the velocity width (b in Eq. 2) to vary. Calibrating Eq. 2 against reverberation BH masses, they find a best-fit value of $b = 0.56$, which is much less than the $b = 2.0$ in the strict virial regime. As a result, the derived BH masses are much less sensitive to the C IV-emission line properties. By contrast our approach is to investigate whether a more complete parametrization of the C IV-emission profile can be used to improve BH-mass estimates based on the conventional virial relation, with $b = 2.0$.

C IV-derived BH masses at low C IV blueshift

The Hα and C IV FWHM (dispersion) of the 10 quasars with C IV blueshifts $<1200\,\mathrm{km\,s^{-1}}$ are linearly correlated, as expected if the dynamics of the BLR clouds are dominated by virial motions. The median C IV/Hα FWHM (dispersion) ratio is 0.91 (1.22) with standard deviation 0.17 (0.28). Thus, the dispersion-based comparison results in a median C IV/Hα consistent with the value of $\simeq 1.4$ from assuming a virial origin for the emission but with a relatively large standard deviation. As predicted in Section 2.5.2, the FWHM-based comparison results in a systematically lower median C IV/Hα. However, the correlation between the C IV and Hα FWHMs is significantly tighter, lending support to the proposal that corrections to BH-mass estimates based on the C IV emission line properties may be possible.

Virial BH masses were calculated using the widely adopted Vestergaard and Peterson, (2006) calibrations. The Vestergaard and Peterson, (2006) C IV FWHM calibration uses the monochromatic continuum luminosity at 1350 Å to predict the BLR radius and corresponds to ($a = 6.66$, $b = 2$, $c = 0.53$) in Eq. 2. The calibration coefficient $a = 6.73$ in their equivalent dispersion-based relation. For the Hβ calibration, Vestergaard and Peterson, (2006) use the monochromatic continuum luminosity at 5100 Å and calibration coefficients corresponding to ($a = 6.91$, $b = 2$, $c = 0.5$). BH masses are computed using the line and continuum properties given in Tables 3 and 4, and we convert our Hα emission-line velocity-width measures to predicted Hβ widths using Eq. 1.

As a direct consequence of the empirically small C IV/Hα FWHM ratio, the C IV-derived BH mass estimates are systematically lower than the corresponding Hα-derived masses when the blueshift is

small. This can be seen in Fig 9, where for every quasar with a C IV blueshift $<1200\,\mathrm{km\,s^{-1}}$(i.e. to the left of the dashed line), the C IV-derived BH mass is smaller than the corresponding Hα-derived mass. The median fractional difference between the two estimates is 0.60.

For the 10 quasars with low C IV blueshifts, we looked for correlations of the C IV/Hα FWHM ratio with other spectral properties. We found marginal evidence for an anti-correlation with the Hα FWHM (Spearman coefficient 0.58 with p-value 0.08). Among the quasars with Hα FWHM $> 4000\mathrm{km\,s^{-1}}$we found the mean C IV/Hα FWHM ratio to be 0.83, compared to 1.01 for the quasars with Hα FWHM $< 4000\mathrm{km\,s^{-1}}$. Similar trends have been observed at low-z; in a sample of Boroson and Green, (1992) quasars, Baskin and Laor, (2005a) found the C IV line to be broader than Hβ when the Hβ FWHM <4000 $\mathrm{km\,s^{-1}}$and narrower when the Hβ FWHM $>4000\,\mathrm{km\,s^{-1}}$.

C IV-derived BH masses at high C IV blueshift

In Section 2.5.1 we have shown that the C IV emission at large C IV-blueshift is not dominated by virial-induced motions due to the BH. The empirically derived increase in the C IV emission FWHM with blueshift leads directly to an overestimate of BH-mass if the trend with blueshift is not taken into account. The availability of the Hα-spectra for the sample allows the quantification of the bias in inferred BH-mass under the assumption that the Hα emission line provides a reliable BH mass.

Figure 9 shows the ratio of the C IV- and Hα-FWHM derived BH masses as a function of the C IV blueshift. We see that for quasars with C IV blueshifts $> 2000\,\mathrm{km\,s^{-1}}$, the C IV-based masses overestimate the Hα-based masses by as much as a factor of ~5.

The existence of a trend in the C IV-dispersion values with C IV blueshift is evident from inspection of the bottom left panel of Fig. 7 but the systematic trend relative to the spread at fixed blueshift is significantly smaller than when using C IV FWHM. Similarly, Fig. 9 shows, at most, only a weak increase in the ratio of C IV- and Hα-derived masses. Without knowledge of the C IV blueshifts the distribution of C IV- and Hα-dispersion based BH masses could be taken to be reassuring. Including the C IV-blueshift information, however, demonstrates that any such interpretation is inherently flawed because the origin of the C IV emission velocity width is not due to virial-motions for a significant range of C IV blueshift. To reiterate the point made above (Sec. 2.5.1), we believe that using a greater knowledge of the line profile (i.e. both the FWHM and blueshift) is a better motivated (and more practical) approach to obtaining more reliable virial BH mass estimates from the C IV line.

The number of objects in our sample is small but an important factor contributing to the significant correlation evident in the FWHM
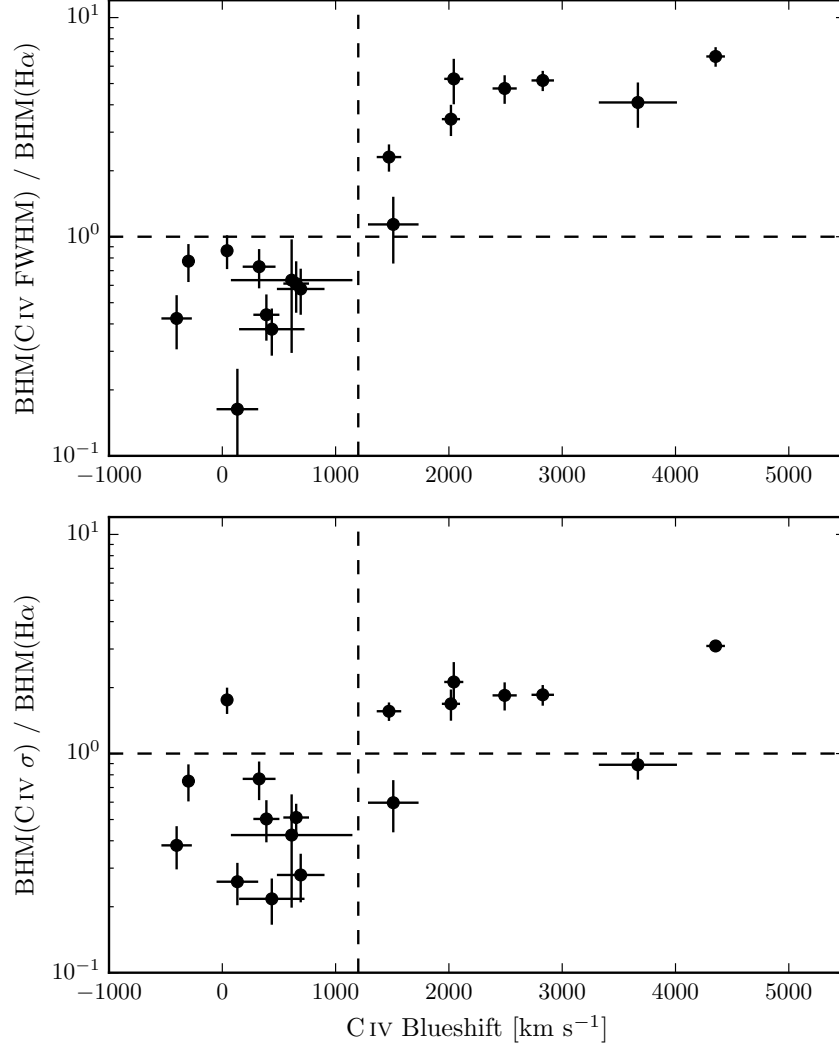
Figure 9: Comparison of virial BH mass estimates based on the C IV FWHM
(*top*) and dispersion σ (*bottom*) and Hα FWHM as a function of
the C IV blueshift. The horizontal line indicates agreement between
C IV and Hα BH masses, and the vertical line demarcates the 'high'
and 'low' C IV blueshift regimes discussed in the text. The BH
masses of quasars with moderate C IV blueshifts are underesti-
mated when using the C IV FWHM, while the masses of quasars
with large blueshifts are severely overestimated. This situation can-
not be corrected by changing the exponent on the FWHM (e.g.
Rafiee and Hall, 2011; Park et al., 2013) or the overall scaling in
standard virial BH mass relations.
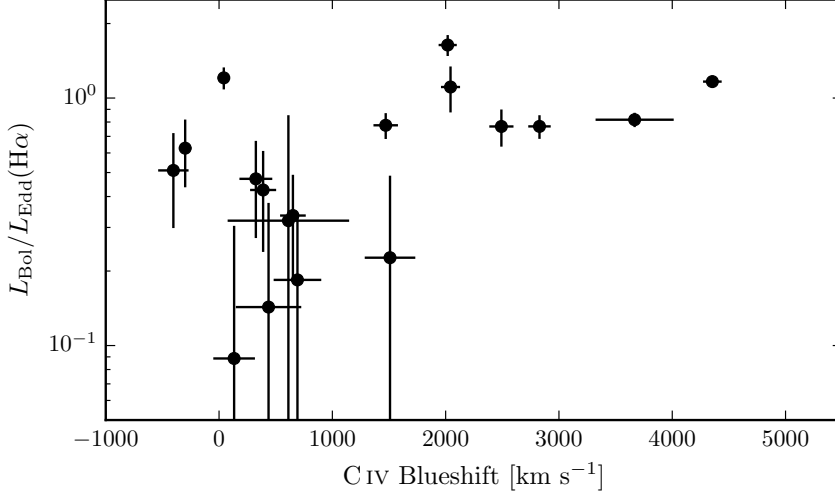
Figure 10: Hα-derived Eddington ratio versus C IV blueshift. At blueshift $\gtrsim$ 2000km s^{-1} all quasars have high accretion rates (L/L$_{Edd}$ $\simeq$ 1). This is in agreement with Kratzer and Richards, (2015), but in contrast to what one would derive from naive use of C IV-based BH mass scaling relations.

version of Fig. 9 is a change in the emission-line shape of Hα as the C IV-blueshift increases. By comparing the distributions of the Hα FWHM and dispersion as a function of C IV-blueshift (shown in the right-panels of Fig. 7), there is trend for the Hα lines to become peakier (with FWHM/σ approaching unity) as the C IV blueshift increases. Whether the size of the true systematic bias in BH masses inferred from C IV-emission FWHM is as large as shown in Fig. 9 will depend on the future parametrization of the reverberation-component present in Hβ (and Hα) profiles for quasars with high luminosities and large C IV blueshifts.

In summary, Fig. 9 illustrates the extent to which key derived physical parameters, including the BH mass and L/L$_{Edd}$, could be systematically in error when C IV-FWHM measures are used without incorporating the information from the C IV blueshifts. Other authors have proposed empirical corrections to C IV-based BH masses based on similar systematic trends seen in the C IV line shape (Denney, 2012) and the continuum-subtracted peak flux ratio of the ultraviolet emission-line blend of Si IV+O IV (at 1400 Å) to that of C IV (Runnoe et al., 2013a). In Section 2.6.1 we apply these corrections the quasars in our sample, and discuss the effect they have on the systematic bias seen in Fig. 9.

Population trends with C IV blueshift

Even with the caveat regarding the small sample size, the differences in the Hα emission-profile as a function of C IV-blueshift (Fig. 6) appear to be systematic. At C IV-blueshift $<$1200 km s^{-1}, the Hα FWHM range is $\simeq 2700 - 8800$ km s^{-1}, with mean $\simeq$5200 km s^{-1}. However, amongst the six quasars with C IV-blueshift $>$2000 km s^{-1}, the mean Hα FWHM=3000 km s^{-1}, with a scatter of just 200 km s^{-1}. The apparent trend of peakier Hα-emission, with FWHM/σ close to unity, at large C IV-blueshift is enhanced by the modest increase in Hα EW with blueshift (Table 3). Amongst the low-C IV-blueshift population there are in addition quasars with broader and more Gaussian-like Hα line profiles, with FWHM/σ $\simeq 2$.

The change in the Hα emission-line profiles as a function of C IV-blueshift means that the Hα-FWHM derived BH masses at high-blueshift are smaller than the sample mean. We transformed the observed luminosity into a mass-normalised accretion rate (Eddington ratio). To convert the monochromatic luminosity, which is observed, in to a bolometric luminosity we use the bolometric correction factor given by Richards et al., (2006a) ($L_{bol} = 9.26L_{5100}$). Although there is evidence that the bolometric correction factor is a function of the luminosity, as well as of other parameters including the C IV blueshift (Krawczyk et al., 2013), the differences are small over the parameter range covered by our sample, and for simplicity we adopt a constant factor.

The results, shown in Fig. 10, show that at large blueshifts quasars are accreting at around their Eddington limits (Fig. 10). The converse is, however, not true, i.e. not all quasars with high Eddington ratios possess large C IV blueshifts (see Baskin and Laor, 2005a).

DISCUSSION

Biases in single-epoch C IV-based BH-mass estimates

The C IV line profiles of the quasars with the largest C IV blueshifts (in the bottom right of Fig. 21) demonstrate that non-virial motions are having a significant effect on the C IV BLR dynamics. At fixed emission-line EW, almost the entire C IV-profile appears to shift blueward and the change in line shape is not simply an enhancement of flux in the blue wing of a symmetric component. It is clear that the virial assumption, on which single-epoch BH-mass measurements are predicated, is not straightforwardly applicable for the C IV-emission line in quasars exhibiting large blueshifts.

Quantitatively, the C IV-shape change is most apparent from the FWHM values, which are strongly correlated with the C IV-blueshift. This trend has previously been identified, by comparison with Mg II

at lower-redshifts (Shen et al., 2008; Shen et al., 2011) and Hβ at higher redshifts (Shen and Liu, 2012). We find that virial BH mass estimates based on the C IV FWHM will overestimate the true mass by a factor of ~5 for objects exhibiting the largest C IV blueshifts.

In contrast, the C IV line dispersion does not show a similarly strong dependence on the blueshift. This is a result of the shape of the C IV line profile being dependent on the blueshift; the low-blueshift profiles are peakier (FWHM/σ $\simeq$ 1) than the high-blueshift profiles (FWHM/σ $\simeq$ 2). Denney, (2012) found the level of contamination in single-epoch spectra from non-reverberating gas to be correlated with the shape (FWHM/σ) of the C IV profile. Their investigation was based on a sample of reverberation mapped quasars, which have a narrow range of C IV-emission line shapes, including the absence of any objects with large C IV blueshifts. The FWHM/σ-based correction to the C IV FWHM proposed by Denney, (2012) increases the inferred BH masses by ~0.2 dex at the low end of our C IV blueshift distribution, thereby reducing part of the systematic trend in the BH mass (Fig. 11). However, it is not applicable at the high C IV blueshift end, where velocity widths are likely dominated by non-virial motions. Based on the typical line shape of C IV in these high-blueshift quasars (FWHM/σ $\simeq$ 2), the Denney, (2012) correction decreases the predicted BH masses by ~0.3 dex, which has only a moderate decreasing effect on the strong systematic (Fig. 11).

While the C IV-line dispersion is largely independent of the blueshift, it does not follow that dispersion-based BH-mass estimates are correct, because the underlying assumption regarding the virial-origin of the C IV emission profile breaks down at large blueshifts. Furthermore, given the difficulty in obtaining reliable dispersion measurements from survey-quality spectra with limited S/N (e.g. Mejía-Restrepo et al., 2016), virial BH-mass estimates for existing large samples of high-redshift quasars are usually based on the FWHM (e.g. Shen et al., 2011). Our work therefore suggests that a viable recipe for obtaining more reliable BH mass estimates for large numbers of quasars at high redshift is to measure both the FWHM and the blueshift, which together can be used to derive a FWHM corrected for the non-virial contribution.

Although we do not have enough quasars in our sample to derive a reliable quantitative correction to BH-masses as a function of C IV blueshift, we are assembling a large sample of quasar spectra with coverage of both C IV and Hβ/Hα in order to empirically validate such a correction. Both Runnoe et al., (2013a) and Shen and Liu, (2012) considered a similar approach, but concluded that a low-ionisation broad line (e.g. Mg II), or features from the quasar NLR, are required to determine the systemic redshift and hence the C IV blueshift. Empirical tests of the reliability of the improved Hewett and Wild, (2010) redshifts for the SDSS DR7 quasars (Shen et al., 2016) and the avail-

ability of the largely SED-independent principal component analysis redshifts for DR10 and DR12 (Pâris et al., 2014; Pâris et al., 2017) already allow meaningful corrections to BH-mass estimates for quasars exhibiting large C IV-blueshifts. Our intention is, however, to determine a definitive correction formula using the redshifts from Allen & Hewett (2016, in preparation) for both DR7 and DR12.

Given the difficulty of measuring reliable C IV blueshifts, Runnoe et al., (2013a) opted instead to use the continuum-subtracted peak flux ratio of the ultraviolet emission-line blend of Si IV+O IV (at 1400 Å) to that of C IV to correct for non-virial contributions to the C IV velocity width. This parameter was chosen because it showed the strongest correlation with the FWHM C IV/Hβ residuals, as well as with the strengths of optical O III and Fe II. The strengths of optical O III and Fe II, being parameters in EV1, are also correlated with the C IV blueshift (Sulentic et al., 2007). As the C IV blueshift increases the EW decreases systematically (Fig. 21). The Si IV+O IV emission-line blend, however, shows significantly less systematic variation. Therefore, while the Runnoe et al., (2013a) Si IV+O IV-based correction is effective in practice, the C IV blueshift measurement provides a more direct measure of the non-virial contributions to the C IV velocity width.

In our sample, we find the 1400 Å/C IV peak flux ratio to be strongly correlated to the C IV blueshift (the Spearman coefficient for the correlation is 0.82, p-value 2E-5). As such, the correction to C IV-based virial masses proposed by Runnoe et al., (2013a, their equation 3) removes a large part of the systematic in the Hα/C IV FWHM residuals with the C IV blueshift (Fig. 11); the median C IV/Hα FWHM ratio at large C IV blueshifts ($>1200 \mathrm{km\,s^{-1}}$) is reduced from 4.5 to 1.5. However, at low ($<1200 \mathrm{km\,s^{-1}}$) C IV blueshifts, the trend for C IV to predict lower BH masses persists, and the scatter between the C IV- and Hα-based masses increases by a factor of two. In accordance with our expectations, we find the FWHM C IV/Hα residuals to be more tightly correlated to the C IV blueshift (Spearman coefficient 0.82, p-value 3E-5) than to the 1400 Å/C IV peak flux ratio (Spearman coefficient 0.72, p-value 7E-4).

Possible systematic trends in Hα BH-mass estimates

In Section 2.5.5, we found that the quasars with large C IV blueshifts have systematically narrower Hα FWHM (Fig. 7). Using the standard virial BH mass calibrations this implies that the high C IV blueshift population have high accretion rates ($L/L_{\mathrm{Edd}} \simeq 1$; Fig. 10). This interpretation requires some caution since the emission-line shape (characterized by the value of FWHM/σ) of Hα is also changing as a function of the C IV blueshift (Fig. 7). At low C IV blueshifts there are a range of shapes, but all of the quasars exhibiting large C IV blueshifts have peaky Hα profiles with FWHM/σ $\simeq$ 1. This raises the question
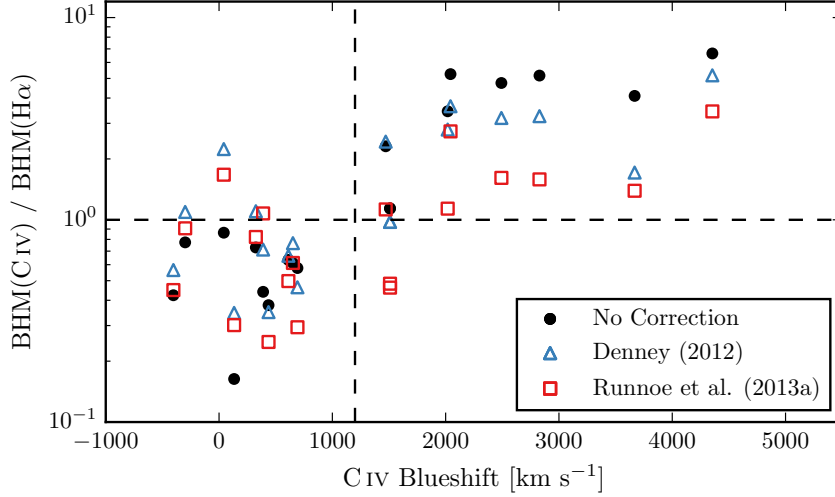
Figure 11: Comparison of BH mass estimates derived from the FWHM of C IV and Hα as a function of the C IV blueshift (*black circles*), and after applying corrections to the C IV-derived mass based on the line shape (*blue triangles*; Denney, 2012) and the peak flux ratio of the Si IV+O IV blend relative to C IV (*red squares*; Runnoe et al., 2013a). While the shape-based correction improves the consistency between BH mass estimates in the low-blueshift population, only the Si IV+O IV/C IV peak flux-based correction is effective at high blueshifts (although a weak systematic remains).

of whether the Hα FWHM is a reliable proxy for the virial-induced velocity dispersion for the full range of Hα line shapes we have in our sample.

When calibrating the virial-product to masses derived independently using the BH mass – stellar velocity dispersion ($M_\odot - \sigma$) relation, Collin et al., (2006) find that the scaling factor, f, is a factor ∼ 2 larger for their Population '1' sources (with FWHM/σ < 2.35 and essentially equivalent to population A of Sulentic and co-workers and to the high-blueshift quasars here) than for their Population 2 (with FWHM/σ > 2.35). For single-epoch BH-mass estimates, assuming a constant value of f, as is normally done (e.g. Vestergaard and Peterson, 2006), means that Population 1 masses will be underestimated and Population 2 will be overestimated. In the context of this result from Collin et al., (2006), our high-blueshift objects all possess peaky Hα-lines and, while our quasar sample probes much higher luminosities and masses, the true BH-masses may also be underestimated. Adopting such an interpretation, the amplitude of the trend seen in Fig. 9 might not be so pronounced.

As mentioned in Section **??** and discussed in Richards et al., (2011), quasars with current reverberation mapping measurements have a restricted range of C IV-line shapes. There are currently very few reverberation-mapping measurements of quasars with large C IV blueshifts

but the results of the large on-going statistical reverberation mapping projects (e.g. Shen et al., 2015) for luminous quasars at high-redshift will go some way to establishing whether the quasar broad line regions producing Balmer emission look the same for objects with very different C IV-emission blueshifts.

Although the EV1-trends (Sulentic et al., 2000; Shen and Ho, 2014) are most likely driven by the accretion rate, orientation may also have a role to play in determining the observed properties of the BLR. Shen and Ho, (2014) argue that a large part of the scatter observed in the Hβ FWHM relates not to a spread in BH masses, but rather to the orientation of the BLR relative to the line-of-sight. For this to be true, the BLR would need to be in a flattened disc-like geometry, in which case the observed line width would increase with the inclination of the disc relative to the line of sight. Brotherton, Singh, and Runnoe, (2015) found that the core-dominance of radio-loud quasars, which is believed to be a reliable proxy for orientation, at least in a statistical sense, is significantly correlated with the Hβ FWHM and hence with the BH-mass estimates. This raises the question of whether the narrow Hα emission lines observed in the quasars with the largest C IV blueshifts could be an orientation effect. However, there is no evidence that the C IV blueshift is dependent on the orientation (inferred from the radio core-dominance; Richards et al., 2011; Runnoe et al., 2014). Furthermore, Leighly, (2004) showed that the He II-1640 emission-line properties of quasars with large C IV blueshifts are more consistent with differences in the SED rather than differences in the orientation. Collin et al., (2006) showed that orientation effects were also sub-dominant to the Eddington ratio in determining the shape of the Hβ line and the Hα line shape trend we observe is consistent with the finding of Marziani et al., (2003) that the Hβ emission profiles of high/low Eddington ratio low-z quasars and type 1 Seyfert nuclei are well fit by Lorentzian and double Gaussian profiles respectively. Overall, therefore, orientation does not appear to be the dominant effect in determining the C IV blueshift and correlated changes in the Hα line profile.

Accretion-rate trends in the quasar population

The blueshifting of C IV is usually interpreted as evidence for strong outflows resulting from the presence of a radiation-driven accretion-disc wind. Richards et al., (2002) found that quasars with large C IV blueshifts have weak He II. This is evidence for weak soft X-ray continuum emission (Leighly, 2004), which would allow a strong line-driven wind to form. The strength of such a wind is predicted to be related to the quasar far-ultraviolet SED, which, in turn, could be related to the mass-accretion rate. This picture is therefore consistent

with our finding that the quasars with large C IV blueshifts have high accretion rates.

All of the objects in our sample which exhibit large C IV blueshifts would be classified as population A in the Sulentic et al., (2000) scheme based on the Hα FWHM (see Section **??**). Our results therefore support the idea of the Sulentic et al., (2000) A/B division being driven by the Eddington ratio, with population A sources possessing higher accretion rates. However, we also observe a number of quasars which have high Eddington ratios but do not have line profiles suggestive of strong outflows in the C IV BLR. This suggests that a high accretion rate is a necessary but not sufficient condition for the existence of outflows (Baskin and Laor, 2005a).

The two-dimensional nature of the C IV emission line parametrization and the apparent anti-correlation between C IV EW and C IV blueshift suggests that the quasar population exhibits a continuum of properties. As such, more accurate C IV blueshift measurements for SDSS-quasars should allow an improved mapping between the C IV-emission properties and key physical parameters of the quasars. This includes improving our understanding of the origin of quasars with exceptionally weak, blueshifted C IV emission (weak emission line quasars; Luo et al., 2015) which could be exotic versions of wind-dominated quasars (Plotkin et al., 2015).

The BAL parent population

Classical high-ionization BAL (HiBAL) quasars are also predominantly Population A objects in the scheme of Sulentic et al., (2000). There are no HiBAL quasars in our sample by design (Section **??**) but it is generally accepted that quasars which show high-ionisation BALs are likely to be radiating with relatively high L/L_{Edd} (e.g. Zhang et al., 2014). We therefore propose that the subset of the quasar population that exhibits large C IV-emission blueshifts, with high-EW and narrow-Hα emission lines, may be directly related to the HiBAL quasar population – perhaps even the 'parent' population (Richards, 2006). A prediction of such a linkage is that near-infrared observations of the rest-frame optical spectra of HiBAL quasars will show strong, relatively narrow, Balmer emission lines, very similar to those of the quasars with high C IV-blueshifts presented in this paper (see Runnoe et al., 2013b, for such a study).

The frequency of quasars with high accretion rates

Quantifying the frequency of quasars producing outflows as a function of key parameters, e.g. quasar luminosity, BH-mass, redshift,... will be important to constrain models of quasar-galaxy evolution. At fixed BH mass, the intrinsic and the observed fraction of quasars ex-

hibiting properties that depend on the Eddington ratio can differ significantly. As an illustration, we consider the implications for the intrinsic fraction of quasars possessing large C IV blueshifts given the observed numbers in the $m_i < 19.1$ flux-limited sub-sample of the SDSS DR7 quasar catalogue, from which our quasar sample is effectively drawn (Section **??**). In order to estimate the size of the selection effect, we considered the detection probability for a much-simplified quasar population. We assume that all quasars with C IV blueshifts $>$1200 km s^{-1} have enhanced accretion rates relative to the 'normal' population (with C IV blueshifts $<$1200 km s^{-1}). If the accretion rate of the high-blueshift population is double the rate of the low-blueshift population (which is true in an average sense – see Fig. 10), then the high-blueshift population will be brighter by $\simeq$0.75 magnitude. Under the assumption that the BH mass distribution is independent of the C IV blueshift, the high-blueshift population will then be over-represented in a flux-limited sample. To estimate the size of the bias, we need to know how many more quasars, at redshifts $2 < z < 2.5$, there are with $m_i < 19.1 + 0.75 = 19.85$ relative to $m_i < 19.1$. This is the fraction of the population which, as a consequence of having enhanced accretion rates, are boosted above the survey flux limit. The main colour-selected SDSS DR7 quasar catalogue extends only to $m_i = 19.1$ and, assuming the luminosity function is continuous[10] we thus use the number counts at $m_i < 19.1$ and $m_i < 18.35$, which differ by a factor of $\simeq 4$.

At redshifts $2 < z < 2.5$, there are 3,834 quasars with C IV blueshifts $<$1200 km s^{-1} and 2,484 with blueshifts $>$1200 km s^{-1} in the SDSS DR7 $m_i < 19.1$ quasar sample, a ratio of ~2:1. The above calculation, although much idealised, suggests that the intrinsic fraction of high-blueshift quasars is a factor of four smaller than in the flux-limited sample (i.e. ~15 per cent of the ultraviolet-selected non-BAL quasar population).

CONCLUSIONS

We have presented an analysis of biases in C IV-derived virial BH masses of high-luminosity ($L_{bol} \sim 47$ erg s^{-1}) quasars at redshifts ~ 2.5 from the Sloan Digital Sky Survey. Many authors have reported a large scatter between C IV- and Hα/Hβ-based masses, and part of this scatter has been shown to correlate with the C IV blueshift (Shen and Liu, 2012). The blueshifting of C IV is usually interpreted as evidence for strong outflows which, most likely, result from the presence of a radiation line-driven accretion-disc wind. Our study is the first to examine this bias systematically across the full range of C IV-emission line blueshifts observed in the SDSS sample. In particular, we have

---

10 The luminosity function and number-counts vary only smoothly (e.g. Ross et al., 2013) for the magnitude and redshift range used here.

used rest-frame optical spectra of 19 quasars in the redshift range $2 < z < 2.7$ to directly compare C IV and Hα emission properties as a function of the C IV blueshift. We reach the following conclusions:

- A strong correlation between C IV-velocity width and blueshift is found and at large blueshifts, $>2000\,\mathrm{km\,s^{-1}}$, the velocity-widths are dominated by non-virial motions. This suggests that the assumption that velocity-widths arise from virial-induced motions, on which single-epoch BH-mass measurements are predicated, is not straightforwardly applicable to these high-blueshift quasars.

- We use the Hα emission line to provide BH-mass estimates that are unbiased by non-virial contributions to the velocity width. We find that the C IV-based BH masses of quasars with low C IV blueshifts are systematically underestimated (by a factor of ~1.7) whereas the masses of quasars with large blueshifts are severely overestimated (by a factor of ~5).

- We find a systematic change in the shape of the Hα line profile as a function of the C IV blueshift. Specifically, the Hα line profiles of the quasars with high C IV blueshifts are all 'peaky' with FWHM/σ close to unity.

- We suggest that the high C IV blueshift quasars are high Eddington-ratio objects that are inherently rare (comprising ~15% of the UV-selected sample), but are being boosted in number by a factor of ~4 in the flux-limited SDSS sample.

With a relatively small sample of 19 quasars we have been able to uncover systematic trends in the C IV and Hα emission line shapes as a function of the C IV blueshift. This confirms the prospect of developing a blueshift-dependent correction to C IV-based single-epoch BH-mass estimates using a larger samples of luminous quasars with both rest-frame UV and rest-frame optical spectroscopy. We are currently in the process of assembling such a sample, which will contain ~300 luminous quasars, 80 per cent at redshifts $z \geqslant 2$. A new SED-independent redshift-estimation algorithm (Allen & Hewett 2016, in preparation) makes it possible to quantify the distribution of C IV-blueshifts in the observed quasar population as a whole, thereby allowing us to make empirical corrections to C IV-based BH-masses for all luminous, high-redshift SDSS/BOSS quasars.

3

BLACK HOLE MASSES

INTRODUCTION

The goal of better understanding the origin of the correlation between the masses of super-massive black holes (BHs) and the masses of host-galaxy spheroids has led to much work focussing on the properties of quasars and active galactic nuclei (AGN) at relatively high redshifts, $z \gtrsim 2$. Extensive reverberation-mapping campaigns (e.g. Kaspi et al., 2000; Kaspi et al., 2007; Peterson et al., 2004; Bentz et al., 2009; Denney et al., 2010) have been used to calibrate single-epoch virial-mass estimates which use the velocity widths of the hydrogen Balmer emission lines and the nuclear continuum luminosity to provide reliable BH masses (e.g. Greene and Ho, 2005; Vestergaard and Peterson, 2006; Vestergaard and Osmer, 2009; Shen et al., 2011; Shen and Liu, 2012; Trakhtenbrot and Netzer, 2012). Single-epoch virial BH mass estimates using Hβ are possible up to redshifts $z \sim 0.7$, and the technique has been extended to redshifts $z \sim 1.9$ via the calibration of the broad Mg II$\lambda\lambda$2796,2803 emission line (McLure and Jarvis, 2002; Onken and Kollmeier, 2008; Wang et al., 2009; Rafiee and Hall, 2011). At redshifts $z \gtrsim 2$, however, ground-based statistical studies of the quasar population generally have no access to the rest-frame optical and near-ultraviolet spectral regions.

Attention has thus been drawn to the properties of the C IV$\lambda\lambda$1498,1501 emission line, which is both relatively strong in the majority of quasars and visible in modern 'optical' spectra, such as those provided by the Sloan Digital Sky Surveys, to redshifts exceeding $z \sim 5$. In contrast to a number of low-ionisation emission lines, such as Mg II, the C IV emission has long been known to exhibit significant displacements to the blue (Gaskell, 1982) and more recent work (e.g. Sulentic, Marziani, and Dultzin-Hacyan, 2000; Richards et al., 2011) has established that the extent of 'blueshifts' in the C IV emission correlates with a number of properties of quasar spectral energy distributions (SEDs). While the physical origin of the blueshifted emission has not been established there is a consensus that the associated gas is not tracing virial-induced velocities, that should allow a BH-mass estimate to be derived. A favoured interpretation associates the blueshifted emission with out-flowing material (see Netzer, 2015, for a recent review), reaching velocities significantly larger than virial-induced velocities associated with the BH (e.g. Sulentic et al., 2007; Richards et al., 2011). Certainly, excess emission-line flux in the blue wing of the C IV emission increases commonly employed measures of

the line-width, notably the full-width at half maximum (FWHM) and the line dispersion (σ). As a consequence, BH-masses derived from C IV emission line velocity-widths are known to be systematically biased compared to masses from the Balmer lines (e.g. Shen et al., 2008; Shen and Liu, 2012; Coatman et al., 2016).

In recent literature, attempts have been made to minimise the influence of the systematic non-virial contribution to the C IV emission on estimates of the BH mass. Strategies include (i) significantly reducing the dependence of the derived masses on the emission-line velocity width (e.g. from the V^2 dependence predicted assuming a virialized broad line region to just $V^{0.56}$ in Park et al. 2013; see also Shen and Liu 2012), (ii) adopting a measure of emission-line velocity-width that is relatively insensitive to changes in the core of the emission-line profile (e.g. Denney et al., 2013) and (iii) estimating the amplitude of the non-virial contribution to the C IV emission-line via comparison with other ultraviolet emission lines (e.g. Si IV+O IVλ1400 in Runnoe et al. 2013a and Brotherton et al. 2015). The increased number of high-quality spectra of quasars where information on both the Balmer lines in the rest-frame optical and C IV in the ultraviolet is available enables a rather different approach. Specifically, to investigate whether, using the properties of the C IV emission line itself, it is possible to reduce, or even remove, the systematic bias in the BH-mass estimates.

In this paper we analyse the spectra of 230 high-luminosity ($10^{45.5} - 10^{48}$ erg s^{-1}), redshift $1.5 < z < 4.0$ quasars for which spectra of the hydrogen Balmer emission lines and the C IV emission line exist. A direct comparison of the emission-line velocity widths is therefore possible, allowing us to determine a highly effective empirical correction to the C IV emission line velocity width as a function of the C IV emission line blueshift.

The paper is structured as follows. Section 2 presents the extensive set of near-infrared spectra that, combined with optical spectra of the quasar ultraviolet rest-frame, provides our spectroscopic catalogue. The scheme adopted to calculate emission-line parameters, which draws heavily on the methodology of Shen et al., (2011), Shen and Liu, (2012) and Shen, (2016), is described in Section 3. The observational results, where the emission-line properties of the Balmer lines and the C IV emission are compared and a quantitative relationship derived, are included as Section 4. Then, in Section 5, the practical application of the new BH-mass estimation formula and the extent of remaining uncertainties are discussed, and our scheme is compared to others presented in the literature. Finally, we summarise the main points of the paper and highlight forthcoming improvements to systemic redshift estimates for quasars that should improve the accuracy of BH-masses from rest-frame ultraviolet quasar spectra even further. Throughout this paper we adopt a ΛCDM cosmology with $h_0 = 0.71$, $\Omega_M = 0.27$, and $\Omega_\Lambda = 0.73$. Vacuum wavelengths are used for both

rest-frame ultraviolet and optical features. Unless otherwise stated, optical (i.e. SDSS) magnitudes are given in the AB system and infrared magnitudes in the Vega system, following the conventions of the original surveys.

QUASAR SAMPLE

The aim of this work is to measure empirically the systematic bias in C IV-based virial BH mass estimates for high-z quasars as a function of the C IV emission-line blueshift. The basis for the C IV blueshift based correction is a large sample of quasars where it is possible to make a direct comparison of the C IV line-width with the line-width of the low-ionisation Balmer lines Hα and Hβ, which are believed to provide reliable proxies for the virial velocity. Such an approach has not been possible hitherto as spectra that cover both the observed-frame optical (where the redshifted C IV appears) and near-infrared (where Hβ and Hα lie) are required.

We have compiled a sample of 307 quasars at redshifts $1.5 < z < 4$ with both optical and near-infrared spectra to enable such a comparison to be performed. Reliable emission line properties were measured for 230 quasars (Section 3.3.5), with 164 possessing Hα line measurements and 144 Hβ line measurements. The sample is considerably larger than previous studies of the rest-frame optical spectra of high-z quasars (e.g. Shen and Liu, 2012). As we demonstrate in Section 3.5.3, the quasars have C IV blueshifts of up to $\sim 5000\,\mathrm{km\,s^{-1}}$, and span the full range observed in the population. Part of this data set has been taken from the literature, but a substantial fraction is presented here for the first time. The infrared spectra were acquired using several different telescope and spectrograph combinations and the contributions from each telescope/spectrograph, along with the instrumental configurations, are summarised in Table 9. We have sub-divided our sample into two overlapping groups: quasars with reliable Hα line measurements (the 'Hα sample') and quasars with reliable Hβ measurements (the 'Hβ sample').

In Fig. 26 we show the luminosities and redshifts of the quasar sample relative to the redshift-luminosity distribution for the Sloan Digital Sky Survey (SDSS; York et al., 2000) Seventh Data Release (DR7; Schneider et al., 2010). Our sample spans a redshift range $1.5 < z < 4.0$ and a bolometric luminosity range $10^{45.5} - 10^{48}$ erg s^{-1}. Spectra were obtained within one or more of the JHK pass-bands and the gaps in our sample coverage at $z \sim 1.8$ and $z \sim 3$ are due to the presence of atmospheric absorption. Obtaining near-infrared spectra of adequate resolution and signal-to-noise ratio (S/N) of even moderately bright quasars remains resource intensive. As a consequence, at fixed redshift, the luminosities of the quasars are brighter than the

Table 5: The numbers of quasars with reliable Hα and Hβ line measurements, the spectrographs and telescopes used to obtain the near-infrared spectra, and the instrumental configurations.

Spectrograph	Telescope	Resolving power $\lambda/\Delta\lambda$	Wavelength coverage μm	Slit width arcsec	
FIRE	MAGELLAN	6000	0.80-2.50	0.6	
GNIRS	GEMINI-N	5400	0.85-2.50	0.3-0.45	
ISAAC	VLT	5100	1.40-1.82	0.6	
LIRIS	WHT	945	1.39-2.42	1.0	
NIRI	GEMINI-N	520-825	1.43-1.96	0.47-0.75	
SINFONI	VLT	2000-3000	1.10-2.45^a		
SOFI	NTT	1000-2000	1.53-2.52^b	0.6	
TRIPLESPEC	ARC-3.5m	2500-3500	0.95-2.46	1.1-1.5	
TRIPLESPEC	P200	2500-2700	1.00-2.40	1.0	
XSHOOTER	VLT	4350-7450	0.30-2.50	0.5-1.6	
			Total		

a J, H or K filters were employed to ensure coverage of the Hβ/[O III] spectral region.
b Both the low resolution red grism and the medium resolution grism, with K and H filters, were employed.

average luminosity of the SDSS sample, although the dynamic range in luminosity is a full 1.5 decades.

Below, we present the key elements of the observations of the six quasar sub-samples that make up the full 230-quasar catalogue.

Near-infrared observations

Coatman et al. (2016) Quasars

Coatman et al., (2016) (hereafter Paper I) observed objects drawn from the SDSS DR7 quasar catalogue. Quasars were selected to i) have redshifts $2.14 < z < 2.51$, ii) be radio-quiet, iii) show no evidence of broad absorption lines (BALs) affecting the C IV emission line, iv) be free from significant dust extinction and v) possess C IV-emission shapes spanning the full range in the population. Near-infrared spectra, including the Hα line, were obtained with the Long-slit Intermediate Resolution Infrared Spectrograph (LIRIS; Manchado et al., 1998) mounted on the 4.2 m William Herschel Telescope (WHT) at the Observatorio del Roque de los Muchachos (La Palma, Spain). The spectra were reduced using standard IRAF[1] packages, as described in Paper I. We have selected 15 quasars with the highest S/N Hα spec-

---

[1] IRAF is distributed by the National Optical Astronomy Observatory, which is operated by the Association of Universities for Research in Astronomy (AURA) under a cooperative agreement with the National Science Foundation.
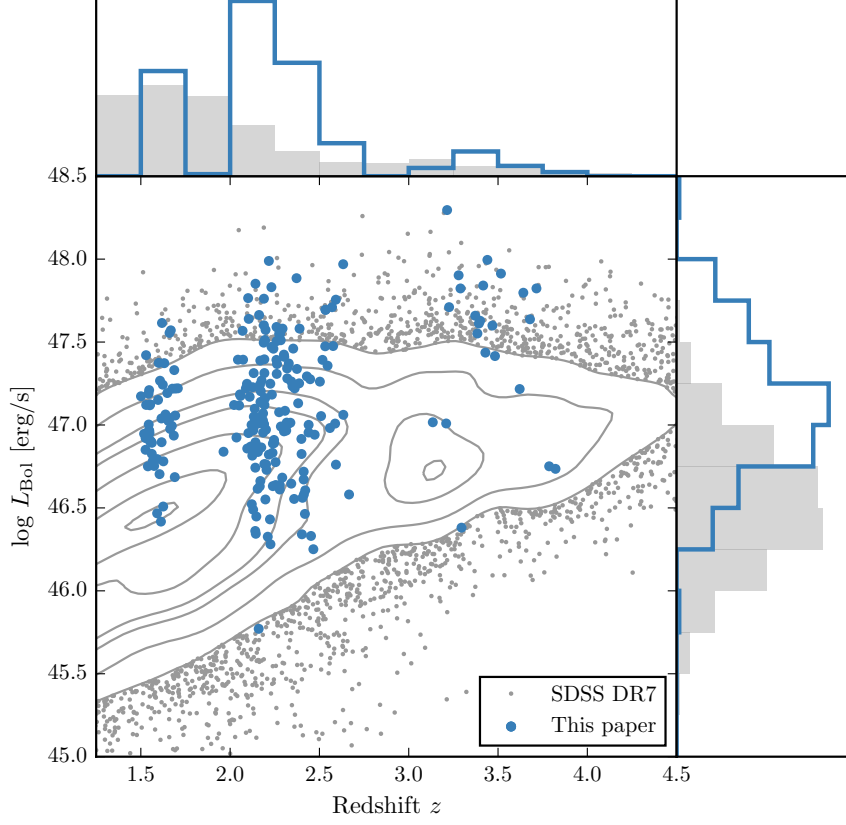
Figure 12: The ranges in redshift and luminosity covered by our sample, relative to the redshift-luminosity distribution of the SDSS DR7 quasar catalogue. In regions of high point-density, contours show equally-spaced lines of constant probability density generated using a Gaussian kernel-density estimator. For the SDSS sample we use Hewett and Wild, (2010) redshifts and bolometric luminosities measured by Shen et al., (2011). For the quasars in this paper the redshift is defined using the peak of the Hα/Hβ emission and the luminosity is measured in the continuum at 1350Å and converted to a bolometric quantity using the same conversion factor employed by Shen et al., (2011).

tra from the original sample of 19 (see Section 3.3.5) and the observational properties of these quasars are summarised in Table **??**.

Shen & Liu (2012) and Shen (2016) Quasars

Shen, (2016) and Shen and Liu, (2012) obtained near-infrared spectroscopy for a sample of 74 luminous, $1.5 < z < 3.5$ quasars selected from the SDSS DR7 quasar catalogue. Targets had to possess good optical spectra covering the C IV line and have redshifts $z \sim 1.5$, 2.1, and 3.3 to ensure that the Hβ-[O III] region was covered in one of the near-infrared JHK bands. Thirty-eight of the quasars were observed with TripleSpec (Wilson et al., 2004) on the Astrophysics Research Consortium (ARC) 3.5 m telescope, and 36 with the Folded-port InfraRed Echellette (FIRE; Simcoe et al., 2010) on the 6.5 m Magellan-Baade telescope. The reduction of the spectra is described in Shen, (2016) and Shen and Liu, (2012). The 57 quasars for which we were able to measure reliable emission line properties (Section 3.3.5) are summarised in Table **??**.

Quasar Pairs

Twenty per cent of our catalogue was observed as part of an ongoing effort to identify quasar pairs at very close projected separations (Quasars Probing Quasars² (QPQ); Hennawi et al., 2006a; Hennawi et al., 2010). The primary science driver of this work is to study the circum-galactic medium of the foreground quasars in absorption (Hennawi et al., 2006b). Very accurate systemic redshift measurements are a requirement and a large amount of effort has gone into obtaining near-infrared spectra which cover low-ionisation broad lines or features from the quasar narrow line region (Prochaska and Hennawi, 2009; Lau, Prochaska, and Hennawi, 2015; Hennawi et al., 2015). From the QPQ data set we identified 46 quasars with good-quality near-infrared spectra covering the Hα and/or Hβ lines and SDSS and/or BOSS spectra covering the C IV line. Twenty-two quasars were observed with the Gemini Near-Infrared Spectrograph (GNIRS; Elias et al., 2006) on the 8.1 m Gemini North telescope, 4 using the Infrared Spectrometer And Array Camera (ISAAC; Moorwood et al., 1998) on the European Southern Observatory (ESO) Very Large Telescope (VLT), 11 with the Near InfraRed Imager and Spectrometer (NIRI; Hodapp et al., 2003) also on Gemini North and 9 with XSHOOTER (Vernet et al., 2011), again, on the VLT. The broad wavelength coverage of XSHOOTER means that the spectra cover the region from C IV to Hα at the redshifts targeted. The XSHOOTER spectra have higher S/N and resolution than the SDSS/BOSS spectra in the rest-frame ultraviolet and therefore the XSHOOTER spectra are used by default to measure the C IV emission.

---

2 www.ucolick.org/~xavier/QPQ/Quasars_Probing_Quasars

The XSHOOTER spectra were reduced with a custom software package developed by George Becker (for details, see Lau, Prochaska, and Hennawi, 2015). The remaining data was processed with algorithms in the LowRedux[3] package (see Prochaska and Hennawi, 2009).

The 46 quasars for which we were able to measure reliable emission line properties are summarised in Table **??**.

VLT SINFONI Quasars

We performed a search of the ESO archive for high-z quasars observed with the SINFONI integral field spectrograph (Eisenhauer et al., 2003; Bonnet et al., 2004) at VLT/UT4. We found 37 quasars with redshifts $1.5 < z < 3.7$ which have H and/or K SINFONI spectroscopy, covering the Hβ and Hα lines respectively, where good optical spectroscopy covering C IV is also available. Thirty of the quasars are from a large programme led by L. Wisotzki (programme 083.B-0456(A)) to study the mass function and Eddington ratios of active BHs at redshifts $z \sim 2$ drawn from the Hamburg/ESO survey (Wisotzki et al., 2000). The Hamburg/ESO optical spectra have a typical $\sim 400 \mathrm{km\,s}^{-1}$ spectral resolution and S/N $\gtrsim 10$ per pixel. A further seven SINFONI spectra are from a programme led by J. D. Kurk (programme 090.B-0674(B)) to obtain reliable BH mass estimates from Hα/Hβ for a sample of radio-loud/radio-quiet SDSS quasars.

The SINFONI spectra were reduced using the package EASYSINF[4]. The package, which is based on the ESO-SINFONI pipeline, is described in Williams et al., (2016).

The 25 quasars for which we were able to measure reliable emission line properties are summarised in Table **??**.

ESO NTT SOFI Quasars

Twelve per cent of the quasar catalogue derives from a large programme (programme 187.A-0645; PI: J. Hennawi) to combine near-infrared spectra from SOFI (Moorwood, Cuby, and Lidman, 1998) on the 3.6 m New Technology Telescope (NTT) with archival high-resolution optical spectra from the UV-Visual Echelle Spectrograph (UVES; Dekker et al., 2000) at VLT/UT2 and the High Resolution Echelle Spectrometer (HIRES; Vogt et al., 1994) at Keck to construct a legacy database of bright, high-redshift ($2 < z < 4$) quasars with both rest-frame optical spectra, covering the Hβ-[O III] complex, and high-resolution rest-frame ultraviolet spectra. The main science goal is to obtain precise systemic redshifts which are crucial for the study of absorption line systems. The SOFI spectra were reduced using a custom data reduction pipeline using algorithms in the LowRedux package.

---

3 www.ucolick.org/~xavier/LowRedux

4 www.mrao.cam.ac.uk/~rw480/easysinf

Eighteen quasars have been targeted as part of the SDSS/BOSS spectroscopic quasar surveys. In addition, 13 reduced and fluxed UVES spectra have been made available to us by A. Dall'Aglio (a description of the reduction procedure is contained in Dall'Aglio, Wisotzki, and Worseck, (2008)). The sample is larger (~100 quasars) but reduced UVES spectra providing rest-frame ultra-violet coverage of C IV are not yet available for the remainder. The spectral resolution of the UVES observations is very high (R~40 000) and the S/N of the spectra re-binned to a resolution of ≃2000 is S/N≃300. The 28 quasars for which we were able to measure reliable emission line properties are summarised in Table **??**.

Over five nights from 2015 August 31 to September 4 we obtained near-infrared SOFI spectra for a further 26 quasars (programme 095.B-0644(A); PI: L. Coatman). These quasars were selected from the SDSS DR7 quasar catalogue using criteria very similar to those described in Paper I (see Section 3.2.1.1). In particular, we selected quasars with large C IV blueshifts to improve the statistics in this region of the C IV emission-line parameter space. The 27 quasars for which we were able to measure reliable emission line properties are summarised in Table **??**.

P200 TripleSpec Quasars

A further 36 quasars in our catalogue are bright SDSS quasars which were observed with the TRIPLESPEC spectrograph on the Palomar 200-inch Hale telescope (P200). The objects were observed with the same science goals as the SOFI NTT large programme. The spectra were reduced using a custom pipeline, again using algorithms in the LowRedux package. The 32 quasars for which we were able to measure reliable emission line properties are summarised in Table **??**.

Optical observations

In the previous sections, we described the infrared spectra of the 230 quasars making up our full spectroscopic catalogue. We will now describe the companion optical spectra, which provide coverage of the C IV emission.

Optical SDSS DR7 spectra are employed for 70 quasars in the full catalogue. The SDSS DR7 spectra are moderate resolution (R≃2000) and S/N (S/N≃20) and cover the observed-frame wavelength interval ~ $3800 - 9180$ Å. Many of the quasars in the SDSS DR7 catalogue have been re-observed as part of the Sloan Digital Sky Survey-III: Baryon Oscillation Spectroscopic Survey (SDSS-III/BOSS; Dawson et al., 2013). As the BOSS-spectra typically have higher S/N than the SDSS DR7 spectra, we have used the BOSS spectra when available (126 quasars). We also use high-resolution optical spectra taken with

VLT/UVES (11 quasars) and VLT/XSHOOTER (8 quasars), and Hamburg/ESO spectra for a further 15 quasars.

In summary, we have assembled a sample of 230 luminous, high-z quasars with optical and near-infrared spectra. This will allow us to directly compare virial BH mass estimates based on the C IV line-width with estimates based on the line-widths of the low-ionisation Balmer lines Hα and Hβ.

SPECTRAL MEASUREMENTS

Conventionally, single-epoch virial estimates of the BH mass are a function of the line-of-sight velocity width of a broad emission line and the quasar luminosity. The velocity width is a proxy for the virial velocity in the broad line region (BLR) and, as revealed in reverberation-mapping studies, the luminosity is a proxy for the typical size of the BLR (the $R - L$ relation; e.g. Kaspi et al., 2000; Kaspi et al., 2007). Most reverberation mapping campaigns have employed Hβ time-lags and velocity widths, but the line-widths of Hα and Mg IIλ2800 have been shown to yield consistent BH masses (e.g. McLure and Jarvis, 2002; Greene and Ho, 2005; Onken and Kollmeier, 2008; Shen et al., 2008; Wang et al., 2009; Rafiee and Hall, 2011; Mejía-Restrepo et al., 2016). In Section 3.4.1 we verify that this is the case for the 99 quasars in our sample with measurements of both Hα and Hβ lines.

At redshifts $z > 2.2$, where the hydrogen Balmer lines and Mg II are no longer accessible in many optical spectra, the C IVλ1550 emission doublet has routinely been used to provide estimates of the virial velocity (e.g. Shen et al., 2011). As has long been recognised (Gaskell, 1982; Tytler and Fan, 1992) the C IV emission line in many quasars includes contributions from gas that does not straightforwardly relate to virial motions within a stable BLR. A number of studies (e.g. Shen et al., 2008; Richards et al., 2011) have shown that the amplitude of the systematic shift of the C IV emission to shorter wavelengths (relative to the systemic velocity) is strongly correlated with the properties of the emission-lines and the overall spectral energy distributions (SEDs).

In our work, a robust measure of the C IV emission-line 'blueshift' provides the basis for the corrected C IV velocity-width measurements, and hence BH masses. The effectiveness of the scheme is validated via a direct comparison of the C IV velocity-widths to the Balmer emission velocity-widths in the same quasars. Our process is as follows. First, an accurate measure of the quasar's systemic redshift is required, for which we adopt the centre of the Balmer emission, where the centre, λ_{half}, is the wavelength that bisects the cumulative total flux. Balmer emission centroids are available for all quasars in the catalogue but we verify that the measure is relatively unbiased through a

comparison of the centroids to the wavelengths of the peak of the narrow [O III]--4960,5008 doublet for the subset of spectra where both are available. Second, the blueshift of the C IV emission line is determined. Again, we adopt the line centroid to provide a robust measure of the C IV emission blueshift. The blueshift (in $\mathrm{km\,s}^{-1}$) is defined as $c\times(1549.48\text{-}\lambda_{\mathtt{half}})/1549.48$ where c is the velocity of light and $1549.48\,\text{Å}$ is the rest-frame wavelength for the C IV doublet, assuming equal contribution from both components. Positive blueshift values indicate an excess of emitting material moving towards the observer and hence out-flowing from the quasar.

Emission-line velocity widths are derived from the full-width-at-half-maximum (FWHM) of the lines but we also compute the line dispersion (calculated from the flux-weighted second moment of the velocity distribution) as some authors have claimed this provides a better estimate of the virial velocity (Denney et al., 2013).

To minimise the impact of the finite S/N of the quasar spectra and the presence of absorption features superposed on the broad emission lines we first fit a parametric model to the continuum and the emission lines. The purpose of the parametric fits is, however, simply to provide higher S/N representations of the emission features. The particular form of the model parametrizations is not important and the fits are used only to provide robust line parameters, such as the centroid λ_{half}, and FWHM, which are measured non-parameterically from the best-fitting model. The models used and the fitting procedure are described below. The issues involved in deriving parameters for broad emission lines from spectra of modest S/N – for example, subtraction of narrow line emission, subtraction of Fe II emission – have been covered comprehensively by other authors (e.g. Shen et al., 2011; Shen and Liu, 2012; Denney et al., 2013; Shen, 2016) and, as far as possible, we follow standard procedures described in the literature.

C IV

The parametrization of the C IV emission line is identical to the one described in Paper I. We first define a power-law continuum, $f(\lambda) \propto \lambda^{-\alpha}$, with the slope, α, determined using the median values of the flux in two continuum windows at 1445-1465 and 1700-1705Å. The continuum emission is subtracted from the spectra, which is then transformed from wavelength units into units of velocity relative to the rest-frame line-transition wavelength for the C IV doublet (1549.98Å, assuming equal contributions from both components). The parametric model is ordinarily fit within the wavelength interval 1500-1600Å (corresponding to approximately $\pm 10\,000\ \mathrm{km\,s}^{-1}$ from the rest-frame transition wavelength), a recipe that is commonly adopted (e.g. Denney et al., 2013). The line-window was extended if more than 5 per cent of the total flux in the profile was present blueward of the short

wavelength limit. Narrow absorption features, which are frequently found superimposed on C IV emission (see, for example, the C IV profile of J0942+3523 in Fig. 13), were masked out during the fit.

The C IV emission was fit with sixth-order Gauss-Hermite (GH) polynomials, using the normalisation of van der Marel and Franx, (1993) and the functional forms of Cappellari et al., (2002). We allowed up to six components, but in many cases a lower order was sufficient (40 and 45 per cent were fit with second- and fourth-order GH polynomials respectively). GH polynomials were chosen because they are flexible enough to model the often very asymmetric C IV line profile. The flip-side of this flexibility, however, is that the model has a tendency to over-fit when spectra possess low S/N. The fits were therefore carefully checked visually and the number of components reduced if over-fitting was evident.

In Paper I we found that using the commonly employed three-Gaussian component model, rather than the GH polynomials, resulted in only marginal differences in the line parameters. Our best-fit parameters are also in good agreement with Shen et al., (2011), who employ a multi-Gaussian parametrization. In the Appendix we demonstrate that the mean difference between our FWHM measurements and the measurements of Shen et al., (2011) is just 200km s^{-1} for the quasars common to both samples, which is much too small to have any significant effect on our results.

Hα

A power-law continuum is fit using two continuum windows at 6000-6250 and 6800-7000 Å. The continuum-subtracted flux is then fit in the wavelength interval 6400-6800 Å. We adopt a rest-frame transition wavelength of 6564.89 Å to transform wavelengths into equivalent Doppler velocities. The broad component of Hα is fit using one or two Gaussians, constrained to have a minimum FWHM of 1200km s^{-1}. When two Gaussians are used, the velocity centroids are constrained to be the same.

The emission-line profiles of both Hβ and Hα frequently include a significant narrow component from the physically more extended narrow line region (NLR). Additional Gaussian components were included in our parametric model to fit the narrow component of Hα as well as [N II]--6548,6584 and [S II]--6717,6731. This resulted in a better fit to the observed flux in 50 per cent of cases. We impose a 1200km s^{-1} upper limit on the FWHM of all narrow lines and the amplitudes of all components must be non-negative. The relative flux ratio of the two [N II] components is also fixed at the expected value of 2.96. In 70 per cent of the spectra the [O III]--4960,5008 doublet is detected at moderate S/N in the Hβ region. In these cases the peak of the [O III] is used to fix the velocity offsets and the FWHMs of the nar-

row line components in the Hα region. For spectra where the [O III] doublet does not constrain the velocity and FWHM accurately, the narrow emission in the Hα and Hβ regions are fitted independently but, for each region, the individual narrow-line velocity offsets and the FWHMs are constrained to be identical. In these objects the narrow line contribution is generally weak, and so does not have a large effect on the line parameters we measure for the broad component.

The model described above is very similar to the one described in Shen, (2016), Shen and Liu, (2012) and Shen et al., (2011), the only major difference being that we do not fit the Hα and Hβ emission regions simultaneously. In Appendix 3.7, we compare our Hα line measurements for the subset of our sample taken from Shen, (2016) and Shen and Liu, (2012), and find a scatter of just 0.07 dex.

Hβ and [O III]

Emission from optical Fe II is generally strong in the vicinity of Hβ. We therefore fit a combination of a power-law continuum and an optical Fe II template – taken from Boroson and Green, (1992) – to two windows at 4435-4700 and 5100-5535 Å. The Fe II template is convolved with a Gaussian, and the width of this Gaussian, along with the normalisation and velocity offset of the Fe II template, are free variables in the pseudo-continuum fit. We use the same model to fit the broad and narrow components of Hβ as was used with Hα. Each line in the [O III] doublet is fit with two Gaussians, to model both the systemic and any outflow contributions. The peak flux ratio of the [O III] 4960 Å and 5008Å lines is fixed at 1:3. As for the fit to the narrow lines in the spectral region around Hα, the width and velocity offsets of all the narrow components are set to be equal, and an upper limit of 1200 km s^{-1} is placed on the FWHM.

Fitting procedure

Model parameters were derived using a standard variance-weighted least-squares minimisation procedure employing the Levenberg-Marquardt algorithm. Prior to the fit, the spectra were inspected visually and regions significantly affected by absorption or of low S/N were masked out.

In Fig. 13 we present our parametric fits to the C IV, Hα and Hβ emission lines in a handful of quasars, which have been chosen to illustrate the range of spectrum S/N and line shapes in the sample. The mean reduced chi-squared values in our Hα, Hβ and C IV fits are 1.69, 1.62, and 1.77 respectively and, in general, there are no strong features observable in the spectrum minus model residuals. Table 6 includes the line parameters of our best-fitting model for each line. The reported line-width measures are corrected for instrumental broaden-

Table 6: The format of the table containing the emission line properties from our parametric model fits. The table is available in machine-readable form in the online journal.

NAME	Units	Description
NAME		Catalogue name
FWHM_BROAD_HA	$km\,s^{-1}$	FWHM of broad Hα line
FWHM_BROAD_HA_ERR	$km\,s^{-1}$	
SIGMA_BROAD_HA	$km\,s^{-1}$	Dispersion of broad Hα line
SIGMA_BROAD_HA_ERR	$km\,s^{-1}$	
Z_BROAD_HA		Redshift from broad Hα line
FWHM_BROAD_HB	$km\,s^{-1}$	FWHM of broad Hβ line
FWHM_BROAD_HB_ERR	$km\,s^{-1}$	
SIGMA_BROAD_HB	$km\,s^{-1}$	Dispersion of broad Hβ line
SIGMA_BROAD_HB_ERR	$km\,s^{-1}$	
Z_BROAD_HB		Redshift from broad Hβ line
FWHM_CIV	$km\,s^{-1}$	FWHM of C IV doublet
FWHM_CIV_ERR	$km\,s^{-1}$	
SIGMA_CIV	$km\,s^{-1}$	Dispersion of C IV doublet
SIGMA_CIV_ERR	$km\,s^{-1}$	
BLUESHIFT_CIV_HA	$km\,s^{-1}$	Blueshift of C IV relative to centroid of broad Hα
BLUESHIFT_CIV_HA_ERR	$km\,s^{-1}$	
BLUESHIFT_CIV_HB	$km\,s^{-1}$	Blueshift of C IV relative to centroid of broad Hβ
BLUESHIFT_CIV_HB_ERR	$km\,s^{-1}$	
LOGL5100	$erg\,s^{-1}$	Monochromatic continuum luminosity at 5100Å
LOGL1350	$erg\,s^{-1}$	Monochromatic continuum luminosity at 1350Å

ing by subtracting the resolution of the spectrograph in quadrature. The spectrograph resolutions, which we estimate from the line widths in the observed sky spectra, range from 25km s^{-1} for XSHOOTER to 477km s^{-1} for the low-resolution LIRIS grism and are therefore small relative to the quasar broad line widths.

Spectra removed from sample

Through visual inspection we flagged and discarded the spectra of quasars for which reliable emission line parameters could not be obtained.

First, we flagged emission lines in spectra that possessed insufficient S/N. A single minimum S/N threshold was not entirely effective and, instead, spectra were flagged when it was judged conservatively that no meaningful constraints could be placed on the velocity centroid and/or width of the emission-line.

J121427.77-030721.0   J103325.93+012836.3

S/N: 18

Hα

S/N: 30

S/N: 22

Hβ

S/N: 25

S/N: 9

C IV

S/N: 14

F_λ [Arbitrary units]

J121140.59+103002.0   J023359.72+004938.5

S/N: 14

Hα

S/N: 8

S/N: 8

Hβ

S/N: 9

S/N: 27

C IV

S/N: 45
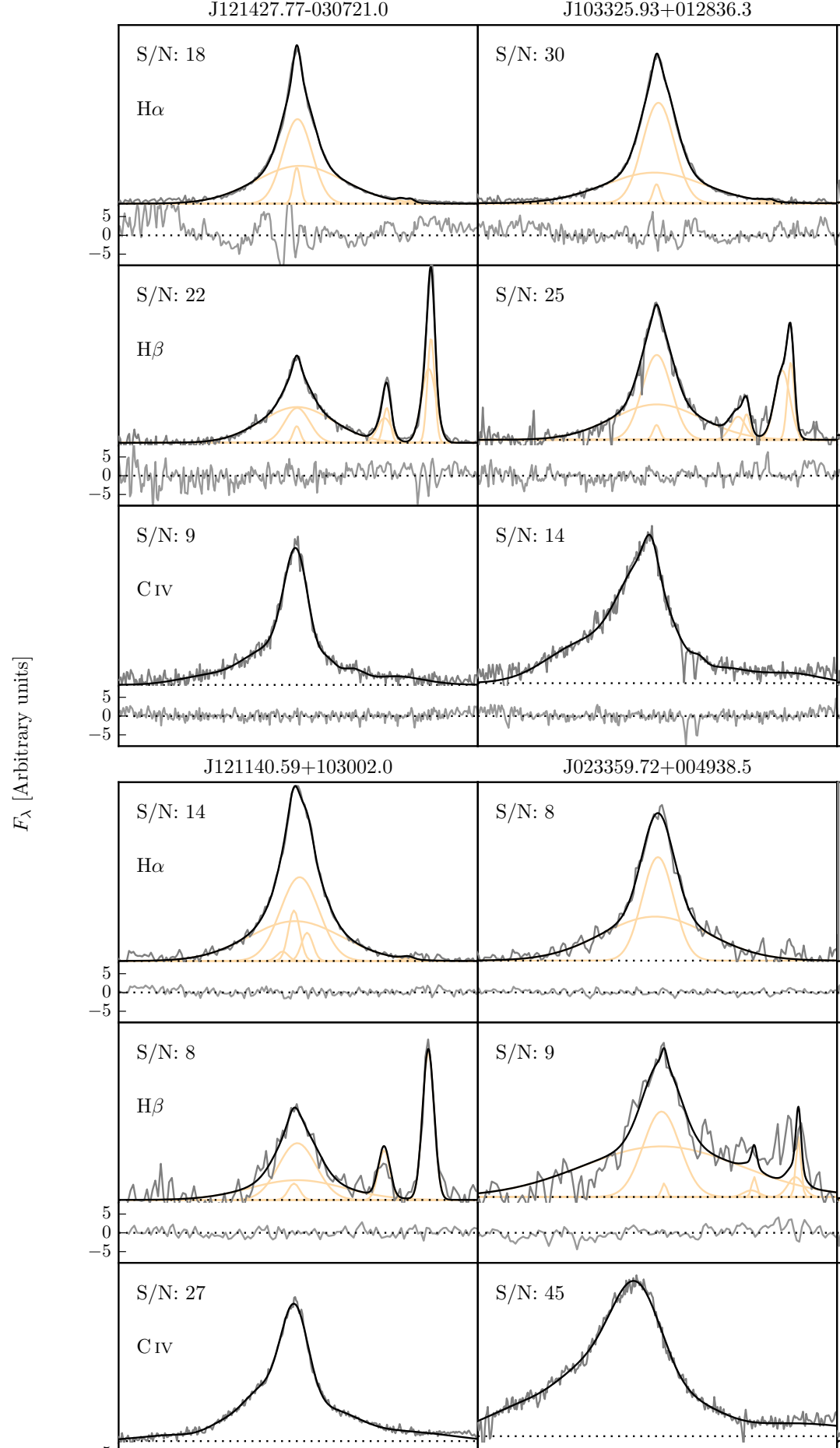
Table 7: The number of spectra removed from our sample by the cuts described in Section 3.3.5.

		Hα sample	Hβ sample
	Total	194	279
Hα/Hβ	Wavelength	6	27
	S/N	8	83
C IV	Wavelength	6	5
	S/N	4	12
	Absorption	6	8
	Total remaining	164	144

Second, we flagged emission lines where significant regions of the continuum and/or emission line fell outside of the wavelength coverage of the spectra. Reliable continuum definition and subtraction is not straightforward for emission lines so affected.

Third, we flagged C IV emission lines because of strong, narrow absorption close to the peak of the line where reliable interpolation across the absorption, using our parametric model, was not possible.

The number of spectra that are removed by each cut is given in Table 7 and the distribution in redshift and luminosity is shown in Fig. 14. Unsurprisingly, there is a preferential removal of intrinsically faint quasars, whose spectra can be of poorer S/N, and a loss of quasars at redshifts $z \sim 2.6$ where the Hα emission falls at the edge of the K-band. Hβ is much weaker than Hα, and the Hβ spectra are generally of lower S/N. As a result, the fraction of Hβ spectra that are flagged – 39 per cent – is particularly high.

Emission-line parameter uncertainties

The 1σ error bars calculated from the covariance matrix in least-squares minimisation will underestimate the true uncertainties on the line parameters, since they do not account for systematic errors such as the significant uncertainty introduced in the continuum subtraction procedure. To calculate more realistic uncertainties on our fitted variables we employed a Monte Carlo approach. One thousand artificial spectra were synthesised, with the flux at each wavelength drawn from a Normal distribution (mean equal to the measured flux and standard deviation equal to the known error). Our emission-line fitting recipe was then implemented on each of these mock spectra. The uncertainty in each parameter is given by the spread in the best-fitting values from the one thousand realisations of the fitting routine. In some cases the standard deviation of the parameter distribution was
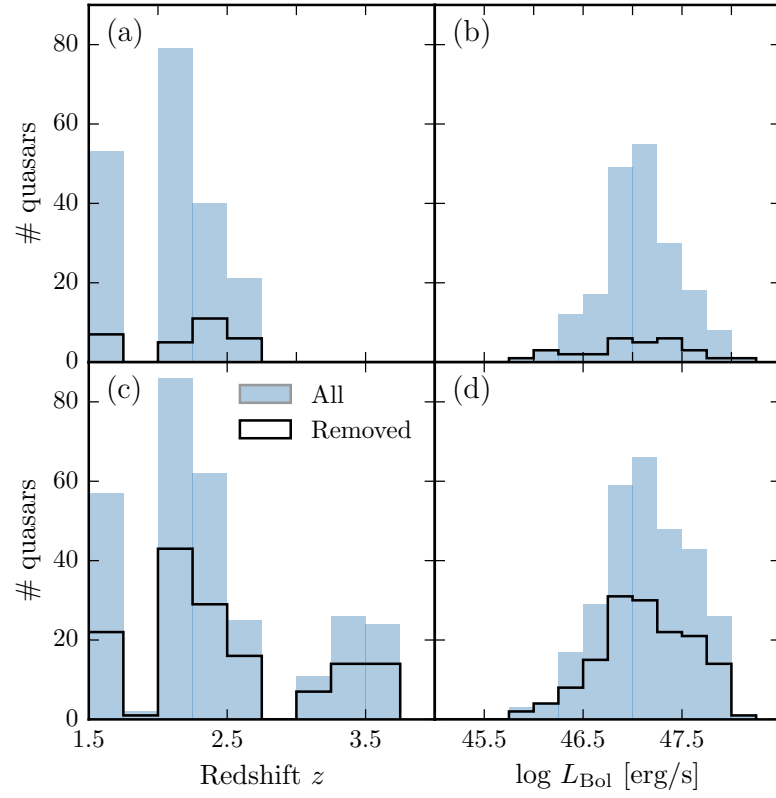
Figure 14: The redshift and luminosity distributions of the spectra removed from our Hα/C IV (a, b) and Hβ/C IV (c, d) samples.

biased by extreme values caused by bad fits[5]. We therefore chose to measure the spread in the parameter distribution by fitting a composite model with two Gaussian components – one to model uncertainty in the parameter and the other any possible outlier component. The uncertainty in each line parameter was then taken to be the width of the narrower Gaussian.

Contemporaneity of spectra

The epochs of the near-infrared and optical spectra can differ by many years. For example, the NTT SOFI spectra were taken ~14 years after the SDSS spectra, and the VLT SINFONI spectra 20 years or more after the Hamburg/ESO observations[6]. If the broad emission line profiles varied significantly on these time-scales the relation between the C IV and Balmer line-width measurements could be blurred.

Cases do exist of dramatic changes in quasar spectra over short time-scales, but this phenomenon is rare (MacLeod et al., 2016). In our spectroscopic catalogue there are 112 SDSS DR7 quasars which are re-observed in BOSS and included in the DR12 quasar catalogue. The mean time elapsed between the two sets of observations is ~8 years. The root-mean-square difference in the C IV FWHM measured from the BOSS and SDSS spectra is a modest $\simeq 500\,\mathrm{km\,s^{-1}}$. Differences in the S/N of the spectra will make a substantial contribution and the scatter due to true variations in the C IV velocity-width will be significantly smaller than $500\,\mathrm{km\,s^{-1}}$. We conclude therefore that any intrinsic changes with time do not materially affect the emission line measurements.

Quasar monochromatic luminosity

Computing virial BH masses also requires the quasar luminosity in an emission-line free region of the continuum adjacent to the broad line being used. The luminosity is used as a proxy for the size of the BLR. The monochromatic continuum flux is generally measured at $1350\,\text{Å}$ for C IV and $5100\,\text{Å}$ for Hα and Hβ.

Relative flux-calibration of the infrared spectra as a function of wavelength has been achieved, to $\simeq 10$ per cent, through observations of appropriate flux standards. The absolute flux levels, however, can be in error by large factors due to variable atmospheric conditions combined with the narrow slit widths. For the majority of the quasars we have, therefore, established the absolute flux scale for each near-infrared spectrum using the same quasar SED-model fitting scheme employed in Paper I. The SED model, described in Maddox et al., (2012), gives a very good fit to the SDSS and UKIDSS magnitudes

---

5 In the analysis of the real spectra such fits are identified via visual inspection.
6 Time differences in the quasar rest-frame are reduced by a factor of $(1 + z)$.

of SDSS DR7 quasars, reproducing the individual magnitudes with a σ <0.1 mag. For 207 quasars, (Y)JHK passband magnitudes from the UKIRT Infrared Deep Sky Survey (UKIDSS; Lawrence et al., 2007) Large Area Survey, the Two Micron All Sky Survey (2MASS; Skrutskie et al., 2006) and the Visible and Infrared Survey Telescope for Astronomy (VISTA) Hemisphere Survey (VHS; McMahon et al., 2013) and Kilo-Degree Infrared Galaxy (VIKING; Edge et al., 2013) survey are available. The SED model was fit to the infrared magnitudes; integrating the SED model through the pass-band transmission functions, to give model magnitudes, and performing a variance weighted least-squares fit to the observed magnitudes. The flux at 5100 Å was then taken from the normalised model.

For 19 of the remaining 23 quasars, where near-infrared photometry was not available, the quasar SED model was fit to the SDSS spectra, the flux calibration of which are known to be excellent. The fit was done using a simple variance-weighted chi-squared minimisation procedure in emission line-free intervals of the optical spectra. The model includes a reddening, $E(B - V)$, based on a Small Magellanic Cloud-like extinction curve, and an overall normalisation of the model as free parameters. In practice, the quasars possess only very modest reddenings, with $E(B - V) \simeq 0.0$-0.1. The flux at 5100 Å was then, again, taken from the normalised SED model. For the four remaining quasars, which possess neither near-infrared photometry nor SDSS DR7 spectra, we fit the SED model to the BOSS DR12 spectra. To avoid the known issues in the flux calibration of the BOSS DR12 quasar spectra at observed-frame blue wavelengths (Lee et al., 2013), our fitting was confined to rest-frame wavelengths long-ward of 1275Å.

Comparison of the 5100 Å luminosity, computed using the photometry- and spectrum-based methods for 177 quasars, showed a scatter of just ~0.1 dex. We therefore assume 0.1 dex to be the measurement uncertainty on the 5100 Å luminosities.

For 34 quasars in the catalogue the optical spectra come from surveys other than SDSS/BOSS and optical magnitudes from recent epochs are not available. In order to obtain an estimate of the luminosity at 1350 Å for the 30 quasars, we take the standard Maddox et al., (2012) quasar SED model, normalised to the near-infrared magnitudes, and read off the flux at 1350 Å.

For all the catalogue quasars, the optical and near-infrared spectra as well as the near-infrared photometry were obtained at different epochs, with rest-frame time differences of up to ~5 years. Intrinsic quasar photometric variability in the rest-frame ultraviolet and optical will therefore add additional scatter of ~0.2 mag (e.g. MacLeod et al., 2010) to the derived 1350- and 5100 Å-luminosities.

Given that the luminosity enters into the calculation of BH-mass only as the square-root, the uncertainty on the luminosities does not
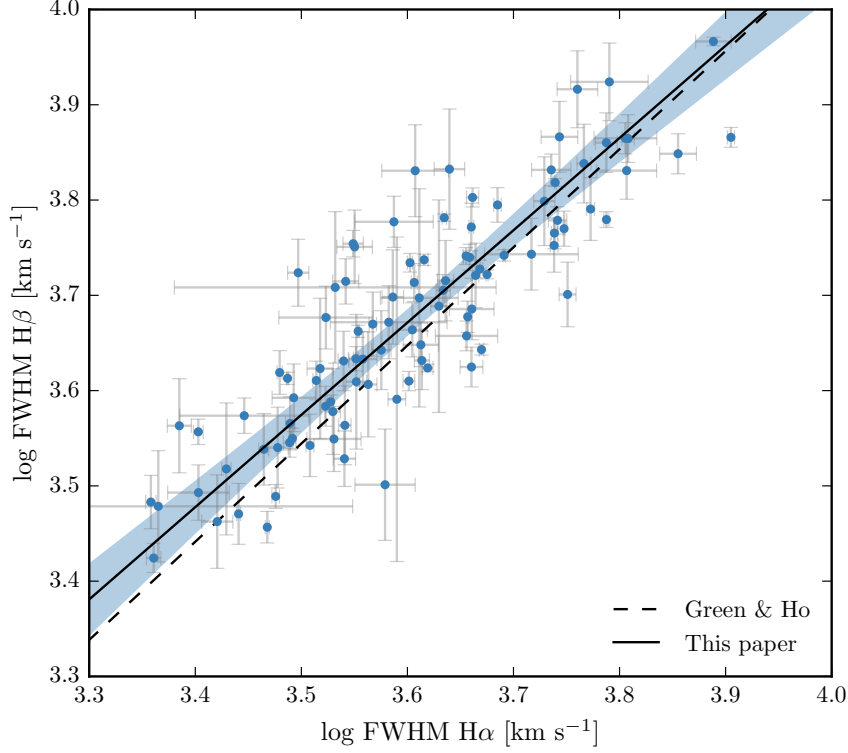
Figure 15: Comparison of Hα and Hβ FWHM measurements for 99 quasars. The solid line is our best-fitting power-law model, and the blue-shaded region shows the 2-σ uncertainties on the model parameters. The dashed line is the relation found by Greene and Ho, (2005) using a sample of $z < 0.35$ SDSS AGN.

make a large contribution to the uncertainties in the BH mass estimates.

AN EMPIRICAL CORRECTION TO C IV-BASED VIRIAL BH-MASS ESTIMATES

Hα/Hβ FWHM comparison

BH-mass calibrations which use the width of the broad Hβ emission line as a proxy for the virial velocity are widely regarded as the most reliable, since most reverberation mapping employs the Hβ line and the $R - L$ relation has been established using Hβ. When Hβ is not available, Hα has been shown to be a reliable substitute (e.g. Greene and Ho, 2005; Shen et al., 2011; Shen and Liu, 2012).

In our sample, we have 99 quasars with reliable measurements of both Hα and Hβ lines. The 99 objects include 21 quasars which were excluded from the main 308-object catalogue because adequate measurements of the C IV FWHM and blueshift could not be acquired.

The line widths are compared in Fig. 15 and, as expected, a tight correlation is observed. Greene and Ho, (2005), using a sample of 162 quasars with high S/N SDSS spectra at $z < 0.35$, established the following relation between the Hα and Hβ FWHMs

$$\text{FWHM}(\text{H}_\alpha) = (1.07 \pm 0.07) \times 10^3 \left(\frac{\text{FWHM}(\text{H}_\beta)}{10^3 \text{ km s}^{-1}} \right)^{(1.03 \pm 0.03)} \tag{3}$$

The relation is shown as the dashed line in Fig. 15. The root-mean-square scatter about this relation is 0.07 dex, compared to the ∼0.1 dex found by Greene and Ho, (2005). However, we find a systematic offset, in the sense that the Hβ line-widths we measure are on average larger by 270km s^{-1} than predicted by the Greene and Ho, (2005) relation. As our sample covers higher redshifts and luminosities than the sample in Greene and Ho, (2005), we derive a new relation between the Hα and Hβ FWHMs.

We assume a relation of the same form used by Greene and Ho, (2005), i.e. a simple power-law, and infer the model parameters by fitting a linear model (with slope α and intercept β) in log-log space. The fit is performed within a Bayesian framework described by Hogg, Bovy, and Lang, (2010). Each data point is treated as being drawn from a distribution function that is a convolution of the projection of the point's covariance tensor, of variance Σ_i^2, with a Gaussian of variance V representing the intrinsic variance in the data. The log-likelihood is then given by

$$\ln\mathcal{L} = -\sum_{i=1}^{N} \frac{1}{2}\ln\left[2\pi\left(\Sigma_i^2 + V\right)\right] - \sum_{i=1}^{N} \frac{\Delta_i^2}{2[\Sigma_i^2 + V]} \tag{4}$$

where Δ_i is the orthogonal displacement of each data point from the linear relationship. An advantage of this approach is that it allows a proper treatment of the measurement errors on both variables, which in this case are comparably large. The model also makes the reasonable assumption that there is an intrinsic scatter in the relationship between the variables that is independent of the measurement errors. Following the suggestion by Hogg, Bovy, and Lang, (2010), the linear model was parametrized in terms of $(\theta, b_\perp)$, where θ is the angle the line makes with the horizontal axis and $b_\perp$ is the perpendicular distance from the line to the origin. Uniform priors were placed on these parameters, and the Jeffreys prior (the inverse variance) was placed on the intrinsic variance. The posterior distribution was sampled using a Markov Chain Monte Carlo (MCMC) method using the Python package emcee (Foreman-Mackey et al., 2013).

The one- and two-dimensional posterior distributions are shown in Fig. 16. The solid line in Fig. 15 is the maximum likelihood solution

$$\mathrm{FWHM(H_\beta)} = (1.23 \pm 0.10) \times 10^3 \left(\frac{\mathrm{FWHM(H_\alpha)}}{10^3 \mathrm{km\,s^{-1}}} \right)^{0.97 \pm 0.05} \qquad (5)$$

and the shaded region shows the 2σ uncertainties on the model parameters.

As discussed above, our relation is displaced to slightly higher Hβ FWHM than the Greene and Ho, (2005) relation – the offset is $210\,\mathrm{km\,s^{-1}}$ for a quasar with Hα FWHM $4500\,\mathrm{km\,s^{-1}}$. We infer a power-law index that, although slightly shallower, is consistent with the Greene and Ho, (2005) index within the quoted uncertainties. The intrinsic scatter in the data, σ_I, we infer from the fit is 0.04 dex. This is smaller than the total scatter seen in Fig. 15 (0.06 dex), which suggests that measurement errors make a significant contribution to the total scatter in the relation.

For 19 of the 99 quasars with Hβ and Hα emission profiles, one of the two Gaussians used to reproduce the Hβ profiles has a FWHM greater than $20\,000\,\mathrm{km\,s^{-1}}$ and a fractional contribution to the total Hβ broad line flux of >0.3 (Marziani et al., 2009; Marziani et al., 2013). Such a broad component is not seen in the Hα profiles and the very broad Hβ-component may be an artifact of the fitting scheme. A particular issue for Hβ is the presence of Fe II emission, often at a significant level. Furthermore, additional lines could be contributing to the underlying continuum (e.g. the He I- -4922,5017 doublet; Véron, Gonçalves, and Véron-Cetty, 2002; Zamfir et al., 2010).

In Sec. 3.4.3 we use the whole of the Hβ profile to derive an unbiased BH mass. If, instead, the FWHM is calculated from the narrower of the two Gaussian components rather than the composite profile, then the Hβ FWHM decreases by $630\,\mathrm{km\,s^{-1}}$ on average. The Hα FWHM, which are calibrated against the Hβ FWHM, will also decrease by the same amount on average. This will enhance the C IV FWHM relative to the Hα/Hβ FHWM by ∼15 per cent and increase the size of the correction which must be applied to the C IV-based BH masses by ∼30 per cent.

Measuring the quasar systemic redshift

An accurate measure of the quasar's systemic redshift is required in order for the blueshift of the C IV emission line to be determined. Balmer emission centroids, where the centroid, λ_{half}, is the wavelength that bisects the cumulative total flux, are available for all quasars in the catalogue and so we use this to define the systemic redshift.

For 83 and 120 quasars in the Hα and Hβ samples respectively narrow [O III] emission is also detected. In the model fit to the Hβ region
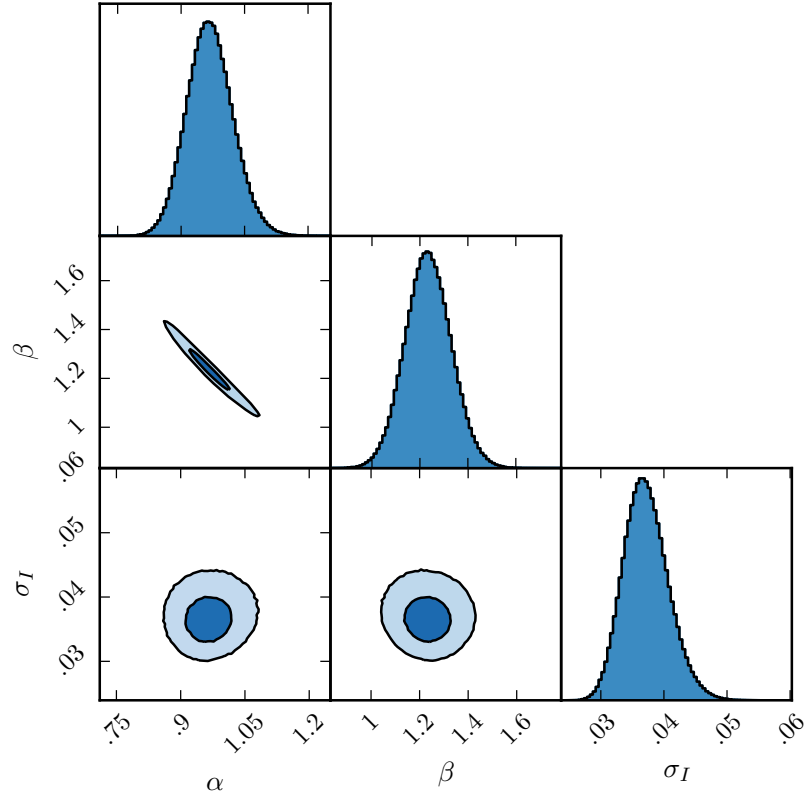
Figure 16: One- and two-dimensional projections of the MCMC sampling of the posterior distribution from the fit in Fig. 15. α is the power-law index, 10^β is the normalisation, and σ_I is the intrinsic scatter. In the two-dimensional projections, 1- and 2-σ contours are shown.

the velocity centroids of the broad Hβ-line and the core component of the [O III] emission were deliberately determined separately. We find the intrinsic difference in the velocity centroids of the Balmer broad emission and the narrow [O III] emission to have a dispersion of 360km s^{-1}, which is very similar to the value found by Shen et al., (2016). However, the median velocity centroid of the narrow component of the [O III] emission is blueshifted by 270km s^{-1} relative to the centroid of the broad Balmer line. Applying our parametric model fitting routine to the composite spectrum from Hewett and Wild, (2010), which is constructed using relatively low redshift SDSS quasars with $L_{Bol} \sim 10^{44}$ erg s^{-1}, the centroids of the broad component of Hβ and the narrow component of [O III] are found to be at essentially identical velocities, suggesting that the blueshifting of narrow [O III] could be luminosity dependent. Regardless, since both the systematic offset and the scatter are small in comparison to the dynamic range in C IV blueshifts, the blueshift-based empirical correction we will derive does not depend on whether the broad Balmer emission or the [O III] centroid is used to define the systemic redshift.

Balmer/C IV line widths as a function of C IV-blueshift

In this section we directly compare the C IV and Hα/Hβ line widths as a function of the C IV blueshift. Because virial BH mass estimates are generally based on the Hβ FWHM, we first convert our Hα FWHM measurements to equivalent Hβ FWHM using Eq. 5. In Fig. 17a and b we show the C IV FWHM relative to both the (Hβ-scaled) Hα FWHM and the Hβ FWHM, as a function of the C IV blueshift.

Employing the same Bayesian fitting framework described in Section 3.4.1, we fit independent linear models to the C IV FWHM relative to the Hα and Hβ FWHM as a function of the C IV blueshift. As before, our model has an additional parameter representing any intrinsic scatter in the relationship between the variables which is independent of measurement errors. We also tested a model where some fraction of the data points (which is free to vary) are drawn from an outlier distribution, represented by a broad Gaussian centered on the mean of the data. We found, however, that the inferred outlier fraction was very low (0.004, corresponding to ~0.7 data points) and so did not include such a component in our model.

In Fig. 18 we show the one- and two-dimensional projections of the posterior distribution from the linear fit to the FWHM C IV/Hα ratio. The projections from the FWHM C IV/Hβ fit (not shown) have very similar appearances. In Fig. 17a we plot the maximum likeli-
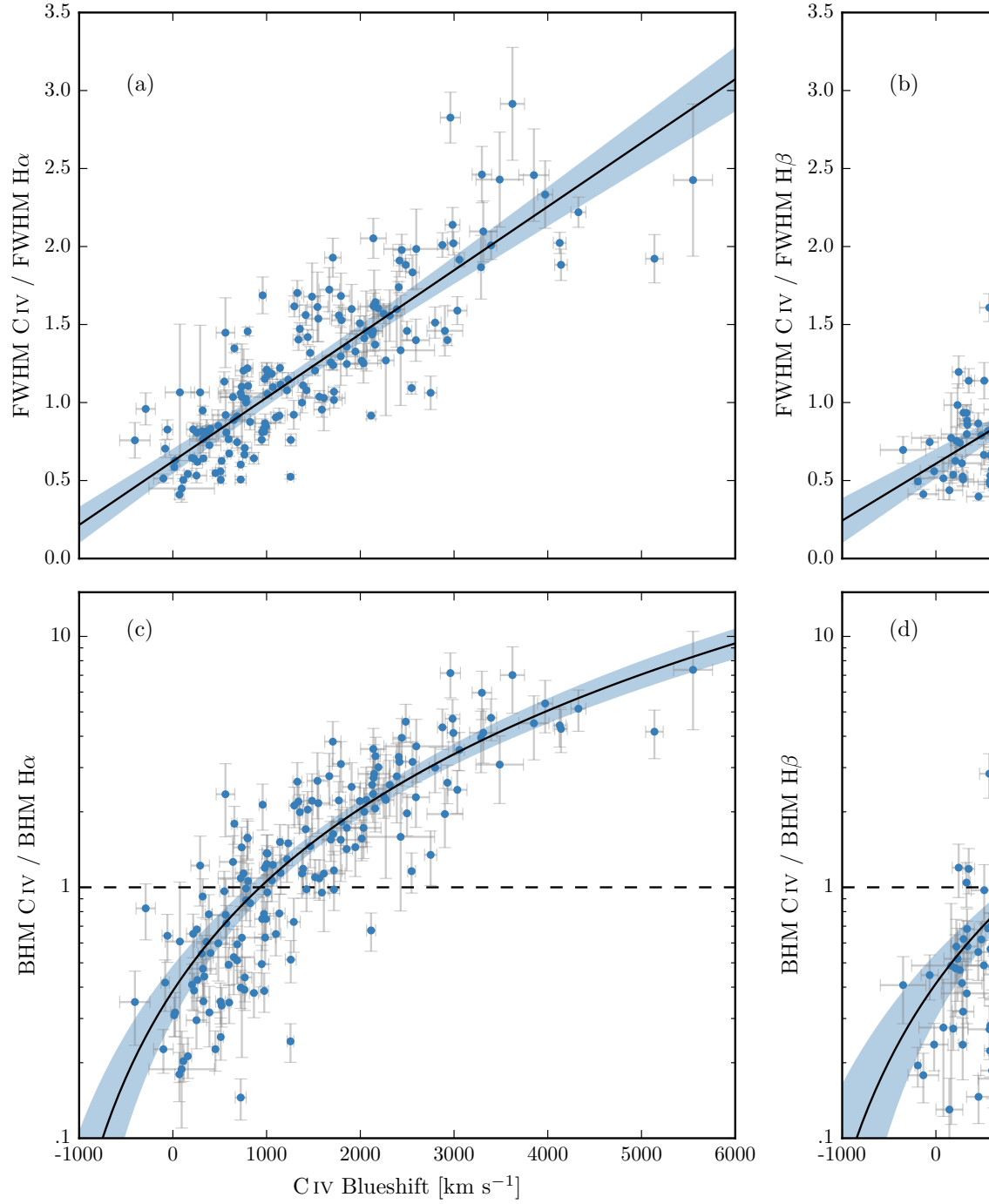
Figure 17: C IV FWHM relative to Hα FWHM (a) and Hβ FWHM (b), and C IV based BH mass (BHM) compared to Hα based mass (c) and Hβ based mass (d), all as a function of the C IV blueshift. The black line is our best-fit linear model, and the shaded region shows the 2-σ uncertainties on the slope and intercept. The Hα FWHM have been scaled to match the Hβ FWHM using Eq. 5.

hood model and the 2σ uncertainties on the model parameters. The maximum likelihood line is given by

$$\text{FWHM(C\,\textsc{iv}, Corr.)} = \frac{\text{FWHM(C\,\textsc{iv}, Meas.)}}{(0.41 \pm 0.02)\left(\frac{\text{C\,\textsc{iv} Blueshift}}{10^3\,\text{km\,s}^{-1}}\right) + (0.62 \pm 0.04)} \quad (6)$$

for the C IV/Hα fit and

$$\text{FWHM(C\,\textsc{iv}, Corr.)} = \frac{\text{FWHM(C\,\textsc{iv}, Meas.)}}{(0.36 \pm 0.03)\left(\frac{\text{C\,\textsc{iv} Blueshift}}{10^3\,\text{km\,s}^{-1}}\right) + (0.61 \pm 0.04)} \quad (7)$$

for the C IV/Hβ fit. The intercepts of the two relations are consistent, while the difference between the slopes is only marginally inconsistent given the quoted uncertainties.

The intrinsic scatter in the data about the linear relation we infer is 0.23 ± 0.02 and 0.25 ± 0.02 for the Hα and Hβ fits respectively. The intrinsic scatter for the Hα fit is represented by the Normal probability density distribution shown in Fig. 19. In the same figure we show the distribution of the orthogonal displacement of each data point from the best-fitting linear relationship. The two distributions are well-matched, which demonstrates that our model is a good representation of the data and the measurement errors on the data points are small relative to the intrinsic scatter.

The overall (intrinsic and measurement) scatter about the best-fitting model is slightly higher when the C IV line-widths are compared to Hβ (0.12 dex) than when compared to Hα (0.10 dex). This is likely due, at least in part, to the generally higher S/N of the Hα emission. In addition, contributions from the strong [O III] doublet in the vicinity of Hβ make de-blending the Hβ emission more uncertain. As a consequence, for quasars where Hα and Hβ are both measured, the mean uncertainty on the Hα FWHM is $130\,\text{km\,s}^{-1}$, compared to $340\,\text{km\,s}^{-1}$ for Hβ.

In the next section we use both the Hα and Hβ lines to calculate unbiased BH masses. We use the Hα measurements to derive an empirical C IV blueshift based correction to the C IV masses (Eq. 8) because of the issues related to the accurate modelling of the Hβ-profile just described. An extra advantage, which is evident in Fig. 17, is that the Hα sample has a better C IV blueshift coverage. However, as can be seen from the similarity of Equations 6 and 7, our results would not change significantly were we instead to use the Hβ sample.

C IV based virial BH mass estimates

We calculate virial BH mass estimates from C IV, Hα and Hβ using the widely-adopted Vestergaard and Peterson, (2006) scaling relations (their equations 5 and 7 for Hα/Hβ and C IV respectively). In Figs. 17c
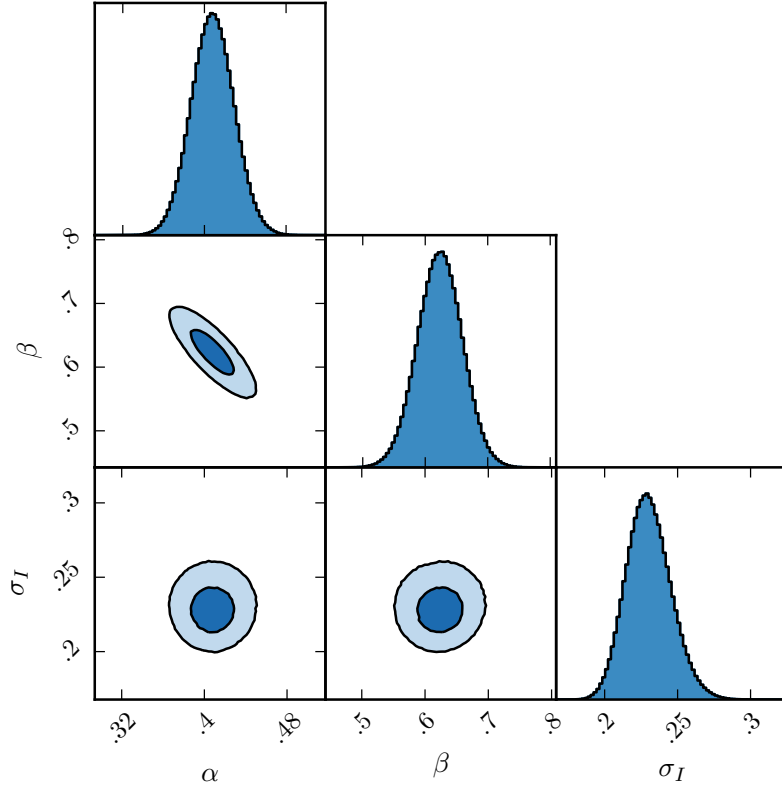
Figure 18: One- and two-dimensional projections of the MCMC sample of the posterior distribution for a linear fit to the FWHM C IV/Hα ratio as a function of the C IV blueshift. In the two-dimensional projections we show 1- and 2-σ contours. The posterior distribution for the linear fit to the FWHM C IV/Hβ ratio, which we do not show, has a very similar appearance.
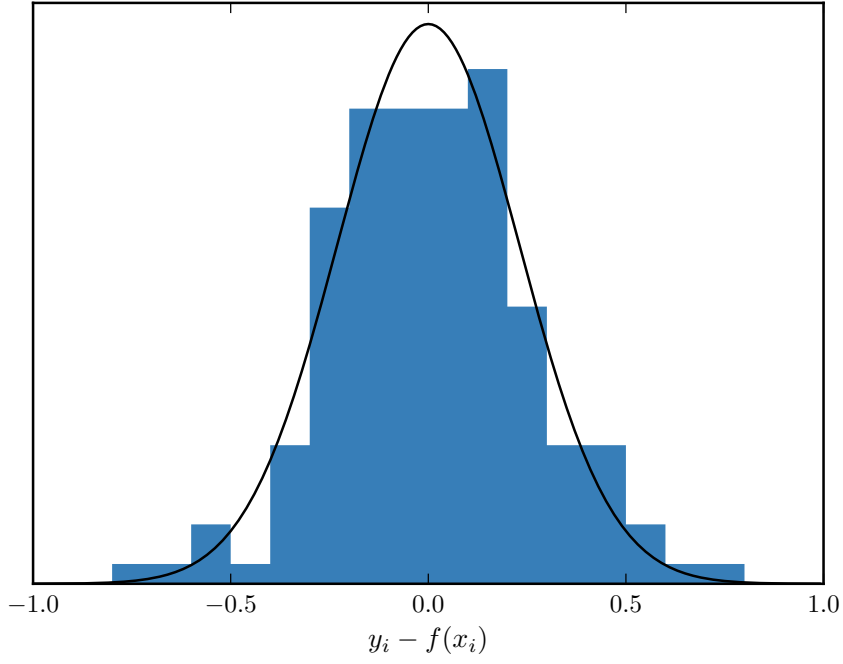
Figure 19: The distribution of the orthogonal displacement of each data point from the best-fitting linear relationship in the fit to FWHM(C IV)/FWHM(Hα) as a function of the C IV blueshift (blue histogram). The black curve is a Normal distribution with a width equal to the intrinsic scatter in the population inferred from the fit. The two distributions are well-matched, which demonstrates that our model is a good representation of the data and the measurement errors on the data points are small relative to the intrinsic scatter.

and d the C IV-based estimates are compared to the Hα/Hβ estimates as a function of the C IV blueshift. There is a strong systematic error in the C IV-based masses as a function of blueshift, which is a direct consequence of the FWHM trend described in the previous section. The C IV emission-based BH-masses are in error by a factor of more than five at $3000 \, \mathrm{km \, s^{-1}}$ in C IV emission blueshift and the overestimate of the BH-masses reaches a factor of 10 for quasars exhibiting the most extreme blueshifts, $\gtrsim 5000 \, \mathrm{km \, s^{-1}}$.

The virial product is the product of the virial velocity squared and the BLR radius (e.g. Shen, 2013), and is proportional to the BH mass. We use the corrected C IV FWHM given by Eq. 6 as an indicator of the virial velocity, and adopt the same $R - L$ relation for the $1350 \, \text{Å}$ continuum luminosity as Vestergaard and Peterson, (2006) (i.e. $R \propto L^{0.53}$). To find the constant scaling factor necessary to transform the virial product in to a BH mass we compute the inverse-variance weighted mean difference between the virial products and the Hα-based masses. The virial BH mass can then be expressed in terms of the corrected C IV FWHM and monochromatic continuum luminosity at $1350 \, \text{Å}$

$$\mathrm{MBH(C \, IV, Corr.)} = 10^{6.71} \left(\frac{\mathrm{FWHM(C \, IV, Corr.)}}{10^3 \, \mathrm{km \, s^{-1}}} \right)^2 \left(\frac{L_{-}(1350\text{Å})}{10^{44} \, \mathrm{erg \, s^{-1}}} \right)^{0.53}$$

(8)

Given measured C IV emission line FWHM and blueshift, equations 4 and 6 can then be used to provide an unbiased estimate of the quasar BH mass.

PRACTICAL APPLICATION OF THE C IV-BASED CORRECTION TO
    VIRIAL BH-MASS ESTIMATES

Recipe for unbiased C IV based BH masses

Equations 4 and 6 together provide an un-biased estimate of the virial BH mass given the FWHM and blueshift of C IV, together with the continuum luminosity at $1350 \, \text{Å}$. The FWHM is readily obtained, either directly from the data, or, via the fitting of a parametric model to the C IV-emission line. The blueshift – defined as the bisector of the cumulative line flux – is also straightforward to measure and our preferred procedure is described in Section 3.3.1. The only potential complication arises in establishing the quasar systemic redshift and hence defining the zero-point for the C IV-blueshift measurement, since both the blueshift and the systemic redshift cannot be determined from C IV alone. In practice, when rest-frame optical lines are accessible, as is the case for the quasar sample here, an accurate systemic redshift can be obtained. The [O III] doublet and the Balmer lines all

have velocity centroids very close to systemic, and the same is true for the broad Mg II doublet. For quasars at very high redshifts, $z \sim 6$, systemic redshifts can also be derived using the [C II] 158 μm emission in the sub-millimetre band (e.g. Venemans et al., 2016). However, in general, for example in determining the BH-masses of quasars at redshifts $z > 2$, if only the rest-frame ultraviolet region is available determining a reliable systemic redshift is non-trivial.

Shen et al., (2016) and our own work shows that there is an intrinsic variation of $\sigma \simeq 220 \mathrm{km\,s^{-1}}$ in the velocity centroids of the broad-line region relative to a systemic-frame defined by the quasar narrow-line regions. As we showed in Paper I, the SDSS DR7 pipeline redshifts are not sufficiently reliable to measure the C IV blueshift accurately because, in part, the C IV emission line itself contributes to the determination of the quasar redshifts (see figure 1 in Paper I). The redshift-determination scheme of Hewett and Wild, (2010) provided much improved redshifts for the SDSS DR7 quasar catalogue, not least because the redshift estimates for the majority of quasars were derived using emission-lines other than the C IV-line itself. The redshifts for quasars in the SDSS DR10 and DR12 catalogues (Pâris et al., 2014; Pâris et al., 2017) possess errors of $\simeq 500\text{-}750 \mathrm{km\,s^{-1}}$ (Pâris et al., 2012; Font-Ribera et al., 2013). The impact of low spectrum S/N for fainter quasars in all the SDSS data releases increases the uncertainty further. Table 8 includes the values for the fractional error in the corrected BH-mass that result from a given error in the determination of the systemic rest-frame. For example, the fractional error in the corrected BH mass is 0.39 for a quasar with a $1000 \mathrm{km\,s^{-1}}$ C IV blueshift when there is a $500 \mathrm{km\,s^{-1}}$ uncertainty in the quasar systemic redshift.

Of potentially more significance for studies of BH-masses as a function of quasar and host-galaxy properties are redshift errors that depend on the form of the quasar ultraviolet SED. The redshifts from Hewett and Wild, (2010) still suffer from systematic errors that are correlated with the shape, and particularly the blueshift, of the C IV emission line. For the Hewett and Wild, (2010) redshifts, and ultraviolet emission-line based redshifts in general, quasars with large C IV EW and modest blueshifts have relatively small ($\simeq 300 \mathrm{km\,s^{-1}}$) SED-dependent redshift errors. Redshift uncertainties as large as $\simeq 1000 \mathrm{km\,s^{-1}}$ for such quasars are unusual and the large relative error in the corrected C IV BH-mass given in Table 8 is pessimistic.

Conversely, systematic redshift errors are greatest for quasars with large blueshifts, reaching $\sim 750 \mathrm{km\,s^{-1}}$ in the extreme for the Hewett and Wild, (2010) values. The associated error in the corrected C IV BH-masses is, however, mitigated somewhat due to the smaller gradient of the MBH(C IV)/MBH(Balmer) relation at large C IV blueshift (see Fig. 17). A definitive quantification of any systematic SED-dependent errors present in the quasar redshifts contained in the SDSS DR12 catalogue is not yet available but the principal component analysis

Table 8: The fractional error on the corrected BH mass as a function of C IV blueshift for different uncertainties in the quasar systemic redshift.

δv (km s^{-1})	C IV blueshift (km s^{-1})			
	0	1000	2000	4000
250	0.33	0.20	0.14	0.09
500	0.65	0.39	0.28	0.18
1000	1.30	0.79	0.57	0.36

(PCA) based redshift estimates are expected to be largely free of SED-dependent systematics. Given the importance of generating more accurate redshifts for the SDSS DR7 and DR12 quasar samples we will publish a catalogue of more accurate redshifts in due course (see Section 3.6).

Systematic trends in residuals

The scatter about the best-fitting line in the C IV/Hα FWHM versus C IV-blueshift relation is ~0.1 dex, an order of magnitude smaller than the size of the C IV-blueshift dependent systematic but, nevertheless, still significant. With a view to reducing the scatter further, we searched for measurable parameters which correlate with the scatter at fixed C IV blueshift, including the luminosity, redshift, [O III] equivalent width (EW), and Fe II EW. The only significant correlation we find is with the Hα FWHM (Fig. 20). Quasars with broad Hα lines tend to lie below the relation while quasars with narrow Hα tend to lie above it. One possibility is that this correlation is simply due to random scatter (either intrinsic or measurement error) in the Hα FWHM which, with the other quasar properties fixed, would naturally produce a correlation between FWHM(C IV)/FWHM(Hα) and FWHM(Hα). However, the fact that we see no such correlation between the model residuals and the C IV FWHM suggests that the Hα FWHM correlation could be revealing somthing more fundamental. The Hα/Hβ FWHM is part of 'eigenvector 1' (EV1), the first eigenvector in a principal component analysis which originated from the work of Boroson and Green, (1992). While a number of parameters have been considered within the EV1 context (e.g. Brotherton and Francis, 1999), Fig. 20 suggests that part of the scatter between the Balmer and C IV velocity widths might be attributed to differences in the spectral properties which are correlated with EV1 (Marziani et al., 2013).

The residuals and the Hα FWHM also correlate with the shape of the line (FWHM/σ, where σ is the dispersion, derived from the second moment velocity; e.g. Kollatschny and Zetzl, 2011; Kollatschny and Zetzl, 2013). The narrow lines are, on average, 'peakier' (with

FWHM/σ ≃ 1) than the broader lines (with FWHM/σ ≃ 2). The origin of the Balmer-line shape correlation is not clear but one possibility is an orientation-dependence of the Hα FWHM (e.g. Shen and Ho, 2014). In this scenario quasars with broader emission lines are more likely to be in an edge-on orientation relative to our line of sight.

At radio wavelengths, the morphology of the radio structure, parametrized in terms of 'core dominance' is believed, at least in a statistical sense, to be a proxy for the orientation of the accretion disk (e.g. Jackson and Browne, 1991). We matched our sample to the FIRST radio catalogue (White et al., 1997) in an attempt to identify orientation-dependent signatures. Following Shen et al., (2011), we classified quasars with matches within 5 arcseconds as core-dominated, while, if multiple matches were found within 30 arcseconds, quasars were classified as lobe-dominated. Twenty core- quasars and six lobe-dominated quasars resulted but no statistically significant differences in the Hα line-widths of the two samples were found. It should be noted that the sub-sample of radio-detected quasars is small and the effectiveness of the test is further compromised by the lack of radio-detected quasars at large blueshifts (see figure 14 of Richards et al., 2011, for example).

There are currently very few reverberation-mapping measurements of quasars with large C IV blueshifts. Looking to the future, the results of the large on-going statistical reverberation mapping projects (e.g. Shen et al., 2015; King et al., 2015) for luminous quasars at high-redshift will shed new light on the Balmer line emitting region of the BLR for quasars with a range of C IV blueshifts and lead to a greater understanding of the relation between the Balmer line profile and the BH mass.

Effectiveness of the C IV blueshift based correction to BH masses

Figure 21 demonstrates that our sample has an excellent coverage of the EW-blueshift parameter space in relation to SDSS DR7 quasars at redshifts $1.6 < z < 3.0$. The systematic offset to higher C IV blueshifts for our catalogue relative to the SDSS quasars as a whole is a result of the higher mean luminosity relative to the SDSS sample (Fig. 26). Our sample includes 21 quasars with C IV blueshifts $>3000 \mathrm{km\,s}^{-1}$, and extends to ~5000 km s^{-1}, i.e. at the very extreme of what is observed in this redshift and luminosity range. Our investigation thus demonstrates that the C IV-blueshift based correction derived in this paper is applicable to very high blueshifts. Conversely, there are no quasars in our catalogue with C IV blueshifts $\lesssim 0 \mathrm{km\,s}^{-1}$ and we caution against extrapolating the correction formula to negative blueshifts.

Figure 22 compares the C IV- and Hα-based BH masses before and after applying the blueshift-based correction to the C IV FWHM. Before the correction, the correlation between the C IV- and Hα-based BH masses is very weak, and the scatter between the masses is 0.4

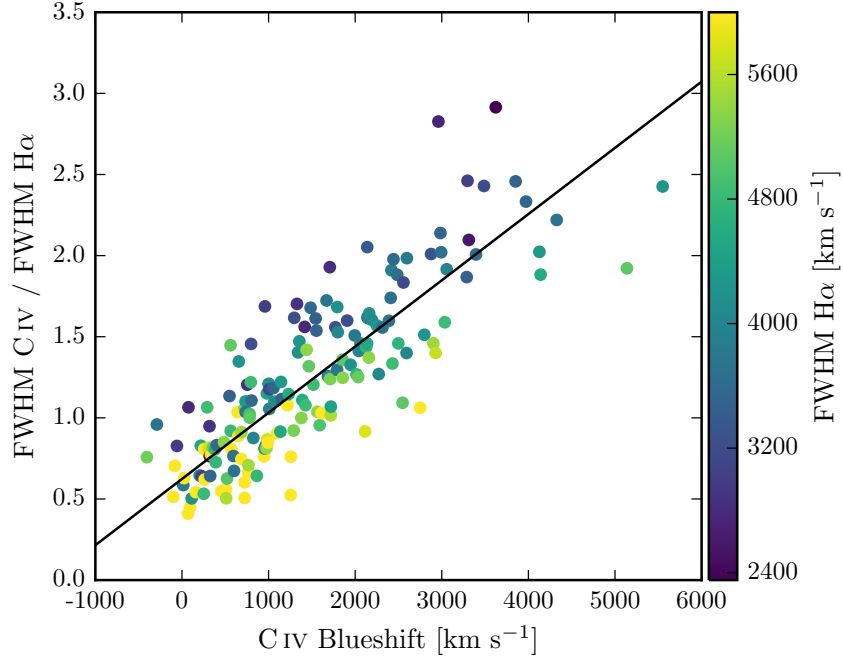Figure 20: Same as Fig. 17a, with the marker colour representing the Hα FWHM. At fixed C IV blueshift, there is a clear Hα FWHM dependent systematic in the model residuals.

dex. After correcting the C IV FWHM for the non-virial contribution, the correlation improves dramatically. The scatter between the corrected C IV-based masses and the Hα-based masses is reduced to 0.2 dex. The scatter is 0.24 dex at low C IV blueshifts ($\sim$0km s^{-1}) and 0.10 dex at high blueshifts ($\sim$3000km s^{-1}).

There has been a considerable amount of attention regarding the relative merits of using the FWHM or dispersion to characterise the velocity width (e.g. Denney et al., 2013). As we showed in Paper I, the line dispersion is relatively insensitive to the blueshift and shape of the C IV line. Therefore, without the blueshift information, using the line dispersion would yield a more accurate BH mass than the FWHM (Fig. 23). The correlation between the Hα and C IV line dispersion is, however, weak. The Pearson coefficient for the correlation is 0.36 (and just 0.15 when the Hβ measurements are used in place of Hα). Furthermore, there is little dynamic range in the line dispersion: the scatter is just 480 and 460km s^{-1} for Hα and C IV respectively. The observation suggests that the line dispersion does not fully trace the dynamic range in BH mass present in the quasar population. At least part of the reason is that the line dispersion is difficult to measure reliably in current survey-quality data, particularly because of the sensitivity to flux ascribed to the wings of the emission line (e.g. Mejía-Restrepo et al., 2016). Figures 22 and 23 demonstrate that estimating a reliable BH mass from the C IV FWHM and blueshift line is
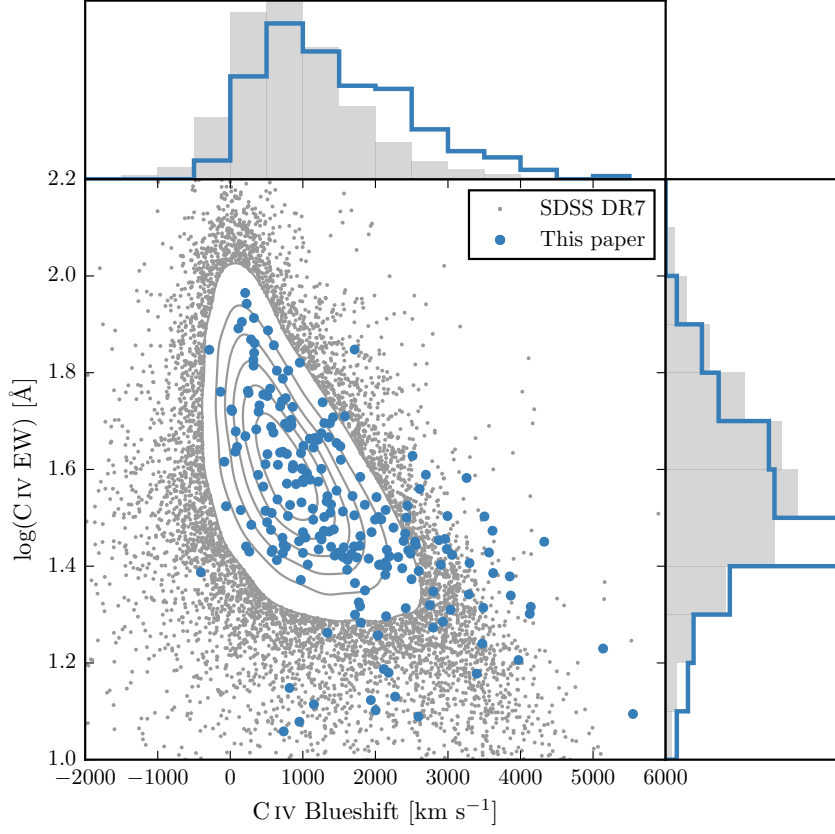
Figure 21: Rest-frame EW versus blueshift of the broad C IV-emission line for 32,157 SDSS DR7 quasars at $1.6 < z < 3.0$ (*grey*) and our sample (*blue*). For the SDSS quasars, the systemic redshifts used to calculate the blueshifts are from Hewett and Wild, (2010) and C IV emission properties are decribed in Paper I. In regions of high point-density, contours show equally-spaced lines of constant probability density generated using a Gaussian kernel-density estimator. Our sample has very good coverage; the shift to high blueshifts is a result of the high luminosity of our sample in relation to the SDSS sample and the correlation between luminosity and blueshift.
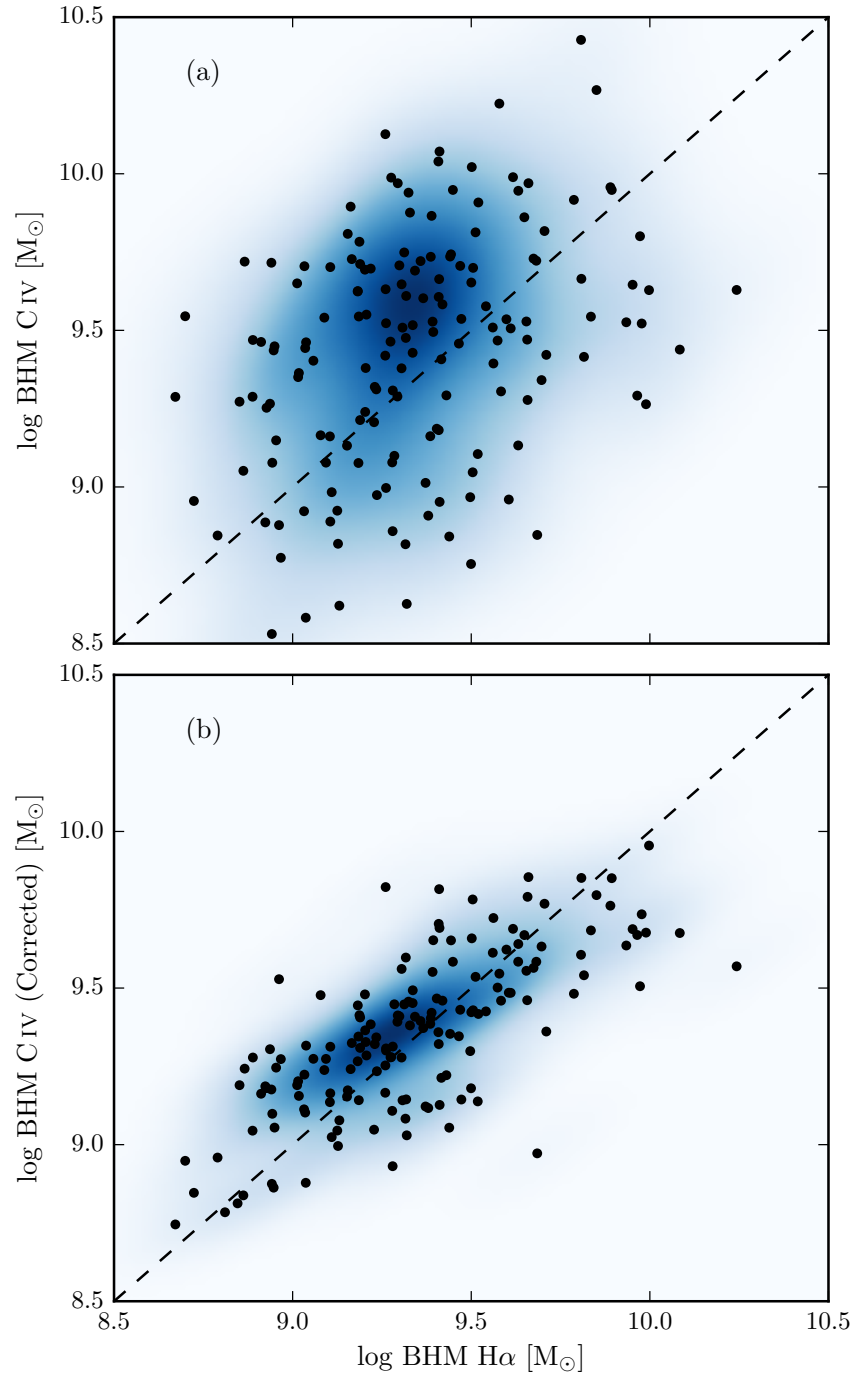
Figure 22: Comparison of the C IV- and Hα-based BH masses before (a) and after (b) applying the C IV blueshift-based correction to the C IV FWHM. The density of the plotted points (estimated using a Gaussian kernel density estimator) is represented by the colour. The correction to the C IV BH masses decreases the scatter by from 0.4 to 0.2 dex.
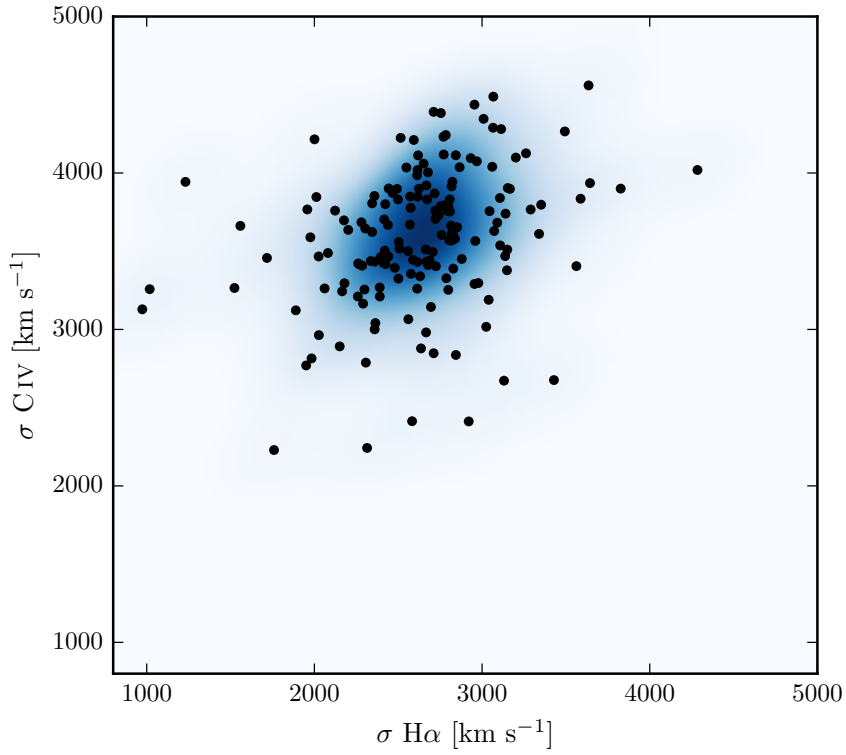
Figure 23: Comparison of the C IV and Hα line dispersion, σ. The density of the plotted points (estimated using a Gaussian kernel density estimator) is represented by the colour. Estimating a reliable BH mass from the C IV FWHM and blueshift line is substantially more effective than using the C IV line dispersion with, or without, the line blueshift. The C IV dispersion values are larger than the corresponding Hα measurements by a factor of 1.4 on average, which is consistent with reverberation mapping measurements (Vestergaard and Peterson, 2006).

substantially more effective than using the C IV line dispersion with, or without, the line blueshift.

Comparison to previous prescriptions

In Fig. 24 we compare the C IV blueshift-based correction presented in this paper to various prescriptions which have been proposed in the literature to derive BH masses from the C IV line which are consistent with the masses derived from the Balmer lines. In each case we compare the corrected C IV-based masses to the Hα-based masses as a function of the C IV blueshift. The correction proposed by Runnoe et al., (2013a) is based on the spectral region at rest-frame wavelengths of ~1400 Å (see below). Therefore, our analysis is based on the 123 quasars which satisfy this requirement.

In Fig 24a the C IV BH masses have been corrected using the C IV shape (FWHM/σ) based correction proposed by Denney, (2012). The correction is not applicable at large C IV blueshifts, since it was calibrated on a sample of low-luminosity AGN which does not include any such objects. Therefore, while the consistency between the Hα- and C IV-based masses at low C IV blueshifts is improved, at high C IV blueshifts the C IV-based masses remain seriously overestimated.

Runnoe et al., (2013a) used the continuum-subtracted peak flux ratio of the ultraviolet emission-line blend of Si IV+O IV (at 1400 Å) relative to C IV to correct for non-virial contributions to the C IV velocity-width. Following Runnoe et al., (2013a), we measure the peak flux by fitting a model with four Gaussian components (two for each emission line) to the continuum-subtracted flux. As is evident from Fig. 21, a correlation exists between the blueshift and equivalent width of C IV: C IV emission which is strongly blueshifted is typically weak. The Si IV+O IV emission-line blend, however, shows significantly less systematic variation. Therefore, the Si IV+O IV-based correction is quite effective in practice: the systematic bias in the C IV BH masses at large C IV blueshifts is reduced to a factor of ~ 2 (Fig. 24b). However, the C IV based masses are still systematically overestimated at large C IV blueshifts.

In contrast to the widely-used Vestergaard and Peterson, (2006) C IV-based virial BH mass calibration, the more recent Park et al., (2013) calibration significantly reduces the dependence of the derived masses on the emission-line velocity width (from the V^2 dependence predicted assuming a virialized BLR to just $V^{0.56}$). As a consequence, the C IV based masses of the quasars with large C IV blueshifts are much reduced (Fig. 24c). However, the systematic error in the C IV-based BH masses as a function of C IV blueshift remains.

As a comparison, the C IV-based masses shown in Fig 24d have been corrected using to the C IV blueshift-based procedure presented
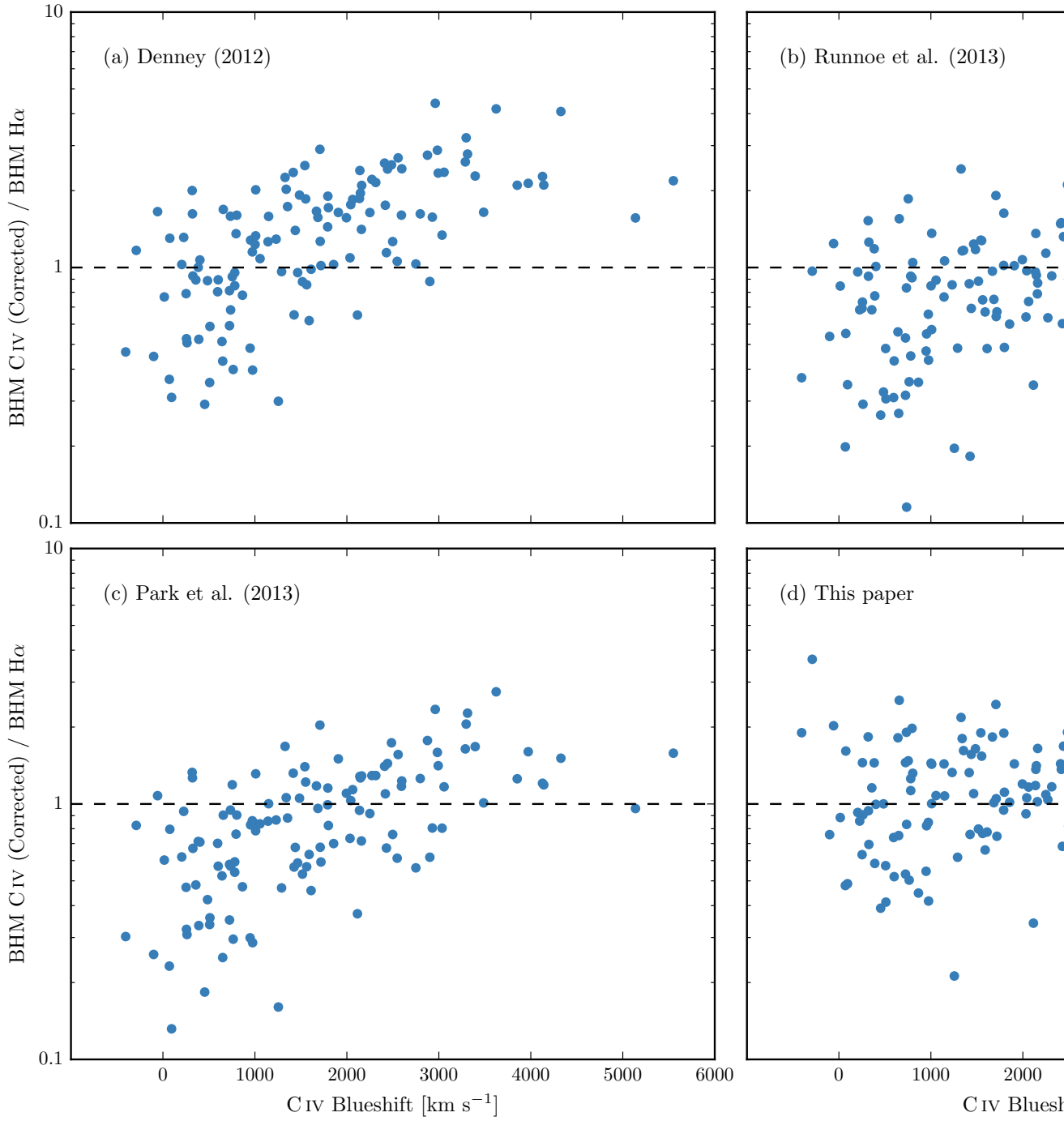
Figure 24: Comparison of BH mass estimates derived from C IV and Hα as a function of the C IV blueshift. Corrections to the C IV-based masses have been applied based on the shape (FWHM/σ) of the C IV emission line (a; Denney, 2012), the peak flux ratio of the Si IV+O IV blend relative to C IV (b; Runnoe et al., 2013a), by significantly reducing the dependence of the derived BH mass on the C IV velocity-width (c; Park et al., 2013), and based on the C IV blueshift (d; this paper).

in this paper. No systematic in the BH masses as a function of the C IV blueshift is evident.

CONCLUSIONS

The main results of this paper are as follows:

- We have analysed the spectra of 230 high-luminosity ($10^{45.5} - 10^{48}$ erg s^{-1}), redshift $1.5 < z < 4.0$ quasars for which spectra of the Balmer emission lines and the C IV emission line exist. The large number of quasars in our spectroscopic catalogue and the wide range in C IV blueshifts the quasars possess has allowed us to directly investigate biases in C IV-based BH mass estimates which stem from non-virial contributions to the C IV emission as a function of the C IV blueshift, which, in turn, depends directly on the form of the quasar ultraviolet SEDs (Richards et al., 2011).

- The C IV emission-based BH-masses are systematically in error by a factor of more than five at 3000km s^{-1} in C IV emission blueshift and the overestimate of the BH-masses reaches a factor of 10 for quasars exhibiting the most extreme blueshifts, $\gtrsim$5000km s^{-1}.

- We have derived an empirical correction formula for BH-mass estimates based on the C IV emission line FWHM and blueshift. The correction may be applied using equations 4 and 6 in Section 3.4.3. The large SED-dependent systematic error in C IV-based BH-masses is removed using the correction formulae. The remaining scatter between the corrected C IV-based masses and the Hα-based masses is 0.24 dex at low C IV blueshifts ($\sim$0km s^{-1}) and 0.10 dex at high blueshifts ($\sim$3000km s^{-1}). This is a significant improvement on the 0.40 dex scatter observed between the un-corrected C IV and Hα BH masses. The correction depends only on the C IV line properties - i.e. the FWHM and blueshift - and allows single-epoch virial BH mass estimates to be made from optical spectra, such as those provided by the SDSS, out to redshifts exceeding $z \sim 5$.

As discussed in Section 3.5.1, uncertainties in redshift estimation and hence the definition of the systemic rest-frame for quasars impact on the accuracy of the corrected BH-masses. Using published redshift estimates, notably those from Hewett and Wild, (2010) for the SDSS DR7 quasars and the BOSS PCA-based redshifts from Pâris et al., (2017) for SDSS DR12, the correction formula given in Section 3.4.3 produces significant improvements to C IV-based BH mass estimates. In a forthcoming work, Allen & Hewett (in preparation) will present

a new redshift-estimation algorithm that produces redshifts independent of the C IV blueshift and other variations in the ultraviolet SEDs of luminous quasars. Allen & Hewett will publish improved redshifts for all quasars in the SDSS DR7 and DR12 which will reduce SED-dependent systematic errors below the apparent inherent dispersion of $\simeq$ 220km s^{-1}associated with broad emission line redshifts (Shen et al., 2016). At the same time we will publish catalogues of unbiased BH masses for both SDSS DR7 and DR12 based on the Allen & Hewett redshifts. The components from the mean-field independent component analysis (see Allen et al., 2013, for an application to astronomical spectra) used in the Allen & Hewett redshift algorithm will also be published. With these components, if a rest-frame ultraviolet spectrum is available, it will be straightforward to determine the systemic redshift, via a simple optimisation procedure, and hence calculate the C IV blueshift.

COMPARISON TO SHEN

In this section we verify the accuracy of our parameter estimation scheme by comparing our FWHM measurements to measurements published in Shen et al., 2011, Shen and Liu, 2012 and Shen, 2016.

The parametric model we fit to the Hβ/[O III] emission region was very similar to the model employed by Shen, (2016). In Fig. 25a we plot our Hβ FWHM measurements against the measurements published in Shen, (2016), for 39 quasars in common to both samples. As expected, we observe a very tight correlation, with a scatter of 0.04 dex.

In Fig. 25b we plot our Hα FWHM measurements against the measurements published in Shen and Liu, (2012), for 51 quasars in common to both samples. There is a strong correlation and, although the scatter is larger than for the Hβ comparison (0.07 dex), no significant systematic bias.

Finally, in Fig. 25c we compare our measurements of the C IV FWHM from the 71 SDSS DR7 spectra in our sample with the measurements published in Shen et al., (2011). Shen et al., (2011) fit the C IV line profile with a composite model comprising up to three Gaussian components, whereas we used (up to order six) Gauss-Hermite polynomials. Nevertheless, there is a very strong agreement between our measurements, with a scatter of 0.05 dex.

4
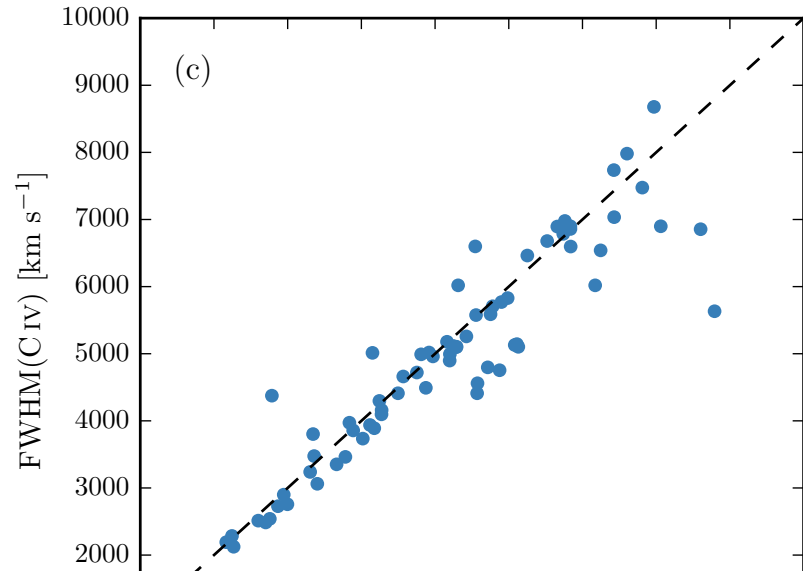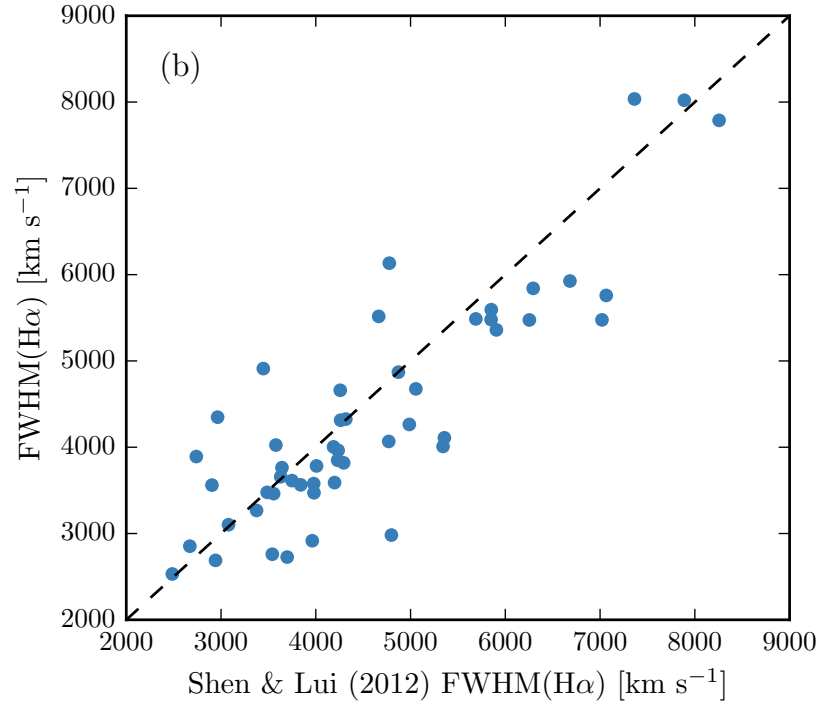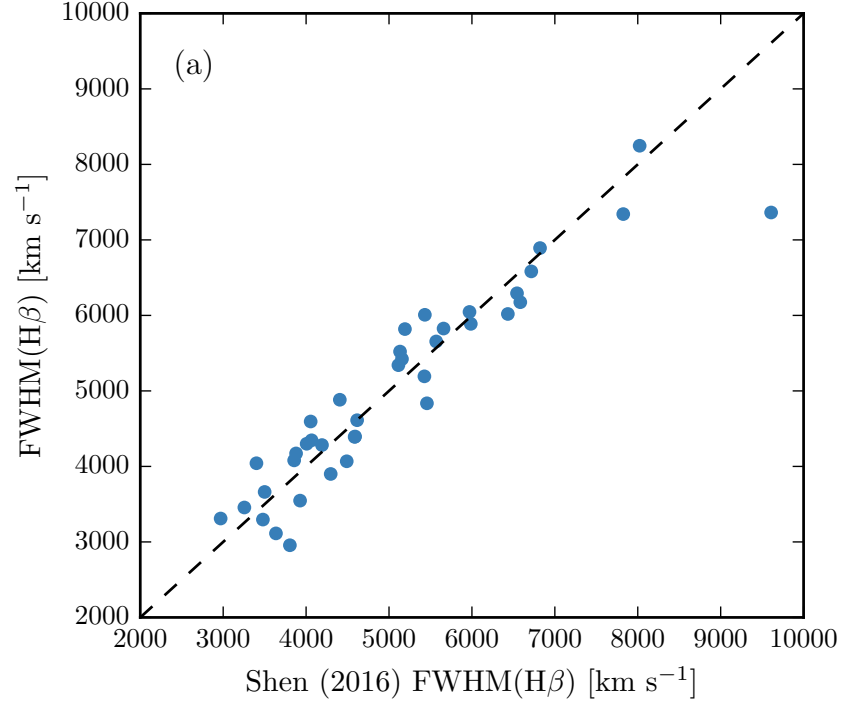
NARROW LINE REGION PROPERTIES

INTRODUCTION

Correlations between the masses of super-massive black holes and properties of the host galaxy bulges in nearby galaxies (Gebhardt et al., 2000; Ferrarese and Merritt, 2000) and the similarity of the cosmic evolution of star formation and black hole activity (Boyle and Terlevich, 1998; Madau and Dickinson, 2014) suggest that the formation and evolution of supermassive black holes and their host galaxies are linked. Active galactic nuclei (AGN) and quasar feedback, in which star formation in the host galaxy is supressed by the energy output from the quasar, is a favoured model. This has motivated a considerable amount of observational work searching for feedback signatures (for recent reviews, see Alexander and Hickox, 2012; Fabian, 2012; Heckman and Best, 2014).

The [O III]--4960,5008 doublet is the strongest feature found in optical quasar spectra. It is forbidden line which traces gas on kiloparsec scales. High velocity dispersions or strong asymmetries in forbidden lines are evidence of high velocity extended ionized outflows. Recent studies have provided constraints on the prevalence of ionized outflows traced by [O III] emission in low-redshift type 2 AGN (e.g. Mullaney et al., 2013; Zakamska and Greene, 2014) using spectra from the Sloan Digital Sky Survey (SDSS; York et al., 2000). However, the signatures of feedback are expected to be stronger at higher redshifts ($z \sim 2$) when the black hole accretion and star formation rates both peak.

In this paper we analyse the [O III] properties of a sample of 358 high-luminosity, redshift $1.5 < z < 4$ quasars. In particular, we search for signs of outflowing gas, which include assymetries and broad velocity widths. Recent near-IR spectroscopy of $z > 1.5$ quasars often report exceptionally large [O III] widths, with FWHM $> 1000 \mathrm{km\,s}^{-1}$ (e.g. Netzer et al., 2004; Nesvadba et al., 2008; Kim et al., 2013; Brusa et al., 2015; Carniani et al., 2015; Perna et al., 2015).

For a subsample where we have spectra covering the rest-frame ultra-violet line C IV, we can test whether the strong outflows, inferred the blueshifting of C IV relative to the systemic redshift, have any effect on the host galaxy on larger scales.

Throughout this paper we adopt a flat ΛCDM cosmology with $h_0 = 0.69$ and $\Omega_M = 0.29$.
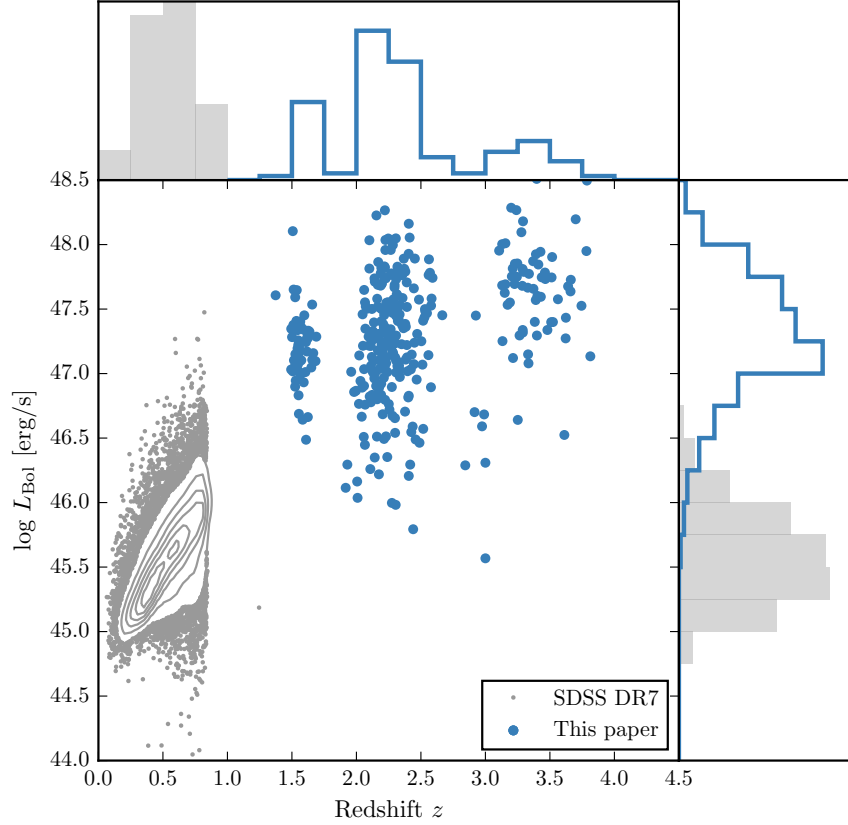
The paper is structured as follows.

Figure 26: The ranges in redshift and luminosity covered by our sample, relative to the redshift-luminosity distribution of the SDSS DR7 quasar catalogue with measured [O III] line properties (Shen et al., 2011). The gaps in our sample coverage at $z \sim 1.8$ and $z \sim 3$ are due to the near-infrared transmission windows. In regions of high point-density, contours show equally-spaced lines of constant probability density generated using a Gaussian kernel-density estimator.

QUASAR SAMPLE

We have assembled a catalogue of 358 high-luminosity, redshift $1.5 < z < 4$ quasars, with spectra taken in the near-infrared. At these redshifts the spectra cover the rest-frame optical region, which includes the broad Balmer Hβ line and the strong, narrow [O III] doublet. There is a significant overlap between the sample presented here and the one used in Coatman et al. (2016b), hereafter paper I. We briefly describe the catalogue below, but refer the reader to Coatman et al. (2016b) for further details, including the reduction procedure.

Two hundred are selected from the SDSS Seventh Data Release (DR7; Schneider et al., 2010). These are observed with LIRIS (Manchado et al., 1998) on the William Herschel Telescope (WHT), Triple-Spec (Wilson et al., 2004) on the Astrophysics Research Consortium

Table 9: The numbers of quasars with [O III] line measurements and the spectrographs and telescopes used to obtain the near-infrared spectra. Further details on the instrumental configurations are given in paper I.

Spectrograph	Telescope	Number
FIRE	MAGELLAN	32
GNIRS	GEMINI-N	29
ISAAC	VLT	8
LIRIS	WHT	5
NIRI	GEMINI-N	29
NIRSPEC	Keck II	3
SINFONI	VLT	76
SOFI	NTT	78
TRIPLESPEC	ARC-3.5m	27
TRIPLESPEC	P200	46
XSHOOTER	VLT	25
		144

(ARC) 3.5 m telescope, FIRE (Simcoe et al., 2010) on the Magellan-Baade telescope, the SINFONI integral field spectrograph (Eisenhauer et al., 2003; Bonnet et al., 2004) on the European Southern Observatory (ESO) Very Large Telescope (VLT), SOFI (Moorwood, Cuby, and Lidman, 1998) on the New Technology Telescope (NTT), and TRIPLE-SPEC on the Palomar 200-inch Hale telescope (P200). One hundred and seventeen were observed to measure accurate redshifts of quasar pairs at very close projected separations (Prochaska and Hennawi, 2009; Lau, Prochaska, and Hennawi, 2015; Hennawi et al., 2015). Spectra were taken with GNIRS (Elias et al., 2006) on the Gemini North telescope, ISAAC (Moorwood et al., 1998) on the European Southern Observatory (ESO) Very Large Telescope (VLT), NIRSPEC (McLean et al., 1998) on the Keck-II telescope, NIRI (Hodapp et al., 2003) also on Gemini North, and XSHOOTER (Vernet et al., 2011), again, on the VLT. Seventy-nine are bright Hamburg-ESO quasars observed with SINFONI, ninety are quasars with archival high-resolution optical spectra observed with SOFI, and four are observed with XSHOOTER and presented in the XQ-100 catalogue (Lopez et al., 2016).

As far as we are aware, this is the largest study of the narrow line region properties of high-z quasars ever undertaken. The redshift and luminosity coverage of the quasars in our sample is shown in Fig. 26, and the quasar sample is summarised in Table 9. Our sample covers much higher redshifts and luminosities than the SDSS sample.

PARAMETERIC MODEL FITS

In this section we describe how we measure the [O III] velocity-width and parameterize asymmeteries in the line. We first fit a parameteric model to the [O III] emission, and the nearby Hβ peak. This step is taken soley to enhance the signal-to-noise (SNR) of the spectra and to decompose the emission from Hβ and the [O III] doublet. We then calculate non-parameteric measures of the line profile from the best-fitting model.

Before the model can be fit, the spectra must first be transformed in to the (approximate) quasar rest-frame. This transformation is only for practical purposes and the emission line parameters we will go on to derive are independent of the exact redshift used. The redshift will later be refined using the results from the fit. The redshift used in this transformation is either derived from a multi-component Gaussian fit to the broad Hα emission (∼ 40 per cent of our sample) or, when this is not possible, from a preliminary fit to the broad Hβ emission (∼ 40 per cent) or narrow [O III] emission (20 per cent). **Should say whether we use peak/median etc.**

The continuum and optical Fe II emission is modelled and subtracted using a recipee that is identical to the one described in paper I. The following model is then fit to the spectra in the wavelength interval 4700-5100 Å. The fit is done as a function of the Doppler velocity shift, and we adopt the wavelength 4862.721Å (the laboratory Hβ wavelength) to transform wavelengths into equivalent Doppler velocities.

Hβ is modelled by two Gaussians with non-negative amplitudes and FWHM greater than 1200km s^{-1}. A handful we fix the centroids of the two Gaussians to be the same, normally because of very low S/N or because the blue wing is below the lower wavelength limit of the spectrograph. Any contribution to the Hβ emission from the narrow-line region is weak in the vast majority of our sample, and so we do not include an additional Gaussian component to model this emission. Note: we do in fact include narrow components for eight objects in our sample. Although, for some objects, this could bias our estimate of the velocity-width of the broad component, this information is not used in the analysis presented in this paper.

Each component of the [O III] doublet is fit with one or two Gaussians, depending on the fractional reduced χ^2 difference between the one- and two-component models. If the addition of the second Gaussian decreases the reduced χ^2 by more than 5 per cent then the double-Gaussian model is accepted. One hundred and twenty-five are fit with a single Gaussian, 147 with two Gaussians, and [O III] is undetected in a further 78 quasars. When a single Gaussian is used to model each line, the peak flux ratio of the [O III] 4960 Å and 5008Å components are fixed at the expected 1:3 ratio and the width and

Table 10: Approximate physical origin of the ICA components.

Component	Origin
w_1	Fe II
w_2	Hβ
w_3	Hβ
w_4	[O III] core
w_5	[O III] core
w_6	[O III] wing

velocity offsets are set to be equal. In the double Gaussian fit, the peak flux ratio of the second components is again fixed at 1:3, and the width and velocity offsets are again set to be equal.

In six quasars a significantly better fit was obtained by allowing the flux ratio between the two components to vary. In these quasars the best-fitting peak ratio varies from 0.50 to 0.84, with mean 0.70. **Check ICA component fits to see if this looks real.**

Model parameters were derived using a standard variance-weighted least-squares minimisation procedure employing the Levenberg-Marquardt algorithm. Prior to the fit, the spectra were inspected visually and regions significantly affected by telluric absorption or of low S/N were masked out.

However, the fits aren't always good. How to be quantative about this? Chi-squared values indicating bad fits? Also the fact that we sometimes model Fe as OIII. Discuss the limitations of using the Boroson & Greene template? Even if don't use results, should discuss Gaussian fits and their limitations, because that's what most people will be using.

Derived Parameters

All [O III] line properties are derived from the [O III]5008 emission, but, as described below, the kinematics of the peak at 4960Å are constrained by our fitting routine to be identical.

We do not to attach any physical meaning to the individual Gaussian components used in the model. While it is true that in some quasars the [O III] emission can be clearly separated in to a narrow component at the systemic redshift and a lower-amplitude, blueshifted broad component (e.g. Shen, 2016), often this decomposition is highly uncertain. Furthermore, often the S/N is not sufficient to statistically justify the addition of a second Gaussian component. Instead, we characterize the [O III] line profile using a number of non-parameteric measures, which are commonly used in the literature (e.g. Zakamska and Greene, 2014; Zakamska et al., 2016). A normalised cumulative velocity distibution is constructed from the best-fitting model,
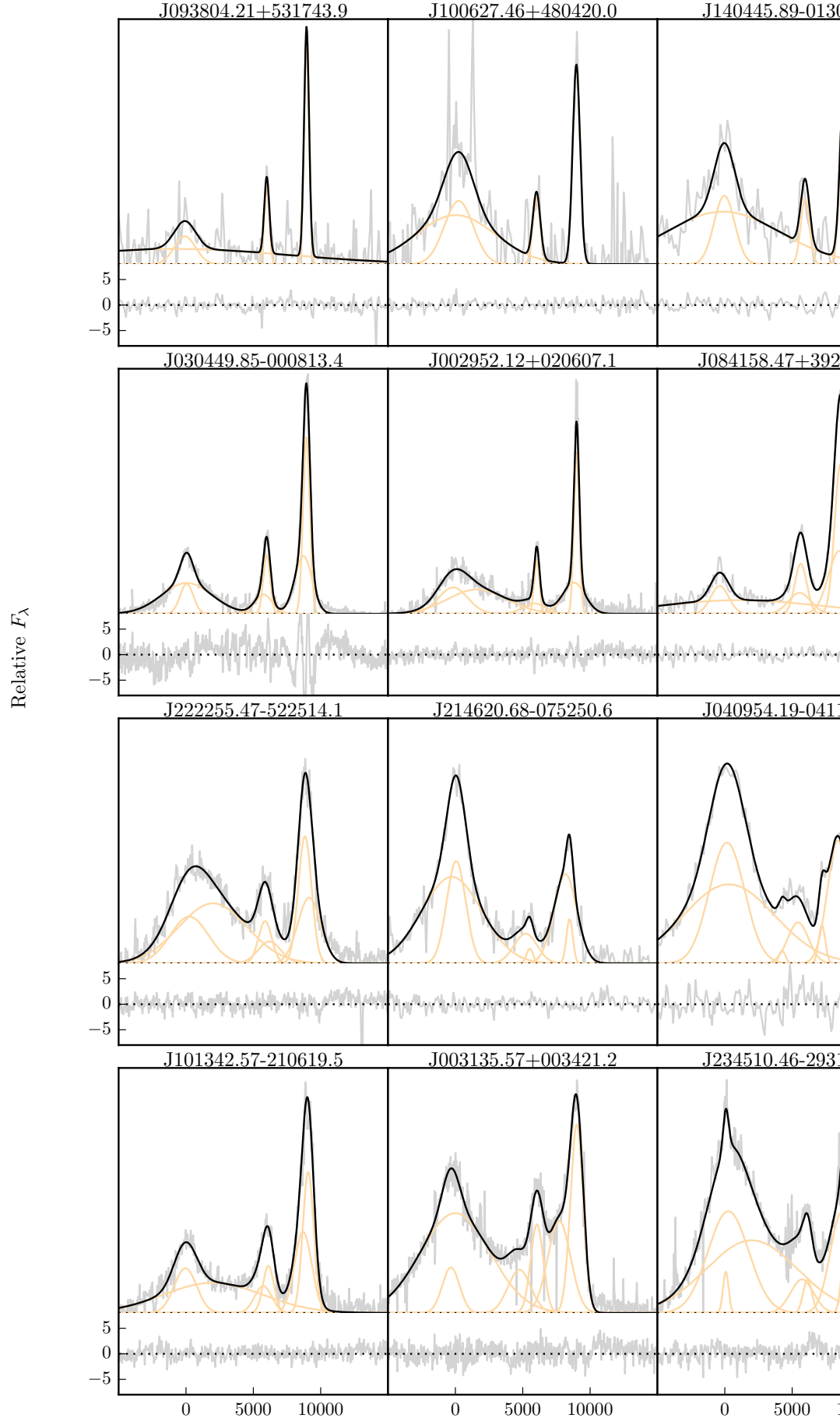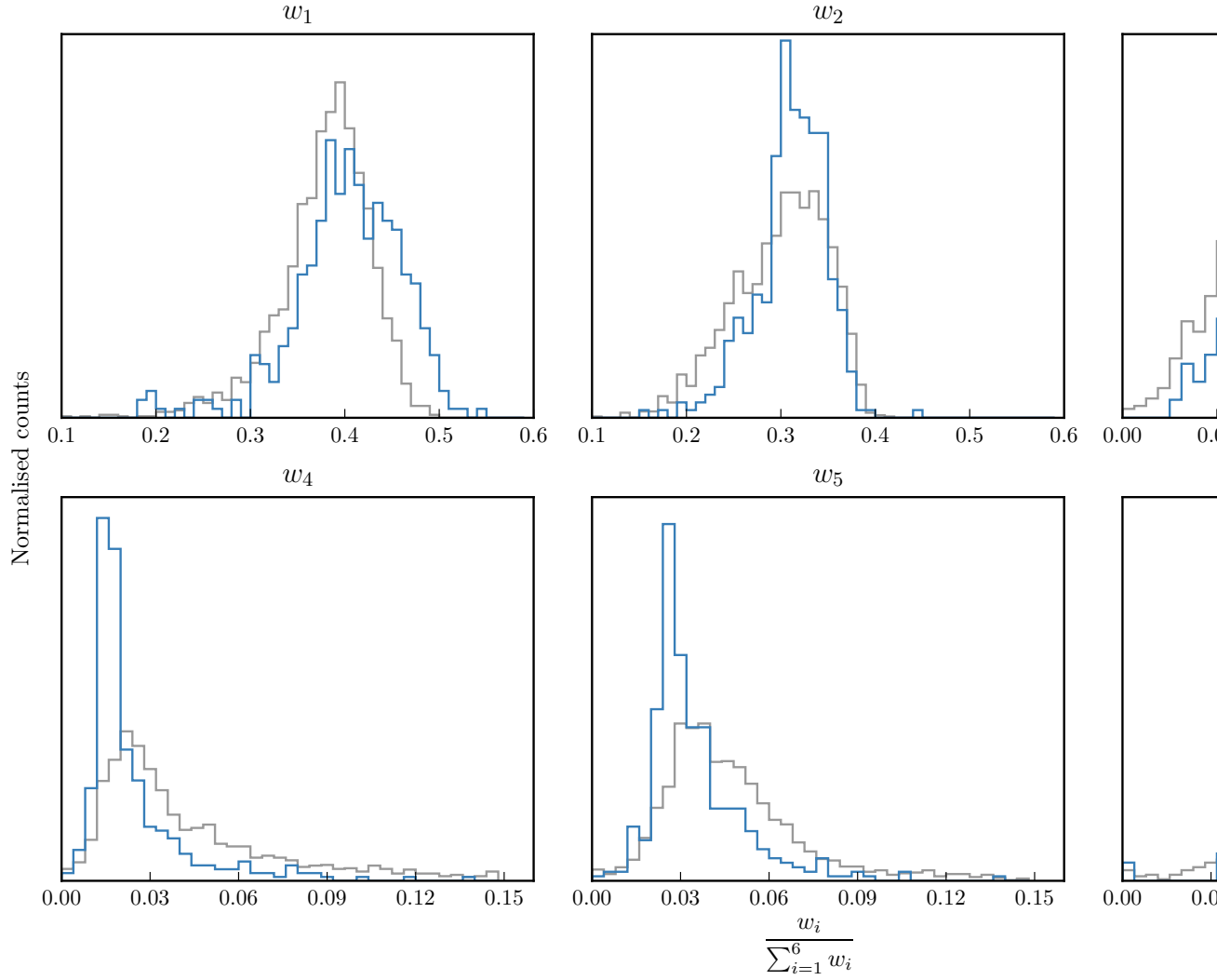
Figure 28: The relative weight in each of the six positive ICA components for the high-luminosity (blue) and low luminosity samples (grey). In the high-luminosity sample Fe II emission is stronger (component w_1). The core [O III] emission is weaker (components w_4, w_5) but the strength of the blueshifted wing is the same (w_6).
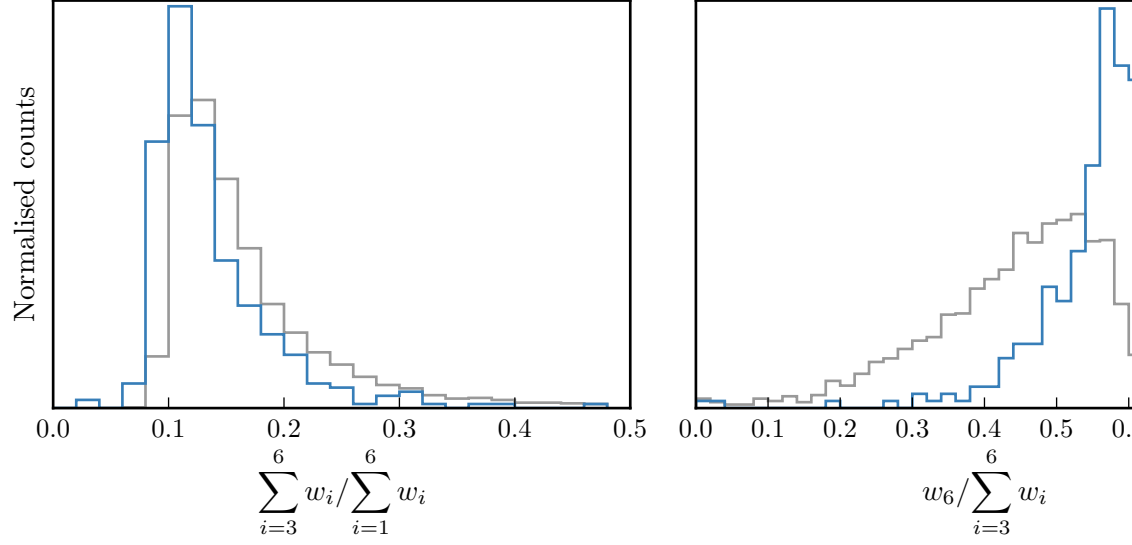
Figure 29: The relative weight in the three ICA components corresponding to [O III] emission (*left*) and the relative weight of the component most closely related to blueshifted [O III] emission relative to all three [O III] components (*right*). [O III] emission is weaker in the high-luminosity sample, but the relative contribution but the fractional contribution from the blueshifted component to the total [O III] emission is higher. Hence [O III] is weaker, broader, and more asymmetric in the high-luminosity sample. See Zakamska discussion.

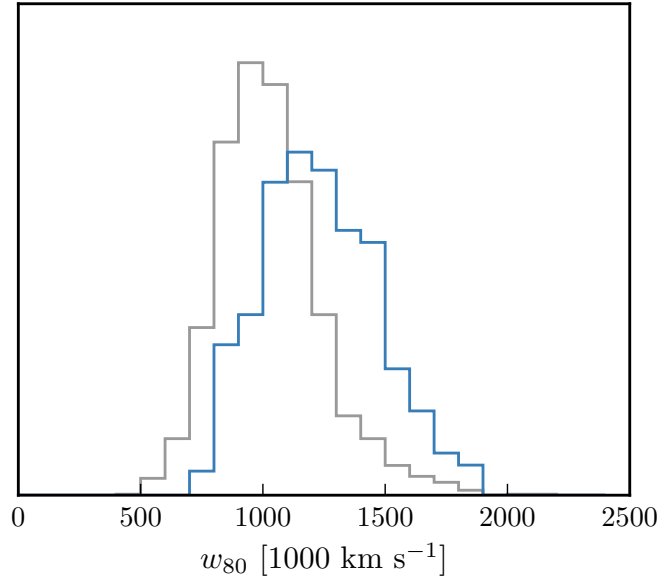Figure 30: Comparison of [O III] velocity-widths in the high and low luminosity samples using the ICA component fits. If keep this need to explain in text how w_{80} is calculated from ICA component fits.
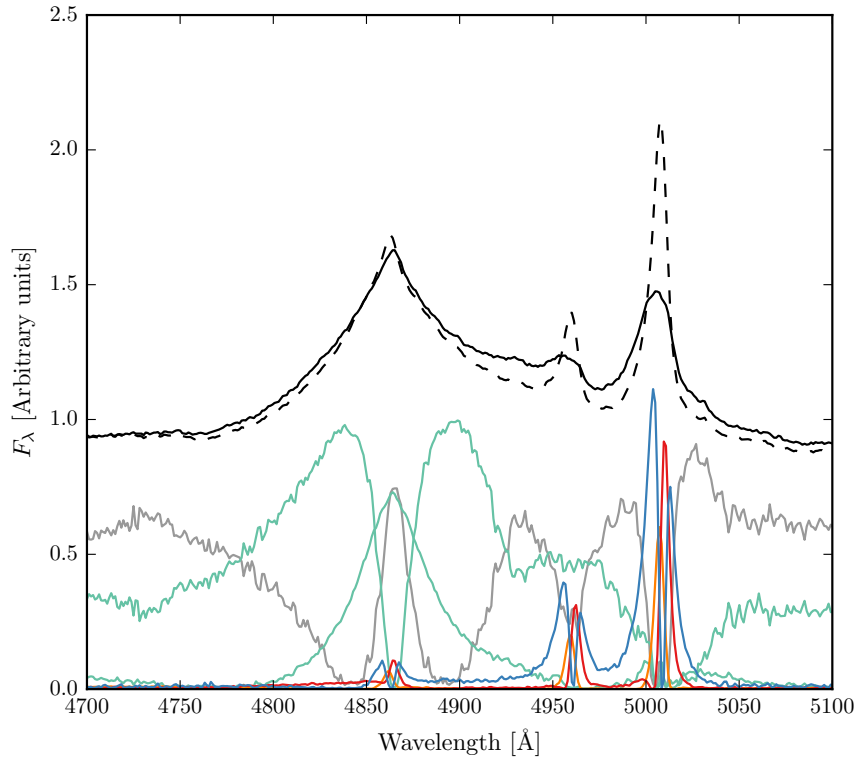
Figure 31: Black solid line is the median from the ICA fits to the high-luminosity sample. Black dashed line shows the median from the low-luminosity sample. The six positive ICA components are also shown.
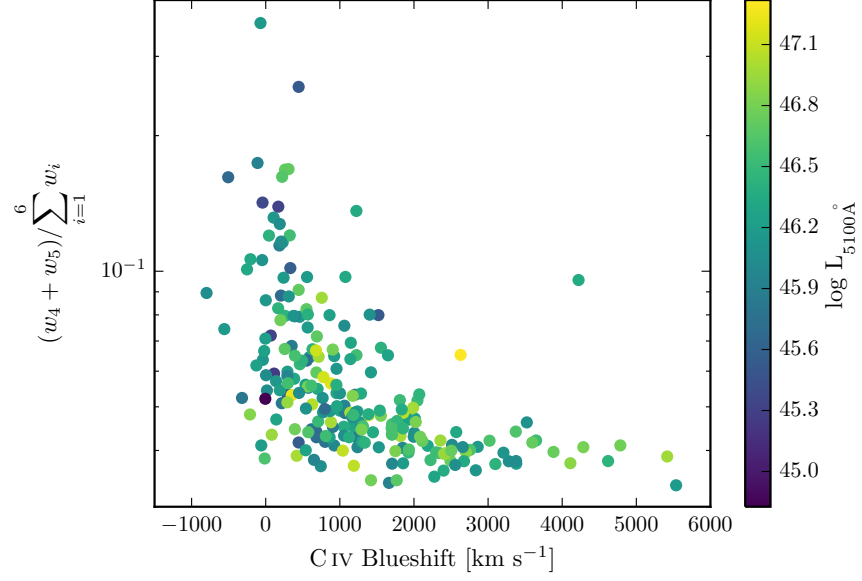
Figure 32: [O III] strength decreases as the C IV blueshift increases, I run in
to problems comparing the C IV blueshift to the [O III] blueshift
/ velocity-width. See similar thing if I use [O III] EQW instead.
Need to fix y ticks. Only showing the core components here. The
C IV blueshift is now measured relative to the NIR ICA redshift.
I think this is trend is mostly being driven by the Eigenvector 1
correlations: as the blueshift increases the Fe II strength increases
and the [O III] strength decreases. Doesn't appear to be driven by
the luminositiy. Is this tighter than EV1 trend shown with Fe/OIII
strength by other authors?
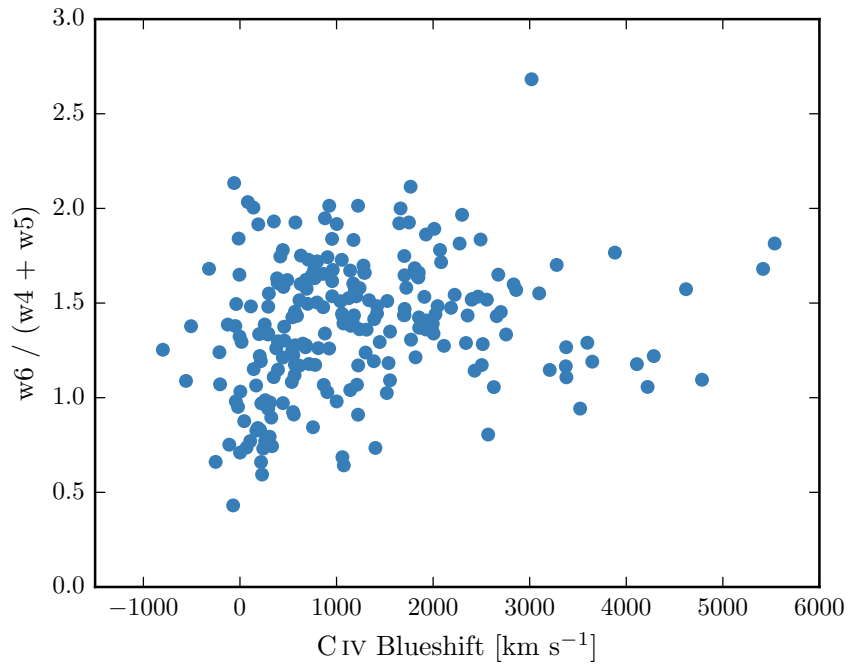
Figure 33: I think there is a trend here but at high blueshifts the OIII is un-
detected / very low S/N. Need to determin when we can believe
OIII paramters. Why at low CIV blueshift is there a much big-
ger dynamic range than in [O III] blueshifts in Fig. 13. Is it just
because we have more objects?
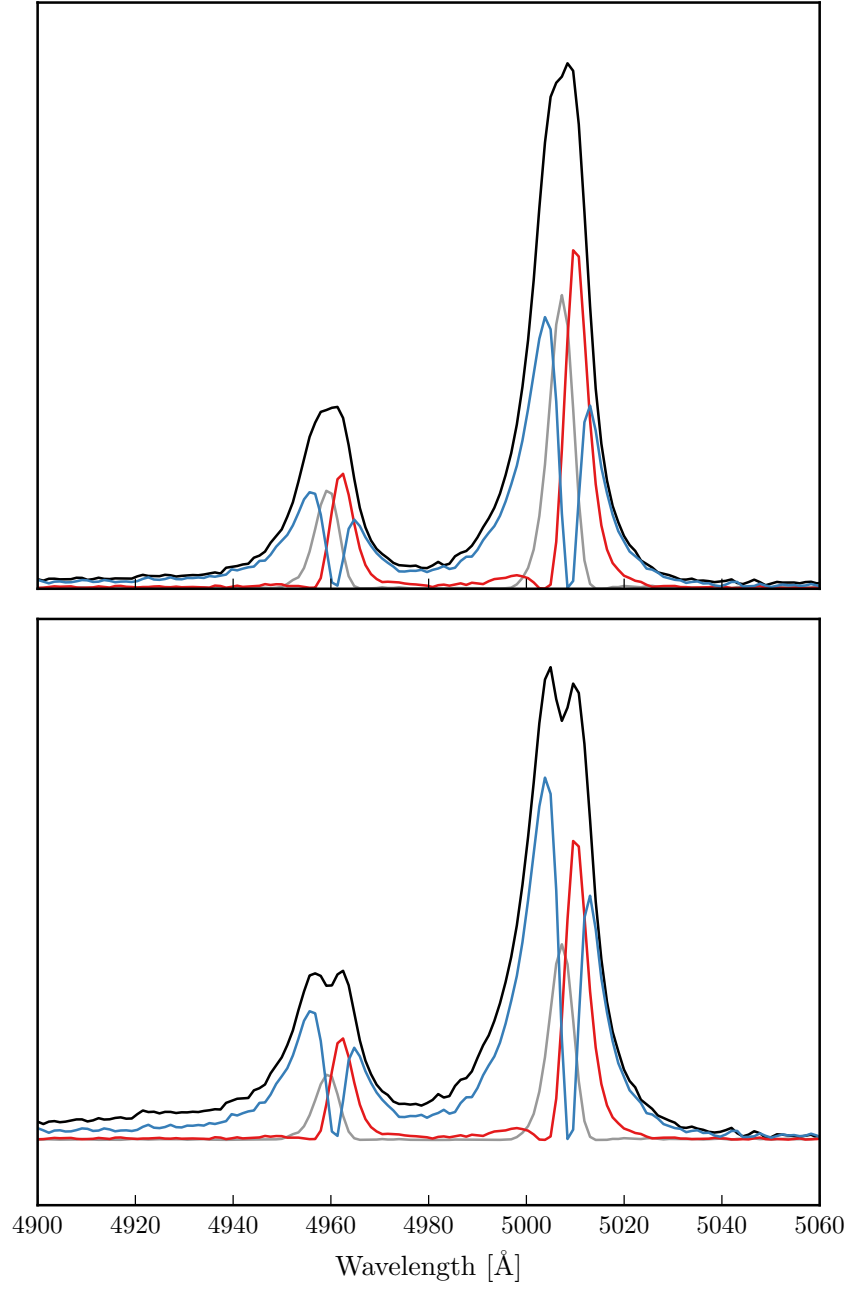
Figure 34: Comparison of median [O III] profiles from ICA fits it low- and high-luminosity samples.
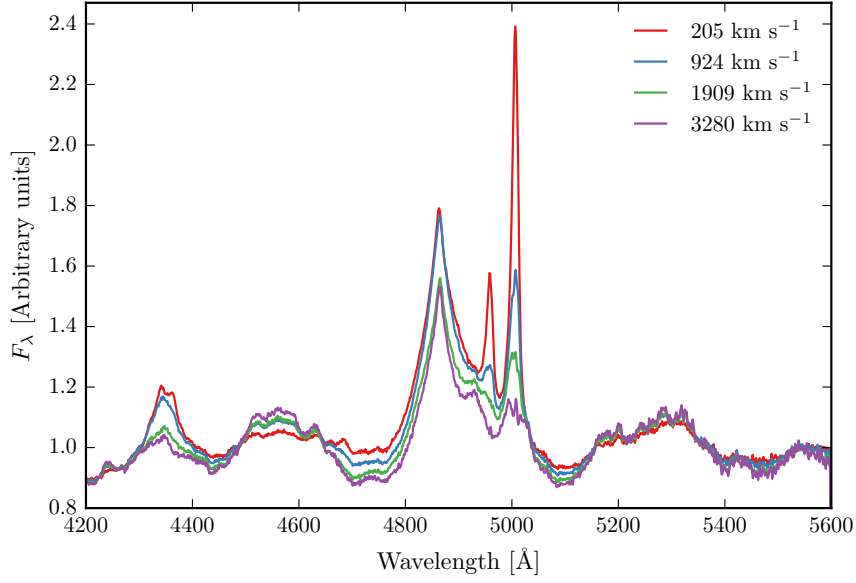
Figure 35: ICA median weights as a functino of the CIV blueshift.
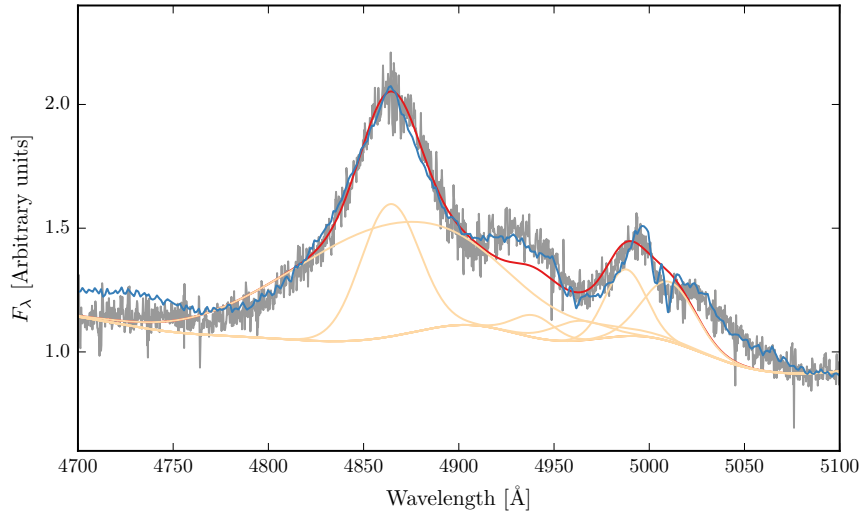
Figure 36: Example where poorly subtracting the iron can be confused with [O III].
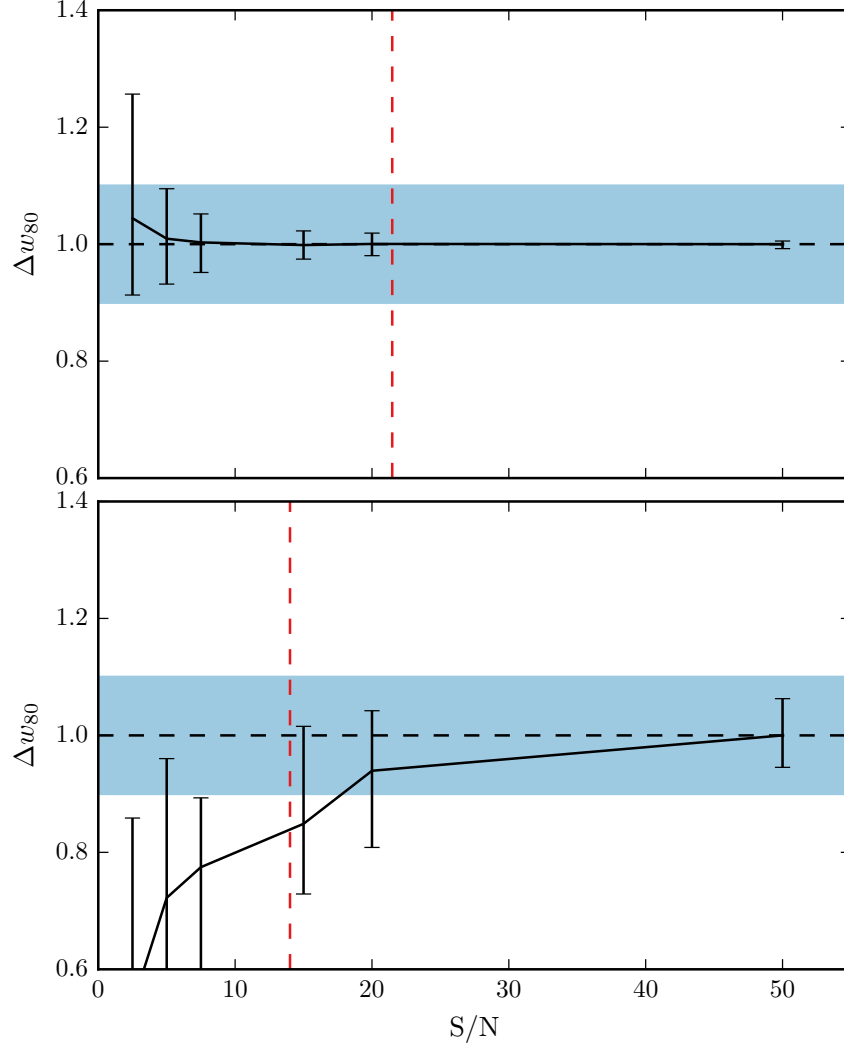
Figure 37

from which the velocities below which 5, 10, 25, 50, 75, 90, and 95 per cent of the total flux accumulates can be read off. The width of the emission line can then be defined, for example, using $w_{80} = v_{90} - v_{10}$. The absolute assymetry in the line profile A is defined as $((v_{95} - v_{50}) - (v_{50} - v_5))/(v_{95} - v_5)$ (Zakamska and Greene, 2014).

We also define the blueshift of the [O III] emission, which is a measure of the velocity shift of the profile from the expected position. This requires a measure of the observed line position, and an accurate measurement of the quasar systemic redshift. We use v_{10} to mesaure the location of the [O III] emission. Note that v_{50} is not suitable because when [O III] is low S/N we fit with single Gaussian.

The line width measures are not at present corrected for instrumental broadening, but this can easily be done.
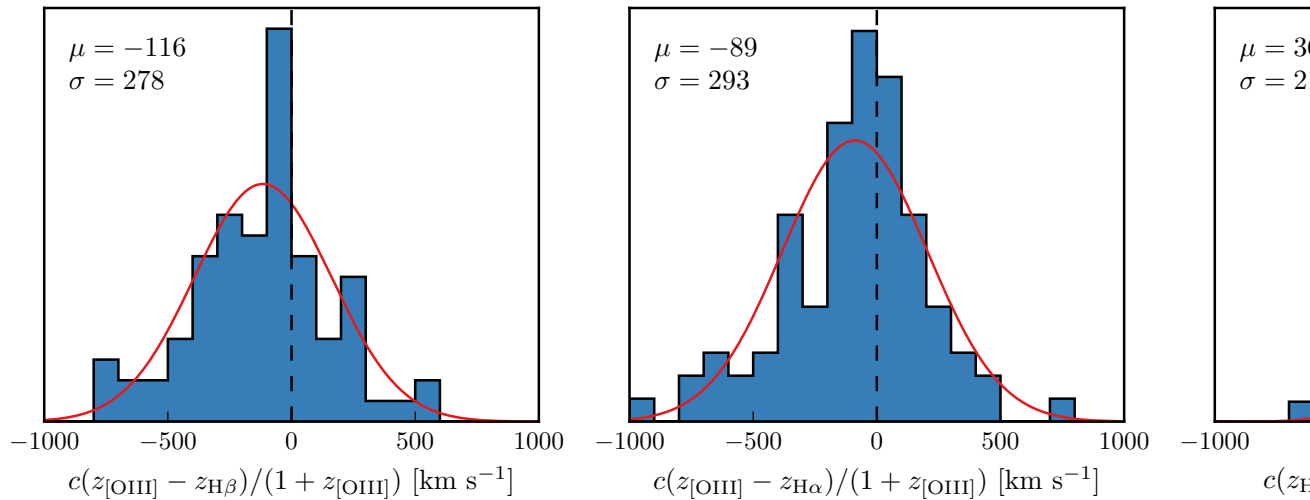
Figure 38: Redshift comparisons. Lots have been excluded from Ha/Hb so need to look at flags greater than one. What is the big peak?

Other flags

Flag 2

Low S/N. Includes some of the strong iron emitters.

Flag 3

74 objects where [O III] is undetected, although I don't have a rigorous definition of what this means. Merge with 2?

ICA COMPONENT FITS

What is the segue here? Sometimes Gaussians give poor fit? Not clear what is Hb, what is OIII, what is Fe? Show some examples of when the multi-Gaussian fits fail. Need to describe sample used in ICA component decomposition and briefly describe method (or refer to Allen & Hewett).

MEASURING THE QUASAR SYSTEMIC REDSHIFT

Explain flags Need to send paul redshifts

Hα

There are 224 quasars in our sample with spectra covering the Hα emission line. We discard seven of these from our sample because of very low S/N (<2.5 measured in the Hα line), leaving 217 To measure the

position of the line we fit a parametric model, which is very similar to the model described in Paper I. The continuum emission is first modeled and subtracted using the procedure described in Paper I. We then test five different models with increasing degrees of freedom to model the Hα emission. The model we select is the simplest model for which the fractional change in the reduced chi-squared from the model with the lowest reduced chi-squared is less than ten per cent.

The models we test are: (1) a single broad Gaussian; (2) two broad Gaussians with identical velocity centroids; (3) two broad Gaussians with different velocity centroids; (4) two broad Gaussians with identical velocity centroids, and additional narrower Gaussians to model the narrow Hα emission, and the narrow components of [N II]--6548,6584 and [S II]--6717,6731; (5) two broad Gaussians with different velocity centroids, and additional narrower Gaussians. If used, the width and velocity of all narrow components are set to be equal in the fit, and the relative flux ratio of the two [N II] components is fixed at the expected value of 2.96. The number of quasars fit by each model is: model 1 - 10; model 2 - 71; model 3 - 32; model 4 - 51; model 5 - 53. The redshift is then measured at the peak flux of the Hα model, including both the broad and narrow components of Hα if appropriate.

Bigger than expected uncertainty in Ha redshifts because of uncertain decomposition in to Hα broad/narrow and [N ii] emission?

ICA

The only sensible way to measure the systemic redshift is using the NIR ICA fit. Hα and Hβ seem to give no systematic offset but large scatter, and they are often asymmetric, so should only use peak. And Hα isn't always available, and have other narrow components need to decompose. O III peak is mostly fine to use, but then there are some objects where the whole line is blueshifted. And critically, at large CIV blueshifts the [O III] emission is often undetected. Can show comparison of NIR ICA redshifts to... Optical ICA? Hewett & Wild?

Should emphasise that most people use [O III] to get the most reliable systemic redshift. While this is fine at low luminosities, at high luminosities this can result in large errors (profile can be dominated by blueshifted component, Fe emission can be improperly subtracted, or [O III] might not be detected at all. Publish ICA components with this paper?

Can also describe what I found trying to get redshifts from broad Hα, Hβ? (Narrow components generally very weak at these luminosities so can't be used.) Generally find no systematic errors but large ($\sim$1000km s^{-1} scatter). Comparing NIR ICA to [O III] for the [O III] with high S/N I find small (few hundred km s^{-1}) scatter.

Should publish [O III] redshifts with this paper for people to use.

Parameter uncertainties and upper limits

Describe how uncertainties on best-fitting parameters were calculated.

In 78 quasars, or approximately 25 per cent of or sample, the [O III] is undetected, or detected with very low S/N. In this section we describe how upper limits on the [O III] equivalent width were calculated. Firstly, the best-fitting model comprising the continuum, Fe II, and Hβ emission is subtracted from the spectra, leaving behind only emission due to [O III]. From this spectra we generate 100 mock spectra, where the flux at each wavelength is randomly drawn from a Normal distribution with a mean equal to the flux convolved with a Gaussian of width $200 \mathrm{km\,s^{-1}}$ and a width equal to the known error. We then perform an error-weighted linear least-squares regression with an [O III] template derived from a fit to a very high S/N low redshift SDSS composite spectra. The equivalent width of the best-fitting model is recorded for each of the 100 realisations of the spectra. The error in the equivalent width is defined as the root-mean-square of these values.

Calculated uncertainties using Monte Carlo. Uncertainties on v10 are very large, which I think makes sense since the wing Gaussian will be appearing and disappering, giving a large dispersion in v10. Or regardles v10 is just very sensitive to the noise. Maybe I should be using v25 instead?

Absolute flux calibration of spectra and continuum luminosities

Relative flux-calibration of the infrared spectra as a function of wavelength has been achieved, to $\simeq 10$ per cent, through observations of appropriate flux standards. The absolute flux levels, however, can be in error by large factors due to variable atmospheric conditions combined with the narrow slit widths. For the majority of the quasars we have, therefore, established the absolute flux scale for each near-infrared spectrum using the same quasar SED-model fitting scheme employed in Paper I. Briefly, the SED-model was fit, with the normalisation and E(B-V) as free varibales, to optical/infrared magnitudes, or SDSS/BOSS spectra (check order I do this.) This allows us to extrapolate from the optical when we do not have photometric data in the near-infrared. The spectra were then normalised to the SED model using a linear error-weighted least-squares regression in the the regions of the spectra covered by the H/K bands. The monochromatic continuum luminosity at 5100Åwas calculated directly from the normalised SED-model. **If this sounds strange can also calculate from fit to normaised spectra. Check if any missing normalisation / monochromatic luminosities.**
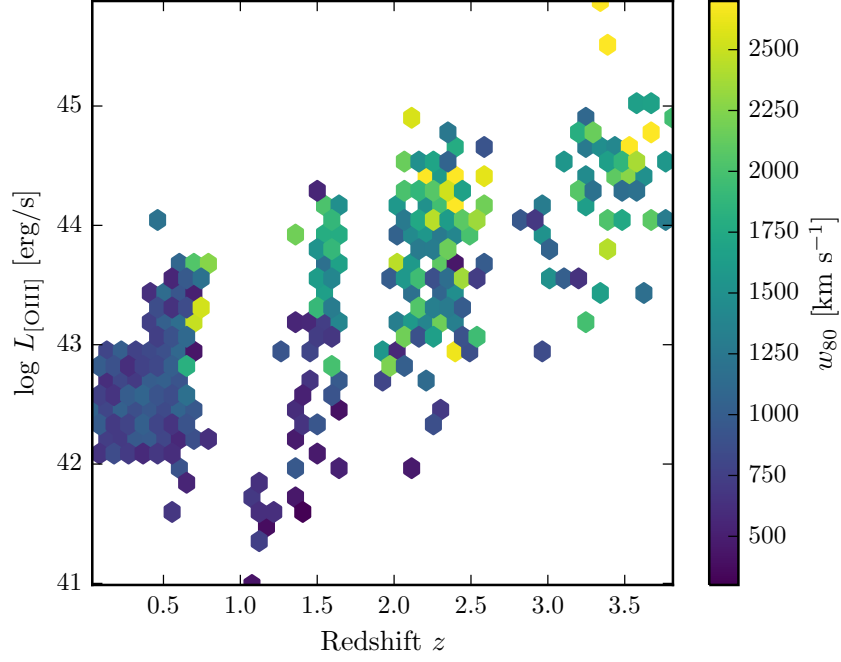
Figure 39: The [O III] velocity-width, characterised by w_{80}, as a function the [O III] luminosity and the quasar redshift. The color of each hexagon denotes the mean w_{80} for the obects in that luminosity-redshift bin. We have suplemented our sample with low-z objects from Zakamska and Greene, (2014) and medium (z ∼1.5) redshift objects from Harrison et al., (2016). If I keep this plot make sure its clear which points belong to which sample.

RESULTS FROM ICA FITS

Need to convince the reader that the ICA components approximately correspond to real components. Explain how non-parameteric measures derived form ICA reconstructions.

We find there is a decreasing symmetric component at high luminosities. Relates directly to Shen and Ho, (2014). A stable narrow line region is removed by the outflowing material. Shen and Ho, (2014) showed that the strength of the core [O III] component decreases with quasar luminosity and optical Fe II strength faster than the wing component, leading to overall broader and more blueshifted profiles as luminoisty and Fe II strength (or C IV blueshift) increases.

LUMINOSITY/REDSHIFT-EVOLUTION OF [O III] PROPERTIES

In this section we look for any luminosity/redshift dependent changes in the [O III] line properties. To do this we extend the dynamic range of our samples in terms of both luminosity and redshift by sup-

plementing our sample with quasars presented by Zakamska and Greene, (2014) and Harrison et al., (2016).

The Zakamska and Greene, (2014) objects are a sample of 568 obscured luminous quasars selected from SDSS (Reyes et al., 2008; Yuan, Strauss, and Zakamska, 2016). They are selected to have [O III] luminosities above $10^{8.5}L_\odot$ and have a median redshift $z = 0.397$.

We also include 40 quasars at redshifts $1.1 \leqslant z \leqslant 1.7$) from the KMOS AGN Survey at High redshift (KASHz) with [O III] line measurements.

We also have the same information for ~20 000 SDSS spectra from Mullaney et al., (2013).

In Figure 39 we show the [O III] velocity width as a function of the [O III] luminosity and the quasar redshift. The lack of any redshift-evolution between $z = 0$ and $z = 1.5$ was reported by Harrison et al., (2016). Our additional data suggests that this continues to $z \sim 2.5$. On the other hand, at fixed redshift, we see a significant correlation between the [O III] velocity width and the luminosity.

The fact that we don't see many broad lines in the Zakamska and Greene, (2014) objects even at luminosities >43 erg/s could be due to the fact that these are all type II quasars, whereas the sample presented in this paper are all type I. Mullaney et al., (2013) showed that the [O III] lines of type I quasars are typically broader than in type II quasars.

Looking at the [O III] velocity width as a function of luminosity tells us about the physical drivers of the outflows observed in [O III]. The correlation with luminosity suggests that the highest velocity outflows are associated with the most luminous AGN. This has been reported for low-redshift AGN, for both ionized and molecular outflows (e.g. Westmoquette et al. 2012; Veilleux et al. 2013; Arribas et al. 2014; Cicone et al. 2014; Hill & Zakamska 2014).

This suggests that the outflows are driven by radiative forces. On the other hand, Mullaney et al., (2013) find that once the correlation between the [O III] luminosity and the radio luminosity has been taken in to account, the [O III] velocity width is more strongly related to the radio luminosity of the AGN.

EQUIVALENT WIDTH

In Fig. 40 we show the [O III]5008 EW as a function of the quasar bolometric luminosity. Bolometric luminosity is estimated from the monochromatic continuum luminoisty at 5100Åusing the correction factor given by Richards et al., (2006a). For comparison, we also show the low-z sample from Shen et al., (2011).

The equivalent width of [O III] has been found to strongly decrease as a function of redshift and/or luminosity (e.g. Brotherton, 1996; Netzer et al., 2004; Sulentic et al., 2004; Baskin and Laor, 2005b).
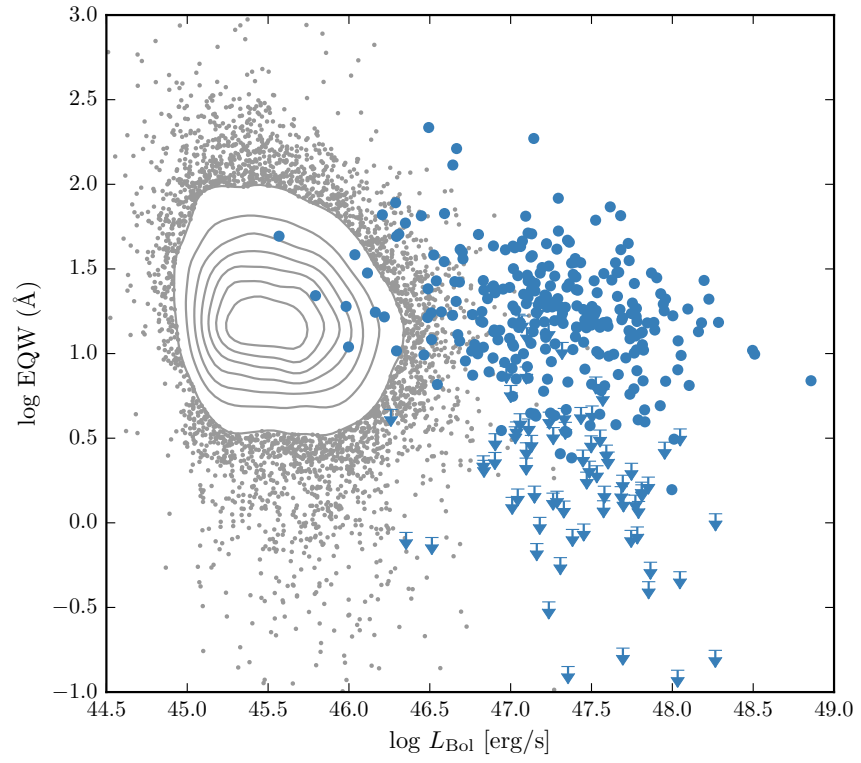
Figure 40: The [O III] EW as a function of the quasar bolometric luminosity for the sample presented in this paper (blue circles) and the low-z SDSS sample (grey points and contours). Upper limits are denoted by the downward arrows.
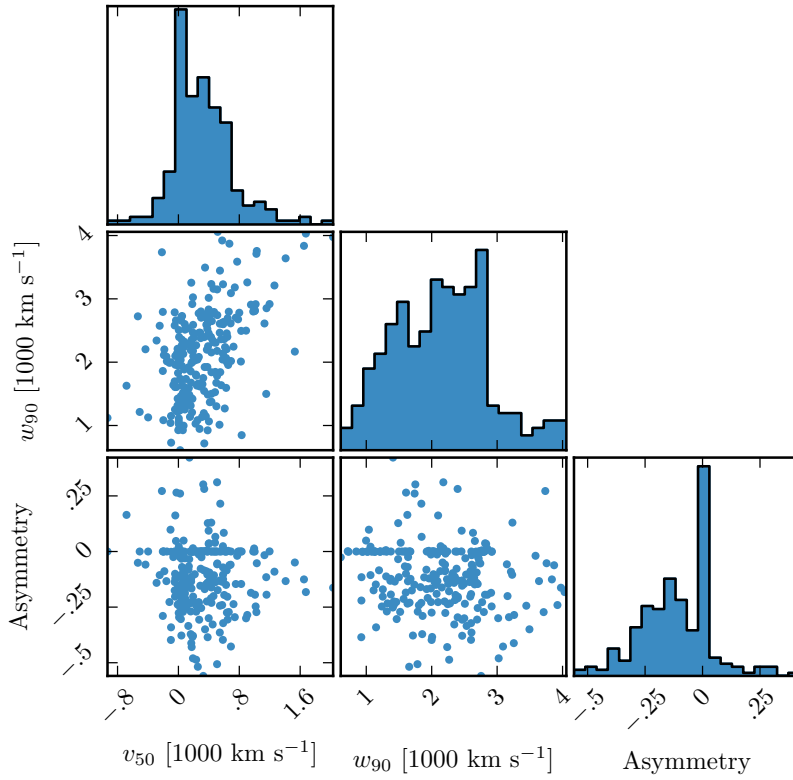
Figure 41: The distributions of and correlations between a subset of the non-parameteric measures we made of the best-fitting [O III] models.

The size of the narrow line region is roughly expected to scale as $L^{0.5}$ (e.g. Netzer et al., 2004). However, for high luminosity quasars with strong [O III] this gives NLR sizes which are unreasonably large (~100 kpc; Netzer et al., 2004).

Netzer et al., (2004) found 1/3 of their high luminosity sample had very weak [O III], whereas quasars with weak [O III] are very rare for nearby AGN. We find a very similar fraction. Netzer et al., (2004) claim that for the population of strong [O III] emitters there is no reduction of EW with increasing source luminosity. On the other hand, there are many weak or no [O III] emitters at high luminosity that could give the impression that the line EQW decreases with increasing source luminoisity.

OIII outflows

Our best-fitting profiles show a strongly blue-asymmetric profile (Fig. 41), with a significant fraction of the total emission in a blue wing. The luminous blueshifted broad wing and the extremely broad profile reveals high-velocity outflowing ionized gas. This can be explained if

the far-side of any outflowing gas, that is moving away from the line of sight, is obscured by dust in the host galaxies (e.g. Heckman et al. 1981; Vrtilek 1985). Observations at both low and high redshifts commonly observe this blueshifted component. Our results, and those of other authors, suggest that kpc-scale outflows in ionized gas are common among the most luminous high-redshift actively accreting SMBHs.

The situtation is very different in nearby AGN, where the [O III] velocity width is dominated by the galactic potential and correlates well with the stellar velocity dispersion. HI, CO and absorption line mesaures of the host galaxy rest frame suggest that [O III] usually gives consistent results within 200 km/s (de Robertis 1985; Whittle 1985; Wilson & Heckman 1985; Condon et al. 1985; Stripe 1990; Alloin et al. 1992; Evans et al. 2001).

We see a correlation between the [O III] velocity width and blueshift. As the blueshift of the line increases it gets broader. This is consistent with Shen and Ho, (2014), where the strength of the narrow core is decreasing, leading to a broader and more blueshifted profile.

[O III] and C IV outflows are linked

As described in Paper I, we have searched for optical counterparts to our near-infrared spectra. Optical spectra are available for XXX quasars in our catalogue, and cover the broad C IV doublet. As we described in Paper I and Coatman et al., (2016), C IV is often blueshifted, which almost certainly signal the presence of strong outflows, most likely originating in a disc wind. In Paper I we demonstrated that the quasars in our sample cover the full range of C IV blueshifts seen in the SDSS quasar population, which makes our sample unique in that it allows us to study properties of the quasar across the full parameter range.

The C IV velocity centroid measurements are taken directly from paper I. We define the 'location' of the [O III] emission using v_{10}, although the results are the same if v_{20}, v_{50} etc. are used instead.

In Figure 42 we show the C IV blueshifts against the [O III] blueshifts. This comparison is done for a sub-sample of 146 objects where we have good measurements of the C IV, [O III], and Hβ (to measure the systemic redshift) profiles. Objects with S/N > 3 are shown as blue filled circles and objects with S/N < 3 as open grey circles. We calculated the median S/N per pixel in the best-fitting model for the [O III]5008 emission.

There is a clear and strong correlation. Similar correlations have been tentatively found in lower redshift quasars and AGN (Zamanov et al., 2002).

The blueshifting of C IV is known to correlate with luminosity (Richards et al., 2011). In [O III], the blueshifted wing becomes relatively more
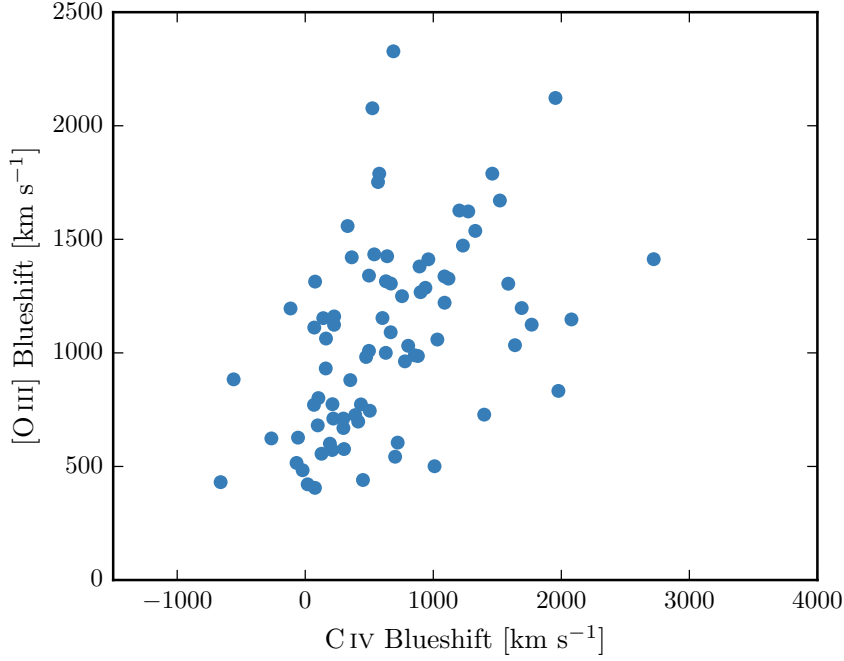
Figure 42: The relation between the blueshifts of C IV and [O III]. Equivalent to Fig 8. We use the Hβ peak in this figure, which I think is responsible for some of the trend. However, we do see a correlation (albeit noisier) using the NIR ICA redshifts. Not a sensible to use the [O III] redshifts, since these become much more unreliable at the high C IV blueshift end (when [O III] is weaker: figure 7. Note that we are using v_{10} for the [O III] position and v_{50} for the C IV position. We can't use v_{50} for [O III] because sometimes we are using a single Gaussian, especially if the [O III] is weaker and we miss the broad component. Need to remake this plot / don't use at all because I don't believe some of the Gaussian fits to [O III], especially at high C IV blueshifts when [O III] is weak and Fe II is strong.) Only objects where fit with two components.
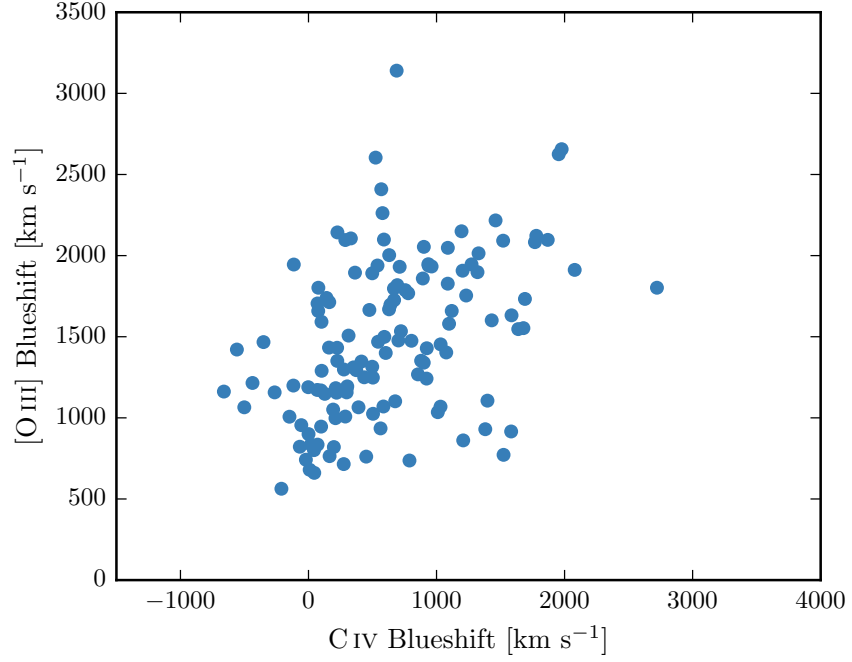
Figure 43

prominent as the luminosity of the quasar increases (Shen and Ho, 2014). Therefore, it is plausible that the correlation between the C IV and [O III] blueshifts is a secondary effect that is driven by the correlation of each with the luminosity. In Figure **??** we color the data points by the luminosity, and no luminosity-dependent trends are apparent. We find that both the [O III] and C IV blueshifts are correlated with the luminosity, but that these correlations are much weaker than the correlation between the [O III] and C IV blueshifts.

EIGENVECTOR ONE CORRELATIONS

In Figure 44 we show the [O III] EQW as a function of the Hβ FWHM and the optical Fe II strength. The optical Fe II strength is defined as the ratio of the Fe II and Hβ EQW, where the Fe II EQW is measured between 4434 and 4684Å. These parameters form part of 'eigenvector 1' (EV1), the first eigenvector in a principal component analysis which originated from the work of Boroson and Green, (1992). In our sample, these parameters follow very similar correlations to what is observed at low-z (e.g. Shen and Ho, 2014). In particular, the anti-correlation between the [O III] and Fe II EQWs.

Same as Shen, (2016), we confirm that the EV1 correlations hold at high luminosities/redshifts. See also Sulentic et al. 2004, 2006; Runnoe et al. 2013. Make sure it's clear that Shen, (2016) quasars make up a significant chunk of our sample.
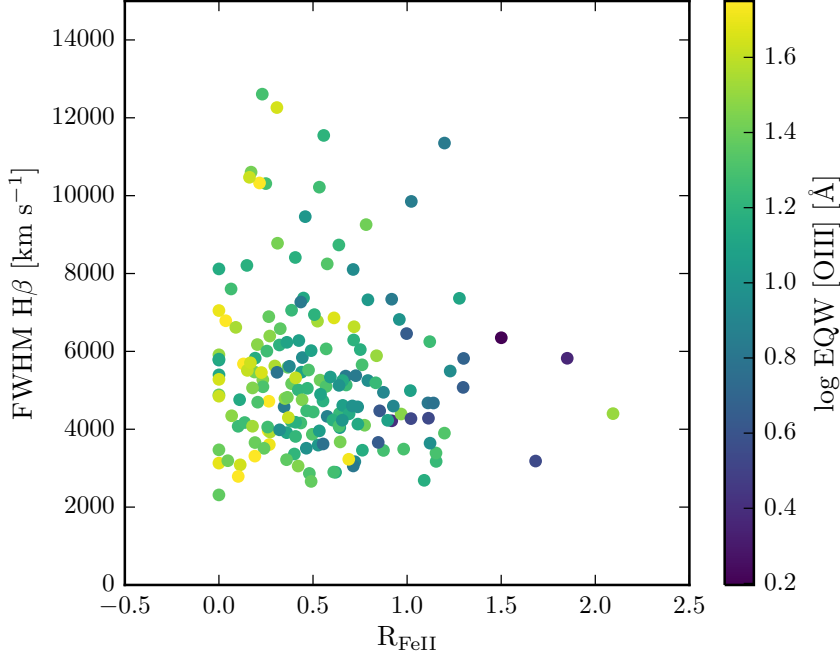
Figure 44: The [O III] EQW as a function of the Hβ FWHM and the optical Fe II strength (EQW Fe II/ EQW Hβ).

SIGNAL TO NOISE TESTS

BROAD ABSORPTION LINE QUASARS

19 quasars in our catalogue are classified as broad absorption line (BAL) quasars, using the either the SDSS classification flags or the Allen et al., (2011) catalogue. We find that the BAL quasars have typically broader [O III] than the rest of the sample. Note that in the Zakamska et al., (2016) sample of very red quasars, the incidence of BALs is very high, and these objects have extremely broad [O III] profiles. A two-sided Kolmogorov-Smirnov statistic on the w_{80} distributions returned a p-value of 0.10. What does this mean? Try with different parameters? Histograms look rubbish so maybe just give the numbers.

DISCUSSION

Type II quasars

Implications of our findings on searches for high-redshift type 2 quasars. It could be that type II quasars exist. If you look at CIV/MgII the narrow line components are very weak. So the contribution from the narrow line region is very weak in luminous quasars, and you just
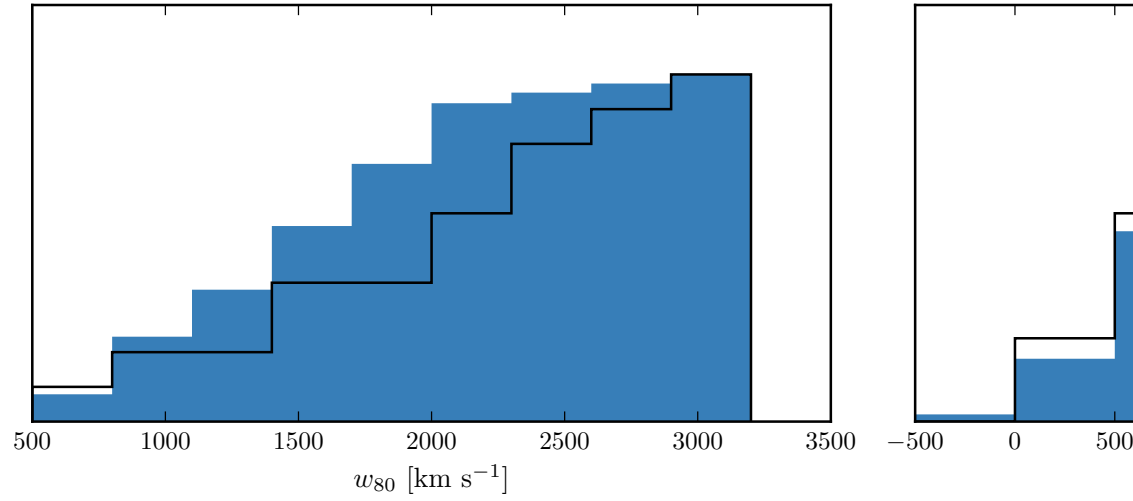
Figure 45: The distribution of w_{80} and v_{10} for the 19 BALs are compared to the distribution for the non-BALs. These look rubbish. Cumulative distributions instead?

won't see it even if the broad line region is obscured. Findings in this paper seem to suggest that the startic narrow line region is very weak in luminous quasars.

Alexander, D. M. and R. C. Hickox (2012). "What drives the growth of black holes?" In: *New Astron. Rev.* 56, pp. 93–121. DOI: 10.1016/j.newar.2011.11.003. arXiv: 1112.1949.

Allen, J. T., P. C. Hewett, N. Maddox, G. T. Richards, and V. Belokurov (2011). "A strong redshift dependence of the broad absorption line quasar fraction." In: *MNRAS* 410, pp. 860–884.

Allen, J. T., P. C. Hewett, C. T. Richardson, G. J. Ferland, and J. A. Baldwin (2013). "Classification and analysis of emission-line galaxies using mean field independent component analysis." In: *MNRAS* 430, pp. 3510–3536. DOI: 10.1093/mnras/stt151. arXiv: 1301.5930.

Assef, R. J. et al. (2011). "Black Hole Mass Estimates Based on C IV are Consistent with Those Based on the Balmer Lines." In: *ApJ* 742, p. 93.

Baskin, A. and A. Laor (2005a). "What controls the CIV line profile in active galactic nuclei?" In: *MNRAS* 356, pp. 1029–1044.

— (2005b). "What controls the [OIII]λ5007 line strength in active galactic nuclei?" In: *MNRAS* 358, pp. 1043–1054. DOI: 10.1111/j.1365-2966.2005.08841.x. eprint: astro-ph/0501436.

Bentz, M. C. et al. (2009). "The Lick AGN Monitoring Project: Broadline Region Radii and Black Hole Masses from Reverberation Mapping of Hβ." In: *ApJ* 705, pp. 199–217. DOI: 10.1088/0004-637X/705/1/199. arXiv: 0908.0003.

Bonnet, H. et al. (2004). "First light of SINFONI at the VLT." In: *The Messenger* 117, pp. 17–24.

Boroson, T. A. and R. F. Green (1992). "The emission-line properties of low-redshift quasi-stellar objects." In: *ApJS* 80, pp. 109–135.

Boyle, B. J. and R. J. Terlevich (1998). "The cosmological evolution of the QSO luminosity density and of the star formation rate." In: *MNRAS* 293, pp. L49–L51.

Brandt, W. N. and G. Hasinger (2005). "Deep Extragalactic X-Ray Surveys." In: *ARA&A* 43, pp. 827–859.

Brotherton, M. S. (1996). "The Profiles of H beta and [O iii] lambda 5007 in Radio-loud Quasars." In: *ApJS* 102, p. 1. DOI: 10.1086/192249. eprint: astro-ph/9507067.

Brotherton, M. S. and P. J. Francis (1999). "The Intermediate Line Region and the Baldwin Effect." In: *Quasars and Cosmology*. Ed. by G. Ferland and J. Baldwin. Vol. 162. Astronomical Society of the Pacific Conference Series, p. 395. eprint: astro-ph/9811088.

Brotherton, M. S., V. Singh, and J. Runnoe (2015). "Orientation and quasar black hole mass estimation." In: *MNRAS* 454, pp. 3864–3871.

Brotherton, M. S., J. C. Runnoe, Z. Shang, and M. A. DiPompeo (2015). "Bias in C IV-based quasar black hole mass scaling relationships from reverberation mapped samples." In: *MNRAS* 451, pp. 1290–1298.

Brusa, M. et al. (2015). "X-shooter reveals powerful outflows in z~1.5 X-ray selected obscured quasi-stellar objects." In: *MNRAS* 446, pp. 2394–2417. DOI: 10.1093/mnras/stu2117. arXiv: 1409.1615.

Cappellari, M., E. K. Verolme, R. P. van der Marel, G. A. Verdoes Kleijn, G. D. Illingworth, M. Franx, C. M. Carollo, and P. T. de Zeeuw (2002). "The Counterrotating Core and the Black Hole Mass of IC 1459." In: *ApJ* 578, pp. 787–805.

Carniani, S. et al. (2015). "Ionised outflows in z ~ 2.4 quasar host galaxies." In: *A&A* 580, A102, A102. DOI: 10.1051/0004-6361/201526557. arXiv: 1506.03096.

Coatman, L., P. C. Hewett, M. Banerji, and G. T. Richards (2016). "CIV emission-line properties and systematic trends in quasar black hole mass estimates." In: *MNRAS* 461, pp. 647–665. DOI: 10.1093/mnras/stw1360. arXiv: 1606.02726.

Collin, S., T. Kawaguchi, B. M. Peterson, and M. Vestergaard (2006). "Systematic effects in measurement of black hole masses by emission-line reverberation of active galactic nuclei: Eddington ratio and inclination." In: *A&A* 456, pp. 75–90. DOI: 10.1051/0004-6361:20064878. eprint: astro-ph/0603460.

Dall'Aglio, A., L. Wisotzki, and G. Worseck (2008). "An unbiased measurement of the UV background and its evolution via the proximity effect in quasar spectra." In: *A&A* 491, pp. 465–481. DOI: 10.1051/0004-6361:200810724. arXiv: 0807.5089.

Dawson, K. S. et al. (2013). "The Baryon Oscillation Spectroscopic Survey of SDSS-III." In: *AJ* 145, p. 10.

Dekker, H., S. D'Odorico, A. Kaufer, B. Delabre, and H. Kotzlowski (2000). "Design, construction, and performance of UVES, the echelle spectrograph for the UT2 Kueyen Telescope at the ESO Paranal Observatory." In: *Optical and IR Telescope Instrumentation and Detectors*. Ed. by M. Iye and A. F. Moorwood. Vol. 4008. Proc. SPIE, pp. 534–545.

Denney, K. D. (2012). "Are Outflows Biasing Single-epoch C IV Black Hole Mass Estimates?" In: *ApJ* 759, p. 44.

Denney, K. D. et al. (2010). "Reverberation Mapping Measurements of Black Hole Masses in Six Local Seyfert Galaxies." In: *ApJ* 721, pp. 715–737.

Denney, K. D., R. W. Pogge, R. J. Assef, C. S. Kochanek, B. M. Peterson, and M. Vestergaard (2013). "C IV Line-width Anomalies: The Perils of Low Signal-to-noise Spectra." In: *ApJ* 775, p. 60.

Edge, A., W. Sutherland, K. Kuijken, S. Driver, R. McMahon, S. Eales, and J. P. Emerson (2013). "The VISTA Kilo-degree Infrared Galaxy (VIKING) Survey: Bridging the Gap between Low and High Redshift." In: *The Messenger* 154, pp. 32–34.

Eisenhauer, F. et al. (2003). "SINFONI - Integral field spectroscopy at 50 milli-arcsecond resolution with the ESO VLT." In: *Instrument Design and Performance for Optical/Infrared Ground-based Telescopes*. Ed. by M. Iye and A. F. M. Moorwood. Vol. 4841. Proc. SPIE, pp. 1548–1561. DOI: 10.1117/12.459468. eprint: astro-ph/0306191.

Elias, J. H., R. R. Joyce, M. Liang, G. P. Muller, E. A. Hileman, and J. R. George (2006). "Design of the Gemini near-infrared spectrograph." In: *Society of Photo-Optical Instrumentation Engineers (SPIE) Conference Series*. Vol. 6269. Proc. SPIE, p. 62694C. DOI: 10.1117/12.671817.

Everett, J. E. (2005). "Radiative Transfer and Acceleration in Magneto-centrifugal Winds." In: *ApJ* 631, pp. 689–706.

Fabian, A. C. (2012). "Observational Evidence of Active Galactic Nuclei Feedback." In: *ARA&A* 50, pp. 455–489. DOI: 10.1146/annurev-astro-081811-125521. arXiv: 1204.4114.

Ferrarese, L. and D. Merritt (2000). "A Fundamental Relation between Supermassive Black Holes and Their Host Galaxies." In: *ApJ* 539, pp. L9–L12.

Font-Ribera, A. et al. (2013). "The large-scale quasar-Lyman α forest cross-correlation from BOSS." In: *J. Cosmology Astropart. Phys.* 5, 018, p. 018. DOI: 10.1088/1475-7516/2013/05/018. arXiv: 1303.1937.

Foreman-Mackey, D., D. W. Hogg, D. Lang, and J. Goodman (2013). "emcee: The MCMC Hammer." In: *PASP* 125, pp. 306–312. DOI: 10.1086/670067. arXiv: 1202.3665 [astro-ph.IM].

Gallagher, S. C., J. E. Everett, M. M. Abado, and S. K. Keating (2015). "Investigating the structure of the windy torus in quasars." In: *MNRAS* 451, pp. 2991–3000.

Gaskell, C. M. (1982). "A redshift difference between high and low ionization emission-line regions in QSOs - Evidence for radial motions." In: *ApJ* 263, pp. 79–86.

Gavignaud, I. et al. (2008). "Eddington ratios of faint AGN at intermediate redshift: evidence for a population of half-starved black holes." In: *A&A* 492, pp. 637–650.

Gebhardt, K. et al. (2000). "A Relationship between Nuclear Black Hole Mass and Galaxy Velocity Dispersion." In: *ApJ* 539, pp. L13–L16.

Greene, J. E. and L. C. Ho (2005). "Estimating Black Hole Masses in Active Galaxies Using the Hα Emission Line." In: *ApJ* 630, pp. 122–129. DOI: 10.1086/431897. eprint: astro-ph/0508335.

Harrison, C. M., D. M. Alexander, J. R. Mullaney, J. P. Stott, A. M. Swinbank, V. Arumugam, F. E. Bauer, R. G. Bower, A. J. Bunker,

and R. M. Sharples (2016). "The KMOS AGN Survey at High redshift (KASHz): the prevalence and drivers of ionized outflows in the host galaxies of X-ray AGN." In: *MNRAS* 456, pp. 1195–1220. DOI: 10.1093/mnras/stv2727.

Heckman, T. M. and P. N. Best (2014). "The Coevolution of Galaxies and Supermassive Black Holes: Insights from Surveys of the Contemporary Universe." In: *ARA&A* 52, pp. 589–660. DOI: 10.1146/annurev-astro-081913-035722. arXiv: 1403.4620.

Hennawi, J. F. et al. (2006a). "Binary Quasars in the Sloan Digital Sky Survey: Evidence for Excess Clustering on Small Scales." In: *AJ* 131, pp. 1–23. DOI: 10.1086/498235. eprint: astro-ph/0504535.

Hennawi, J. F. et al. (2006b). "Quasars Probing Quasars. I. Optically Thick Absorbers near Luminous Quasars." In: *ApJ* 651, pp. 61–83. DOI: 10.1086/507069. eprint: astro-ph/0603742.

Hennawi, J. F. et al. (2010). "Binary Quasars at High Redshift. I. 24 New Quasar Pairs at z ~ 3-4." In: *ApJ* 719, pp. 1672–1692. DOI: 10.1088/0004-637X/719/2/1672. arXiv: 0908.3907.

Hennawi, J. F., J. X. Prochaska, S. Cantalupo, and F. Arrigoni-Battaia (2015). "Quasar quartet embedded in giant nebula reveals rare massive structure in distant universe." In: *Science* 348, pp. 779–783. DOI: 10.1126/science.aaa5397. arXiv: 1505.03786.

Hewett, P. C. and V. Wild (2010). "Improved redshifts for SDSS quasar spectra." In: *MNRAS* 405, pp. 2302–2316.

Higginbottom, N. and D. Proga (2015). "Coronae and Winds from Irradiated Disks in X-Ray Binaries." In: *ApJ* 807, p. 107.

Hodapp, K. W. et al. (2003). "The Gemini Near-Infrared Imager (NIRI)." In: *PASP* 115, pp. 1388–1406. DOI: 10.1086/379669.

Hogg, D. W., J. Bovy, and D. Lang (2010). "Data analysis recipes: Fitting a model to data." In: *ArXiv e-prints*. arXiv: 1008.4686 [astro-ph.IM].

Jackson, N. and I. W. A. Browne (1991). "Optical Properties of Quasars - Part Two - Emission Line Geometry and Radio Properties." In: *MNRAS* 250, p. 422. DOI: 10.1093/mnras/250.2.422.

Jarvis, M. J. and R. J. McLure (2006). "Orientation dependency of broad-line widths in quasars and consequences for black hole mass estimation." In: *MNRAS* 369, pp. 182–188.

Kaspi, S., P. S. Smith, H. Netzer, D. Maoz, B. T. Jannuzi, and U. Giveon (2000). "Reverberation Measurements for 17 Quasars and the Size-Mass-Luminosity Relations in Active Galactic Nuclei." In: *ApJ* 533, pp. 631–649.

Kaspi, S., W. N. Brandt, D. Maoz, H. Netzer, D. P. Schneider, and O. Shemmer (2007). "Reverberation Mapping of High-Luminosity Quasars: First Results." In: *ApJ* 659, pp. 997–1007.

Kelly, B. C. and Y. Shen (2013). "The Demographics of Broad-line Quasars in the Mass-Luminosity Plane. II. Black Hole Mass and Eddington Ratio Functions." In: *ApJ* 764, p. 45.

Kelly, B. C., M. Vestergaard, X. Fan, P. Hopkins, L. Hernquist, and A. Siemiginowska (2010). "Constraints on Black Hole Growth, Quasar Lifetimes, and Eddington Ratio Distributions from the SDSS Broad-line Quasar Black Hole Mass Function." In: *ApJ* 719, pp. 1315–1334.

Kim, M., L. C. Ho, C. J. Lonsdale, M. Lacy, A. W. Blain, and A. E. Kimball (2013). "Evidence for Active Galactic Nucleus Driven Outflows in Young Radio Quasars." In: *ApJ* 768, L9, p. L9. DOI: 10.1088/2041-8205/768/1/L9. arXiv: 1303.7194.

King, A. L. et al. (2015). "Simulations of the OzDES AGN reverberation mapping project." In: *MNRAS* 453, pp. 1701–1726.

King, A. and K. Pounds (2015). "Powerful Outflows and Feedback from Active Galactic Nuclei." In: *ARA&A* 53, pp. 115–154.

Kollatschny, W. and M. Zetzl (2011). "Broad-line active galactic nuclei rotate faster than narrow-line ones." In: *Nature* 470, pp. 366–368. DOI: 10.1038/nature09761.

— (2013). "The shape of broad-line profiles in active galactic nuclei." In: *A&A* 549, A100, A100. DOI: 10.1051/0004-6361/201219411. arXiv: 1211.3065.

Kollmeier, J. A. et al. (2006). "Black Hole Masses and Eddington Ratios at $0.3 < z < 4$." In: *ApJ* 648, pp. 128–139. DOI: 10.1086/505646. eprint: astro-ph/0508657.

Konigl, A. and J. F. Kartje (1994). "Disk-driven hydromagnetic winds as a key ingredient of active galactic nuclei unification schemes." In: *ApJ* 434, pp. 446–467.

Kormendy, J. and L. C. Ho (2013). "Coevolution (Or Not) of Supermassive Black Holes and Host Galaxies." In: *ARA&A* 51, pp. 511–653.

Kratzer, R. M. and G. T. Richards (2015). "Mean and Extreme Radio Properties of Quasars and the Origin of Radio Emission." In: *AJ* 149, p. 61.

Krawczyk, C. M., G. T. Richards, S. S. Mehta, M. S. Vogeley, S. C. Gallagher, K. M. Leighly, N. P. Ross, and D. P. Schneider (2013). "Mean Spectral Energy Distributions and Bolometric Corrections for Luminous Quasars." In: *ApJS* 206, p. 4.

Lau, M. W., J. X. Prochaska, and J. F. Hennawi (2015). "Quasars Probing Quasars VIII. The Physical Properties of the Cool Circumgalactic medium Surrounding z ˜ 2-3 Massive Galaxies." In: *ArXiv e-prints*. arXiv: 1510.06018.

Lawrence, A. et al. (2007). "The UKIRT Infrared Deep Sky Survey (UKIDSS)." In: *MNRAS* 379, pp. 1599–1617.

Lee, K.-G. et al. (2013). "The BOSS Lyα Forest Sample from SDSS Data Release 9." In: *AJ* 145, 69, p. 69. DOI: 10.1088/0004-6256/145/3/69. arXiv: 1211.5146.

Leighly, K. M. (2004). "Hubble Space Telescope STIS Ultraviolet Spectral Evidence of Outflow in Extreme Narrow-Line Seyfert 1 Galaxies. II. Modeling and Interpretation." In: *ApJ* 611, pp. 125–152.

Lopez, S. et al. (2016). "XQ-100: A legacy survey of one hundred 3.5 < z < 4.5 quasars observed with VLT/XSHOOTER." In: *ArXiv e-prints*. arXiv: 1607.08776.

Luo, B. et al. (2015). "X-ray Insights into the Nature of PHL 1811 Analogs and Weak Emission-line Quasars: Unification with a Geometrically Thick Accretion Disk?" In: *ApJ* 805, p. 122.

MacLeod, C. L. et al. (2010). "Modeling the Time Variability of SDSS Stripe 82 Quasars as a Damped Random Walk." In: *ApJ* 721, pp. 1014–1033. DOI: 10.1088/0004-637X/721/2/1014. arXiv: 1004.0276 [astro-ph.CO].

MacLeod, C. L. et al. (2016). "A systematic search for changing-look quasars in SDSS." In: *MNRAS* 457, pp. 389–404. DOI: 10.1093/mnras/stv2997. arXiv: 1509.08393.

Madau, P. and M. Dickinson (2014). "Cosmic Star-Formation History." In: *ARA&A* 52, pp. 415–486. DOI: 10.1146/annurev-astro-081811-125615. arXiv: 1403.0007.

Maddox, N., P. C. Hewett, C. Péroux, D. B. Nestor, and L. Wisotzki (2012). "The large area KX quasar catalogue - I. Analysis of the photometric redshift selection and the complete quasar catalogue." In: *MNRAS* 424, pp. 2876–2895. DOI: 10.1111/j.1365-2966.2012.21427.x. arXiv: 1206.1434.

Manchado, A. et al. (1998). "LIRIS: a long-slit intermediate-resolution infrared spectrograph for the WHT." In: *Infrared Astronomical Instrumentation*. Ed. by A. M. Fowler. Vol. 3354. Proc. SPIE, pp. 448–455.

Marziani, P., R. K. Zamanov, J. W. Sulentic, and M. Calvani (2003). "Searching for the physical drivers of eigenvector 1: influence of black hole mass and Eddington ratio." In: *MNRAS* 345, pp. 1133–1144.

Marziani, P., J. W. Sulentic, G. M. Stirpe, S. Zamfir, and M. Calvani (2009). "VLT/ISAAC spectra of the Hβ region in intermediate-redshift quasars. III. Hβ broad-line profile analysis and inferences about BLR structure." In: *A&A* 495, pp. 83–112. DOI: 10.1051/0004-6361:200810764. arXiv: 0812.0251.

Marziani, P., J. W. Sulentic, I. Plauchu-Frayn, and A. del Olmo (2013). "Is MgIIλ2800 a reliable virial broadening estimator for quasars?" In: *A&A* 555, A89, A89. DOI: 10.1051/0004-6361/201321374. arXiv: 1305.1096.

Marziani, P., M. A. Martínez Carballo, J. W. Sulentic, A. Del Olmo, G. M. Stirpe, and D. Dultzin (2016). "The most powerful quasar outflows as revealed by the Civ λ1549 resonance line." In: *Ap&SS* 361, 29, p. 29. DOI: 10.1007/s10509-015-2611-1. arXiv: 1512.00381.

McGill, K. L., J.-H. Woo, T. Treu, and M. A. Malkan (2008). "Comparing and Calibrating Black Hole Mass Estimators for Distant Active Galactic Nuclei." In: *ApJ* 673, pp. 703–714.

McLean, I. S. et al. (1998). "Design and development of NIRSPEC: a near-infrared echelle spectrograph for the Keck II telescope." In: *Infrared Astronomical Instrumentation*. Ed. by A. M. Fowler. Vol. 3354. Proc. SPIE, pp. 566–578.

McLure, R. J. and M. J. Jarvis (2002). "Measuring the black hole masses of high-redshift quasars." In: *MNRAS* 337, pp. 109–116. DOI: 10.1046/j.1365-8711.2002.05871.x. eprint: astro-ph/0204473.

McMahon, R. G., M. Banerji, E. Gonzalez, S. E. Koposov, V. J. Bejar, N. Lodieu, R. Rebolo, and VHS Collaboration (2013). "First Scientific Results from the VISTA Hemisphere Survey (VHS)." In: *The Messenger* 154, pp. 35–37.

Mejía-Restrepo, J. E., B. Trakhtenbrot, P. Lira, H. Netzer, and D. M. Capellupo (2016). "Active galactic nuclei at z~1.5 - II. Black hole mass estimation by means of broad emission lines." In: *MNRAS* 460, pp. 187–211.

Moorwood, A., J.-G. Cuby, and C. Lidman (1998). "SOFI sees first light at the NTT." In: *The Messenger* 91, pp. 9–13.

Moorwood, A. et al. (1998). "ISAAC sees first light at the VLT." In: *The Messenger* 94, pp. 7–9.

Mullaney, J. R., D. M. Alexander, S. Fine, A. D. Goulding, C. M. Harrison, and R. C. Hickox (2013). "Narrow-line region gas kinematics of 24 264 optically selected AGN: the radio connection." In: *MNRAS* 433, pp. 622–638. DOI: 10.1093/mnras/stt751. arXiv: 1305.0263.

Murray, N., J. Chiang, S. A. Grossman, and G. M. Voit (1995). "Accretion Disk Winds from Active Galactic Nuclei." In: *ApJ* 451, p. 498.

Nesvadba, N. P. H., M. D. Lehnert, C. De Breuck, A. M. Gilbert, and W. van Breugel (2008). "Evidence for powerful AGN winds at high redshift: dynamics of galactic outflows in radio galaxies during the "Quasar Era"." In: *A&A* 491, pp. 407–424. DOI: 10.1051/0004-6361:200810346. arXiv: 0809.5171.

Netzer, H. (2015). "Revisiting the Unified Model of Active Galactic Nuclei." In: *ARA&A* 53, pp. 365–408. DOI: 10.1146/annurev-astro-082214-122302. arXiv: 1505.00811.

Netzer, H., O. Shemmer, R. Maiolino, E. Oliva, S. Croom, E. Corbett, and L. di Fabrizio (2004). "Near-Infrared Spectroscopy of High-Redshift Active Galactic Nuclei. II. Disappearing Narrow-Line Regions and the Role of Accretion." In: *ApJ* 614, pp. 558–567. DOI: 10.1086/423608. eprint: astro-ph/0406560.

Onken, C. A. and J. A. Kollmeier (2008). "An Improved Method for Using Mg II to Estimate Black Hole Masses in Active Galactic Nuclei." In: *ApJ* 689, p. L13.

Onken, C. A. and B. M. Peterson (2002). "The Mass of the Central Black Hole in the Seyfert Galaxy NGC 3783." In: *ApJ* 572, pp. 746–752. DOI: 10.1086/340351. eprint: astro-ph/0202382.

Pâris, I. et al. (2012). "The Sloan Digital Sky Survey quasar catalog: ninth data release." In: *A&A* 548, A66, A66. DOI: 10.1051/0004-6361/201220142. arXiv: 1210.5166.

Pâris, I. et al. (2014). "The Sloan Digital Sky Survey quasar catalog: tenth data release." In: *A&A* 563, A54.

Pâris, I. et al. (2017). "The Sloan Digital Sky Survey Quasar Catalog: Twelfth data release." In: *A&A* 597, A79.

Park, D., J.-H. Woo, K. D. Denney, and J. Shin (2013). "Calibrating C-IV-based Black Hole Mass Estimators." In: *ApJ* 770, p. 87.

Perna, M. et al. (2015). "Galaxy-wide outflows in z ~ 1.5 luminous obscured quasars revealed through near-IR slit-resolved spectroscopy." In: *A&A* 574, A82, A82. DOI: 10.1051/0004-6361/201425035. arXiv: 1410.5468.

Peterson, B. M. (1993). "Reverberation mapping of active galactic nuclei." In: *PASP* 105, pp. 247–268.

— (2010). "Toward Precision Measurement of Central Black Hole Masses." In: *Co-Evolution of Central Black Holes and Galaxies*. Ed. by B. M. Peterson, R. S. Somerville, and T. Storchi-Bergmann. Vol. 267. IAU Symposium, pp. 151–160.

— (2014). "Measuring the Masses of Supermassive Black Holes." In: *Space Sci. Rev.* 183, pp. 253–275.

Peterson, B. M. et al. (2004). "Central Masses and Broad-Line Region Sizes of Active Galactic Nuclei. II. A Homogeneous Analysis of a Large Reverberation-Mapping Database." In: *ApJ* 613, pp. 682–699.

Plotkin, R. M. et al. (2015). "Detection of Rest-frame Optical Lines from X-shooter Spectroscopy of Weak Emission Line Quasars." In: *ApJ* 805, p. 123.

Prochaska, J. X. and J. F. Hennawi (2009). "Quasars Probing Quasars. III. New Clues to Feedback, Quenching, and the Physics of Massive Galaxy Formation." In: *ApJ* 690, pp. 1558–1584. DOI: 10.1088/0004-637X/690/2/1558. arXiv: 0806.0862.

Proga, D., J. M. Stone, and T. R. Kallman (2000). "Dynamics of Line-driven Disk Winds in Active Galactic Nuclei." In: *ApJ* 543, pp. 686–696.

Rafiee, A. and P. B. Hall (2011). "Supermassive Black Hole Mass Estimates Using Sloan Digital Sky Survey Quasar Spectra at 0.7 < z < 2." In: *ApJS* 194, 42, p. 42. DOI: 10.1088/0067-0049/194/2/42. arXiv: 1104.1828.

Reyes, R., N. L. Zakamska, M. A. Strauss, J. Green, J. H. Krolik, Y. Shen, G. T. Richards, S. F. Anderson, and D. P. Schneider (2008). "Space Density of Optically Selected Type 2 Quasars." In: *AJ* 136,

pp. 2373–2390. DOI: 10.1088/0004-6256/136/6/2373. arXiv: 0801.1115.

Richards, G. T. (2006). "AGN Outflows in Emission and Absorption: The SDSS Perspective." In: *AGN Winds in the Caribbean*. arXiv: astro-ph/0603827.

Richards, G. T., D. E. Vanden Berk, T. A. Reichard, P. B. Hall, D. P. Schneider, M. SubbaRao, A. R. Thakar, and D. G. York (2002). "Broad Emission-Line Shifts in Quasars: An Orientation Measure for Radio-Quiet Quasars?" In: *AJ* 124, pp. 1–17.

Richards, G. T. et al. (2006a). "Spectral Energy Distributions and Multiwavelength Selection of Type 1 Quasars." In: *ApJS* 166, pp. 470–497.

Richards, G. T. et al. (2006b). "The Sloan Digital Sky Survey Quasar Survey: Quasar Luminosity Function from Data Release 3." In: *AJ* 131, pp. 2766–2787.

Richards, G. T., N. E. Kruczek, S. C. Gallagher, P. B. Hall, P. C. Hewett, K. M. Leighly, R. P. Deo, R. M. Kratzer, and Y. Shen (2011). "Unification of Luminous Type 1 Quasars through CIV Emission." In: *AJ* 141, p. 167.

Ross, N. P. et al. (2013). "The SDSS-III Baryon Oscillation Spectroscopic Survey: The Quasar Luminosity Function from Data Release Nine." In: *ApJ* 773, p. 14.

Runnoe, J. C., M. S. Brotherton, Z. Shang, and M. A. DiPompeo (2013a). "Rehabilitating C IV-based black hole mass estimates in quasars." In: *MNRAS* 434, pp. 848–861.

Runnoe, J. C., M. S. Brotherton, Z. Shang, B. J. Wills, and M. A. DiPompeo (2013b). "The orientation dependence of quasar single-epoch black hole mass scaling relationships." In: *MNRAS* 429, pp. 135–149.

Runnoe, J. C., M. S. Brotherton, M. A. DiPompeo, and Z. Shang (2014). "The behaviour of quasar C IV emission-line properties with orientation." In: *MNRAS* 438, pp. 3263–3274.

Schneider, D. P. et al. (2010). "The Sloan Digital Sky Survey Quasar Catalog. V. Seventh Data Release." In: *AJ* 139, p. 2360.

Shen, Y. (2013). "The mass of quasars." In: *Bulletin of the Astronomical Society of India* 41, pp. 61–115.

— (2016). "Rest-Frame Optical Properties of Luminous $1.5 < z < 3.5$ Quasars: The Hβ-[O III] Region." In: *ApJ* in press. DOI: 10.1088/0004-6256/141/5/167. arXiv: 1512.00005.

Shen, Y. and L. C. Ho (2014). "The diversity of quasars unified by accretion and orientation." In: *Nature* 513, pp. 210–213.

Shen, Y. and X. Liu (2012). "Comparing Single-epoch Virial Black Hole Mass Estimators for Luminous Quasars." In: *ApJ* 753, p. 125.

Shen, Y., J. E. Greene, M. A. Strauss, G. T. Richards, and D. P. Schneider (2008). "Biases in Virial Black Hole Masses: An SDSS Perspective." In: *ApJ* 680, pp. 169–190.

Shen, Y. et al. (2011). "A Catalog of Quasar Properties from Sloan Digital Sky Survey Data Release 7." In: *ApJS* 194, p. 45.

Shen, Y. et al. (2015). "The Sloan Digital Sky Survey Reverberation Mapping Project: Technical Overview." In: *ApJS* 216, p. 4.

Shen, Y. et al. (2016). "The Sloan Digital Sky Survey Reverberation Mapping Project: Velocity Shifts of Quasar Emission Lines." In: *ArXiv e-prints*. arXiv: 1602.03894.

Simcoe, R. A. et al. (2010). "The FIRE infrared spectrometer at Magellan: construction and commissioning." In: *Ground-based and Airborne Instrumentation for Astronomy III*. Vol. 7735. Proc. SPIE, p. 773514. DOI: 10.1117/12.856088.

Skrutskie, M. F. et al. (2006). "The Two Micron All Sky Survey (2MASS)." In: *AJ* 131, pp. 1163–1183. DOI: 10.1086/498708.

Sulentic, J. W., P. Marziani, and D. Dultzin-Hacyan (2000). "Phenomenology of Broad Emission Lines in Active Galactic Nuclei." In: *ARA&A* 38, pp. 521–571.

Sulentic, J. W., T. Zwitter, P. Marziani, and D. Dultzin-Hacyan (2000). "Eigenvector 1: An Optimal Correlation Space for Active Galactic Nuclei." In: *ApJ* 536, pp. L5–L9.

Sulentic, J. W., G. M. Stirpe, P. Marziani, R. Zamanov, M. Calvani, and V. Braito (2004). "VLT/ISAAC spectra of the Hβ region in intermediate redshift quasars." In: *A&A* 423, pp. 121–132. DOI: 10.1051/0004-6361:20035912. eprint: astro-ph/0405279.

Sulentic, J. W., P. Repetto, G. M. Stirpe, P. Marziani, D. Dultzin-Hacyan, and M. Calvani (2006). "VLT/ISAAC spectra of the Hβ region in intermediate-redshift quasars. II. Black hole mass and Eddington ratio." In: *A&A* 456, pp. 929–939. DOI: 10.1051/0004-6361:20054153. eprint: astro-ph/0606309.

Sulentic, J. W., R. Bachev, P. Marziani, C. A. Negrete, and D. Dultzin (2007). "C IV λ1549 as an Eigenvector 1 Parameter for Active Galactic Nuclei." In: *ApJ* 666, pp. 757–777. DOI: 10.1086/519916. arXiv: 0705.1895.

Tilton, E. M. and J. M. Shull (2013). "Ultraviolet Emission-line Correlations in HST/COS Spectra of Active Galactic Nuclei: Single-epoch Black Hole Masses." In: *ApJ* 774, p. 67.

Trakhtenbrot, B. and H. Netzer (2012). "Black hole growth to z = 2 - I. Improved virial methods for measuring M_{BH} and L/L_{Edd}." In: *MNRAS* 427, pp. 3081–3102. DOI: 10.1111/j.1365-2966.2012.22056.x. arXiv: 1209.1096.

Tytler, D. and X.-M. Fan (1992). "Systematic QSO emission-line velocity shifts and new unbiased redshifts." In: *ApJS* 79, pp. 1–36. DOI: 10.1086/191642.

Venemans, B. P., F. Walter, L. Zschaechner, R. Decarli, G. De Rosa, J. R. Findlay, R. G. McMahon, and W. J. Sutherland (2016). "Bright [C ii] and Dust Emission in Three z > 6.6 Quasar Host Galaxies

Observed by ALMA." In: *ApJ* 816, 37, p. 37. DOI: `10.3847/0004-637X/816/1/37`. arXiv: `1511.07432`.

Vernet, J. et al. (2011). "X-shooter, the new wide band intermediate resolution spectrograph at the ESO Very Large Telescope." In: *A&A* 536, A105, A105. DOI: `10.1051/0004-6361/201117752`. arXiv: `1110.1944 [astro-ph.IM]`.

Véron, P., A. C. Gonçalves, and M.-P. Véron-Cetty (2002). "The "red shelf" of the Hβ line in the Seyfert 1 galaxies RXS J01177+3637 and HS 0328+05." In: *A&A* 384. DOI: `10.1051/0004-6361:20020072`. eprint: `astro-ph/0201240`.

Vestergaard, M. (2002). "Determining Central Black Hole Masses in Distant Active Galaxies." In: *ApJ* 571, pp. 733–752.

— (2004). "Early Growth and Efficient Accretion of Massive Black Holes at High Redshift." In: *ApJ* 601, pp. 676–691.

Vestergaard, M. and P. S. Osmer (2009). "Mass Functions of the Active Black Holes in Distant Quasars from the Large Bright Quasar Survey, the Bright Quasar Survey, and the Color-selected Sample of the SDSS Fall Equatorial Stripe." In: *ApJ* 699, pp. 800–816.

Vestergaard, M. and B. M. Peterson (2006). "Determining Central Black Hole Masses in Distant Active Galaxies and Quasars. II. Improved Optical and UV Scaling Relationships." In: *ApJ* 641, pp. 689–709.

Vestergaard, M., X. Fan, C. A. Tremonti, P. S. Osmer, and G. T. Richards (2008). "Mass Functions of the Active Black Holes in Distant Quasars from the Sloan Digital Sky Survey Data Release 3." In: *ApJ* 674, pp. L1–L4.

Vogt, S. S. et al. (1994). "HIRES: the high-resolution echelle spectrometer on the Keck 10-m Telescope." In: *Instrumentation in Astronomy VIII*. Ed. by D. L. Crawford and E. R. Craine. Vol. 2198. Proc. SPIE, p. 362.

Wang, H., F. Xing, K. Zhang, T. Wang, H. Zhou, and S. Zhang (2013). "Outflow and Hot Dust Emission in High-redshift Quasars." In: *ApJ* 776, p. L15.

Wang, J.-G., X.-B. Dong, T.-G. Wang, L. C. Ho, W. Yuan, H. Wang, K. Zhang, S. Zhang, and H. Zhou (2009). "Estimating Black Hole Masses in Active Galactic Nuclei Using the Mg II λ2800 Emission Line." In: *ApJ* 707, pp. 1334–1346. DOI: `10.1088/0004-637X/707/2/1334`. arXiv: `0910.2848`.

White, R. L., R. H. Becker, D. J. Helfand, and M. D. Gregg (1997). "A Catalog of 1.4 GHz Radio Sources from the FIRST Survey." In: *ApJ* 475, pp. 479–493.

Williams, R. J., R. Maiolino, Y. Krongold, S. Carniani, G. Cresci, F. Mannucci, and A. Marconi (2016). "An ultra-dense fast outflow in a quasar at z=2.4." In: *ArXiv e-prints*. arXiv: `1605.08046`.

Wilson, J. C. et al. (2004). "Mass producing an efficient NIR spectrograph." In: *Ground-based Instrumentation for Astronomy*. Ed. by A.

F. M. Moorwood and M. Iye. Vol. 5492. Proc. SPIE, pp. 1295–1305. DOI: `10.1117/12.550925`.

Wisotzki, L., N. Christlieb, N. Bade, V. Beckmann, T. Köhler, C. Vanelle, and D. Reimers (2000). "The Hamburg/ESO survey for bright QSOs. III. A large flux-limited sample of QSOs." In: *A&A* 358, pp. 77–87. eprint: `astro-ph/0004162`.

Wu, X.-B., R. Wang, M. Z. Kong, F. K. Liu, and J. L. Han (2004). "Black hole mass estimation using a relation between the BLR size and emission line luminosity of AGN." In: *A&A* 424, pp. 793–798.

York, D. G. et al. (2000). "The Sloan Digital Sky Survey: Technical Summary." In: *AJ* 120, pp. 1579–1587.

Yuan, S., M. A. Strauss, and N. L. Zakamska (2016). "Spectroscopic identification of type 2 quasars at z < 1 in SDSS-III/BOSS." In: *MNRAS* 462, pp. 1603–1615. DOI: `10.1093/mnras/stw1747`. arXiv: `1606.04976`.

Zakamska, N. L. and J. E. Greene (2014). "Quasar feedback and the origin of radio emission in radio-quiet quasars." In: *MNRAS* 442, pp. 784–804. DOI: `10.1093/mnras/stu842`. arXiv: `1402.6736`.

Zakamska, N. L., F. Hamann, I. Pâris, W. N. Brandt, J. E. Greene, M. A. Strauss, C. Villforth, D. Wylezalek, R. M. Alexandroff, and N. P. Ross (2016). "Discovery of extreme [O III] λ5007 Å outflows in high-redshift red quasars." In: *MNRAS* 459, pp. 3144–3160. DOI: `10.1093/mnras/stw718`. arXiv: `1512.02642`.

Zamanov, R., P. Marziani, J. W. Sulentic, M. Calvani, D. Dultzin-Hacyan, and R. Bachev (2002). "Kinematic Linkage between the Broad- and Narrow-Line-emitting Gas in Active Galactic Nuclei." In: *ApJ* 576, pp. L9–L13. DOI: `10.1086/342783`. eprint: `astro-ph/0207387`.

Zamfir, S., J. W. Sulentic, P. Marziani, and D. Dultzin (2010). "Detailed characterization of Hβ emission line profile in low-z SDSS quasars." In: *MNRAS* 403, pp. 1759–1786. DOI: `10.1111/j.1365-2966.2009.16236.x`. arXiv: `0912.4306`.

Zhang, S., H. Wang, T. Wang, F. Xing, K. Zhang, H. Zhou, and P. Jiang (2014). "Outflow and Hot Dust Emission in Broad Absorption Line Quasars." In: *ApJ* 786, p. 42.

van der Marel, R. P. and M. Franx (1993). "A new method for the identification of non-Gaussian line profiles in elliptical galaxies." In: *ApJ* 407, pp. 525–539.

DECLARATION

Put your declaration here.

Saarbrücken, September 2015

Liam Coatman